POLITECNICO DI TORINO

Master of Science
in Energy and Nuclear Engineering

Master's Degree Thesis

Thermal analysis of a solar parabolic trough - ORC - biomass cogeneration plant of electricity and cooling applied to a shopping centre

Thesis advisor:
Vittorio Verda

Autor:
Cristina Ballerini

External thesis advisors:
Miguel Ángel Lozano Serrano,
Luis María Serra de Renobales

-Academic year 2017/2018-

Alla mia famiglia che è sempre stata fiera di me

e a mia sorella che con un "puoi fare meglio"

mi ha sempre spronata.

A chi mi ha permesso e mi permetterà

di vivere la vita

come una grande locura.

Contents

1. Abstract

The main objective of this works is the design of a renewable system which function is covering the electrical and cooling annual demand of a shopping centre in Zaragoza, Spain.

The analysis of the system includes sizing of a parabolic trough collector solar field, integrated with a biomass boiler. The assembly has to provide the thermal energy needed in a power Organic Rankine Cycle which produces electricity for chillers and for other uses of the shopping centre, besides a possible connection to the city's power grid is considered.

The aim of the analysis is basically to employ a parabolic trough collector solar field designed using the software System Advisor Model [NREL. System Advisor Model 2017.9.5] and which parameters have been varied to analyse the system response and to provide different possible solutions. In order to present the technologies, a case study has been presented.

The solar field has been placed within a location where the annual global horizontal radiation is significant: 1651 kWh/m^2 [Meteonorm, www.meteonorm.com, 2018]. The site is Zaragoza where the study of the thesis has taken place. Two tanks, a hot and a cold tank, are employed to store the exceeding quantity produced during the hours of peak production. The system is also composed by a biomass boiler that complements the energy produced by the solar field to supply an organic Rankine cycle with almost a pre-set thermal input. The working fluid that flows through the power cycle is the refrigerant R245fa, chosen after comparing alternatives commercial fluids. Different possible operating results of the ORC, due to climatic conditions, are discussed.

Afterwards, an application of the whole system is presented. As it has been mentioned earlier, cooling and electrical demands of a shopping centre in Zaragoza are analysed and thought to be covered by the electricity produced by the ORC. An integration with the power grid allows the whole system not to be oversized whilst, in condition of surplus of electrical energy produced, the grid connection additionally enables to sell the exceeding electricity.

In order to better combine all the components, the ORC cycle and the solar field are designed, adjusting the plant following the demand. The total nominal power of the chillers, needed for cooling the shopping centre is the value that imposes the size of the ORC plant. The results of the case study analysed are presented as mean hourly values of a typical day for each month of the year.

2. Introduction

2.1. Energy related environmental problems

One of the most widely accepted definitions of sustainable development is: *development that meets the needs of the present without compromising the ability of future generations to meet their own needs* [Gro Harlem Bruntland, 1987].
It is generally considered true that a fully sustainable supply of energy is a target to aim at in the next years. Moreover, secure and constant supply of energy is necessary, and it has to be available for everyone and at reasonable cost without causing emission of toxic substances or any dangerous elements.

Until the 1970s the energy demand was concerned with researching the cheaper and more convenient source. Although in the early 1970s, after the oil crisis, the concern was on the cost of energy, during the past two decades, the risk and reality of environmental degradation have become more apparent. The interest in the maintenance of the energy sources has increased and the development of renewable energies and energy saving has been stimulated [Soteris A. Kalogirou, 2004].

The increasing of environmental problems strongly depends on energy consumption, and this is only expected to increase in the coming years. The growing of the population is a factor that will affect the energy production for private uses as well as for industrial activities. Besides, the life quality of underdeveloped regions increases and the developed regions of the world are not permitting any decrease in economic growth. Therefore, the future of the world situation is more industrialization and higher consumption of energy resources.

The impact of these activities will lead to a continuous degradation of the environment due to the emissions in the environment of pollutants and hazardous substances worsening already existing environmental impacts such as global warming, eutrophication, stratospheric ozone depletion and acid precipitation.

As an attempt to reduce the negative results of increasing in the energy production, alternatives to fossil fuel technologies have to assume the main role in energy production. Economic, safety and environmental aspects will be important characteristics that will be taken into account when vetting their applications in energy production.

2.2. Renewable energy

Renewable energies are energy sources whose use does not compromise natural resources available and the environment. Moreover, the great advantage of these sources is their inexhaustibility, which aim is to fully replace the traditional sources.

The renewable energy technologies use the Sun’s energy and its direct and indirect effects on Earth, gravitational forces and the heat of Earth’s core as the resources from which energy is produced [Soteris A. Kalogirou, 2004].

The main renewable energy sources are:

- Solar energy, employed as solar thermal or photovoltaic; respectively, to produce thermal energy in the form of hot fluid or to directly produce electricity.
- Wind energy that exploits the power of the air flowing through wind turbines, they transform the kinetic energy in the wind into mechanical power and then converted into electricity.
- Hydraulic energy, that is based on the transformation in electricity of the gravitational potential energy of water reservoirs at higher elevation than the area where the transformation takes place.
  The gravitational potential energy is exploitable via a water flow that, reducing its elevation, rises its kinetic energy. At the bottom of the hydraulic system, the water flows through a hydraulic turbine and rotates its shaft. This process converts the kinetic energy in mechanical energy that is consequentially transformed in electricity by an alternator.
- Biomasses are organic materials that can be used as fuels. They can be of different kinds, considering their origins:
  - Wood from forests and plant material from agriculture
  - Animal and human sewage
  - Solid waste
- Geothermal energy, that allows to use the heat from within Earth and beneath the soil. The temperature generally increases going deeper in the interior of the Earth. In certain areas, where the geothermal gradient reaches high values, high temperature can be found at reachable depths. Thus, the corresponding technology is feasible.

2.3. Document's objective

This work agrees with the idea of an energetic sustainable development, based on the exploitation of renewable sources and maximizing the efficiency of the system developed.

This document focuses on the technology of concentrating solar thermal collectors, complemented by a biomass boiler in substitution of a traditional boiler fed by fossil fuel, integrated with an organic Rankine cycle. Physical models have been studied to describe the behaviour of the devices and equipment employed.
The purpose of the thesis is to design and to analyse, throughout the year, a solar thermal parabolic trough field equipped with two tanks, a hot and a cold tank that extend the production time and reduce the variability in the production. The system is hybridized with a biomass boiler that guarantees a constant production even in the absence of solar radiation. The sole exploitation of renewable sources would be permitted through the integration of this technology. The assembly is connected to a heat exchanger that feeds a power cycle, which is an organic Rankine cycle (ORC). An organic fluid flows through the power cycle, its pressure is risen by a pump and it is warmed up throughout the heat exchanger. When its temperature is at the maximum value of the cycle, it goes into a turbine to be expanded. The work of the turbine is to produce mechanical energy exploiting the high enthalpy of the fluid (high temperature and pressure) that enters in the turbine, thus the turbine is able to convert the reduction of enthalpy into mechanical energy.
Then, an alternator directly connected to the turbine shaft, transforms the mechanical energy in electricity.
The system studied has been thought to produce electricity to supply a shopping centre, which requires a high amount of electricity throughout the year. Hence, the electrical demand of a shopping centre sited in Zaragoza has been analysed and used as input to design the system. The needed electricity is employed for three cooling machines, for lighting and for electrical demand of other devices. Monthly and daily demand profiles are evaluated to obtain for the entire year, the hourly electrical demand of a

typical day for each month, both for weekdays and for holidays. The cooling demand profiles are then converted in electrical demand necessary to supply the mechanical chillers that are employed in the shopping centre.

Covering the electrical nominal demand of the three chillers has been the criterion chosen to design the ORC cycle. This choice is a compromise between trying to cover, at least, the cooling demand and not oversizing the whole system. Nonetheless, the production of this system does not assure to cover the whole electrical demand. In order to provide the necessary electricity to cover the entire electrical demand of the shopping centre, a connection to the grid has proved to be necessary.

Thus, having the opportunity to buy electricity from the grid assures a constant supply, and selling to the grid gives the chance to have an economic return of the investment, even when the production exceeds the demand of the shopping centre.

2.4. State of the art

Projects that employ the technologies analysed in this document have already been built and are in operation, as the cases shown in this paragraph. Herein are presented some parabolic trough solar field coupled with ORC technology, different integration and variations are applied for each project.
In the coming section cases in which some plants where the integration between different renewable technologies are considered. Biomass and solar trough field or solar thermal and photovoltaic and geothermal energy, are duly described. Besides, it is considered the possibility to combine a renewable source, such as the solar energy, with a fossil-based technology, i.e. a combined cycle composed by a gas turbine, one heat recovery steam generator and one steam turbine.

The data shown as follows is taken from the National Renewable Energy Laboratory web site [www.nrel.gov, 07/2018], where projects carried on by more developers and owners, are listed and presented.

2.4.1. Brønderslev

Aalborg CSP A/S [www.aalborgcsp.com, 07/2018], in close cooperation with Brønderslev Forsyning A/S [www.bronderslevforsyning.dk, 07/2018], established a 0.8 MWth test facility to investigate the possibility of using concentrated solar energy to optimize a biomass-based Organic Rankine Cycle (ORC) plant. Based on the positive results, Aalborg CSP awarded the order to develop and deliver a 16.6 MWt solar heating plant, which contributes to a greener production of both electricity and heat to the citizens of Brønderslev.

Figure 1: Aalborg CSP-Brønderslev project [Aalborg CSP, www.aalborgcsp.com, video screenshot,07/2018]

The solar thermal plant demonstrates how CSP technology can be combined with other green solutions, in this case a biomass-based ORC system, even under Danish weather conditions, that are not favourable for solar collector technologies.

The plant contains a total of 5 km receiver pipes. The receiver tube is encircled by a vacuum glass tube, and inside the tube runs a thermal oil that is heated only by the sun. This high temperature can have an electric turbine to produce electricity, and the flexibility of CSP technology also allows to produce lower temperatures for district heating. The solar heating system can thus switch between supplying combined electricity and district heating through the ORC plant or supplying district heating exclusively. To have a more feasible system, electricity is produced depending on the market development and the waste heat is utilised for district heating [Aalborg CSP, www.aalborgcsp.com, 07/2018].

Project Name:	Aalborg CSP-Brønderslev CSP with ORC project
Country:	Denmark
Location:	Brønderslev (North Jutland)
Owner(s):	Brønderslev Forsyning
Lat/Long Location:	57°15′ 16.0″ North, 9°59′ 19.0″ East
Technology:	Parabolic trough
Status:	Operational
Start Year:	2016
Contact(s):	Webmaster Solar
Key References:	Web site
Break Ground:	apr-16
Start Production:	December 30, 2016
Solar-Field Aperture Area:	26929 m²
# of Solar Collector Assemblies (SCAs):	40
# of SCAs per Loop:	4
SCA Aperture Area:	674 m²
SCA Length:	125 m
# of Modules per SCA:	10
SCA and HCE Manufacturer:	Aalborg CSP
# of Heat Collector Elements (HCEs):	1.2
Solar-Field Inlet Temp:	252°C
Solar-Field Outlet Temp:	312°C
Turbine Capacity (Gross):	16.6 MW
Turbine Description:	MWth for production of heat and electricity
Output Type:	Organic Rankine
Thermal Storage Type:	None

Table 1: Project Overview [www.nrel.gov,Aalborg CSP, 05/2017]

2.4.2.ISCC Kuraymat

The Kuraymat plant is located at about 87 km south of Cairo, Capital of Egypt, on the eastern side of the River Nile. The Integrated Solar Combined-Cycle (ISCC) technology combines the benefits of solar energy with the benefits of a combined cycle. The solar resource partially substitutes the fossil fuel. The Kuraymat project has an overall capacity of 140 MW (120 MW combined cycle, 20 MW solar input).

Figure 2: Solar parabolic trough collectors of the Kuraymat plant [www.protenders.com, 07/2018]

The solar irradiation, which is channelled to parabolic-shaped mirrors, is reflected onto an absorber pipe, the receiver, in the focal line of the collector. The vacuum-isolated absorber pipes contain a circulating heat transfer fluid [www.protenders.com, 07/2018].

The solar heat transfer from the solar field collectors (PTCs) to the steam cycle is done by the HTF (heat transfer fluid) system. The HTF is Therminol VP-1 from Solutia. The Combined Cycle Island consists of one gas turbine, one heat recovery steam generator (HRSG), one steam turbine, solar heat exchangers plus all associated control and balance of plant equipment and installations [A. Temraz et al., 2018].

Project Name:	ISCC Kuraymat (ISCC Kuraymat)
Country:	Egypt
Location:	Kuraymat (100 km south of Cairo)
Lat/Long Location:	29°16′ 43.0″ North, 31°14′ 56.0″ East
Owner(s):	NREA (100%)
Technology:	Parabolic trough
Status:	Operational
Solar Resource:	2431 kWh/m2/yr
Electricity Generation:	34000 MWh/yr (Expected)
Contact(s):	Bothayna Rashed
Company:	NREA
Start Production:	June 2011
Project Type:	Commercial
Solar-Field Aperture Area:	130800 m²
# of Solar Collector Assemblies (SCAs):	160
# of Loops:	40
# of SCAs per Loop:	4
# of Modules per SCA:	12
SCA Manufacturer (Model):	Flagsol (SKAL-ET)
Mirror Manufacturer (Model):	Flabeg (RP3)
Heat-Transfer Fluid Type:	Therminol VP-1
Solar-Field Inlet Temp:	293°C
Solar-Field Outlet Temp:	393°C
Turbine Capacity:	Net: 20.0 MW, Gross: 20.0 MW
Turbine Manufacturer:	Siemens
Output Type:	Steam Rankine
Cooling Method	Wet cooling
Description:	Cooling towers
Thermal Storage Type:	None

Table 2: Project Overview [www.nrel.gov, ISCC Kuraymat, 02/2013]

The scheme configuration of the integrated solar combined plant is presented in the Figure 3.

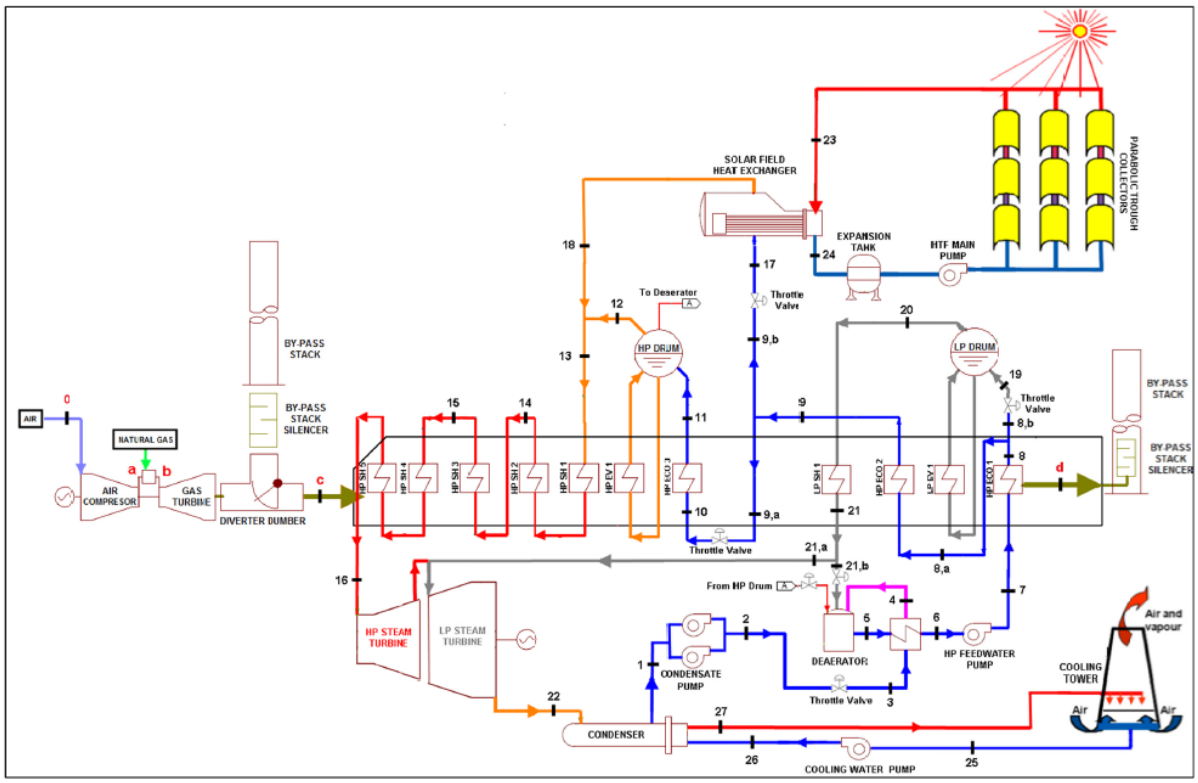

Figure 3: Flow Diagram of ISCC in Kuraymat, Egypt with state points illustration [A. Temraz et al., 2018]

2.4.3. Saguaro Power Plant

The power plant of Saguaro, a concentrating solar power (CSP) project, is located in Red Rock, Arizona (USA).

The APS Saguaro solar facility features more than 100000 square feet of parabolic trough-shaped mirrors aligned in six rows, providing enough electricity to meet the demand of 200 homes.

The Saguaro solar power project is the first to combine solar trough technology with an organic Rankine cycle power block, typically used in geothermal and biomass applications. The block allows the plant to produce more power at lower temperatures. [www.protenders.com, 07/2018]

The Saguaro Station power plant was built by Solargenix [www.nrel.gov, 07/2018], a solar energy development company based /in Raleigh, N.C. and a subsidiary of ACCIONA Energy of Spain [www.acciona-energia.com, 07/2018], a world leading company devoted to renewables [www.greenprogress.com, 07/2018].

Figure 4: Solar collectors site [www.protenders.com, 07/2018]

Project Name:	Saguaro Power Plant
Country:	United States
Location:	Red Rock, Arizona (Southwest USA)
Owner(s):	Arizona Public Service (100%)
Lat/Long Location:	32°32′ 52. 0″ North, 111°17′ 34.0″ West
Technology:	Parabolic trough
Status:	Currently Non-Operational
Start Year:	2006
Solar Resource:	2636 kWh/m2/yr
Electricity Generation:	2000 MWh/yr (Expected/Planned)
Cost (approx):	6000000 USD
Project Type:	Production
Solar-Field Aperture Area:	10340 m²
# of Solar Collector Assemblies (SCAs):	24
# of Loops:	3
# of SCAs per Loop:	8
SCA Length:	97 m
# of Modules per SCA:	12 and 8
SCA Manufacturer (Model):	Starnet (LS-2)
# of Heat Collector Elements (HCEs):	528
HCE Manufacturer (Model):	Schott Glass (Schott PTR70)
Heat-Transfer Fluid Type:	Xceltherm 600 (solar field); n-pentane (ORC working fluid)
HTF Company:	Radco Industries
Solar-Field Inlet Temp:	248°F
Solar-Field Outlet Temp:	572°F
Turbine Capacity:	Net: 1.0 MW, Gross: 1.16 MW
Turbine Manufacturer:	Ormat (Israel)
Output Type:	Organic Rankine
Cooling Method:	Wet cooling
Thermal Storage Type:	None

Table 3: Project Overview [www.nrel.gov, Saguaro Power Plant, 04/2017]

2.4.4. Stillwater GeoSolar Hybrid Plant

Stillwater Solar Geothermal Hybrid Project in Fallon, Nevada is a first of its kind renewable energy power plant. Stillwater integrates 33 MW of geothermal power with 26.4 MW of solar photovoltaic and 2 MW of solar thermal capacity. The Stillwater geothermal project is located in Nevada, USA, and is owned and operated by Enel Green Power North America, Inc. (EGP-NA). The first phase of the project began with a geothermal plant, a 33 MW gross binary plant which was commissioned in 2009.

Figure 5: Stillwater hybrid geothermal-solar plant, Nevada [Enel, video screenshot,07/2018]

A desire to increase output led EGP to add 26 MW of solar photovoltaic (PV) power to the project in 2012. The solar PV project size was tailored to complement the geothermal plant output degradation during hot summer temperatures. In 2013, design began on an additional solar project using Concentrated Solar Power (CSP) thermal technology [Giuseppe DiMarzio et al., 2015].

Project Name:	Stillwater GeoSolar Hybrid Plant
Country:	United States
Location:	Fallon, Nevada
Owner(s):	Enel Green Power
Lat/Long Location:	39°32′ 53.0″ North, 118°33′ 20.0″ West
Technology:	Parabolic trough
Status:	Operational
Start Year:	2015
Land Area:	21 acres
Electricity Generation:	3000 MWh/yr (Estimated)
Contact(s):	Craig Turchi
Company:	NREL
Start Production:	March 2015
PPA/Tariff Period:	20 years
SCA Aperture Area:	656 m²
SCA Length:	115 m
# of Modules per SCA:	8
SCA Manufacturer (Model):	SkyFuel (SkyTrough®)
Mirror Manufacturer (Model):	SkyFuel (ReflecTech®)
HTF Company:	Demineralised water
Turbine Capacity:	Net: 2.0 MW Gross: 2.0 MW
Turbine Description:	Thermal
Output Type:	Organic Rankine
Thermal Storage Type:	None

Table 4: Project Overview [www.nrel.gov, Stillwater GeoSolar Hybrid Plant, 10/2016]

3. The solar field

This paragraph focuses on the solar thermal technology and how the software SAM [NREL. System Advisor Model 2017.9.5] develops models to calculate and study solar thermal plants.
Moreover, a parametrical analysis of the solar field is presented and the equations that describe the thermodynamic processes that take place in the elements of the system are introduced.
The analysis is conducted through the design of a parabolic trough solar field using the software SAM.

3.1. Solar thermal technology

Solar thermal collectors are used to convert the incident solar radiation on their area, into thermal energy. This process is conducted by a transport medium, going through the loop that absorbs the solar radiation in order to rise its temperature [Pedro Horta, FhG ISE, 2012].
The solar energy thus collected is carried through from the circulating fluid either to a heat exchanger to be directly employed as heat source for a secondary loop; or to a thermal storage from which can be withdrawn when the instantaneous production is not sufficient.
The efficiency is related to the operating temperatures because both the fluid flowing through the collectors and the structure is at a higher temperature than the air temperature. Therefore, higher temperatures lead to higher thermal losses and to lower efficiencies.

To reduce thermal losses, occurring either by means of conduction, convection and radiation, solar collectors might also dispose of thermal insulation and glazing materials [Pedro Horta, FhG ISE, 2012].
It is worth pointing out that, considering the factors that reduce the efficiency, a key element is the optical efficiency. Optical losses play an essential role in reducing the incident radiation on the collectors.

Different solar collector technologies have been developed, which can be mainly divided into two categories:

- Stationary collectors: Non-concentrating collectors that have the same area for interception and absorption or a very moderate ratio between aperture and absorber areas (ratio<2). They are thus suitable for fixed positioning. They are flat-plate collectors, evacuated tube collectors and compound parabolic concentrator collectors.
- Concentrating collectors: Solar energy is optically concentrated before being transferred into heat. The reflected radiation is concentrated in a focal zone, where the receiver is positioned. The typical ratio between aperture and absorber areas is more than ten, for this kind of collectors. In order to be more efficient, these collectors require the use of tracking systems to follow the Sun throughout the day and/or the year. They are parabolic trough collectors and linear Fresnel reflector concentrator [Soteris A. Kalogirou, 2004], [Pedro Horta, FhG ISE, 2012].

Hereunder, the focus is given to the solar trough collectors, chosen in this document to be analysed as the technology that exploits the solar source.

3.2. Parabolic trough collectors

The main advantage of the parabolic trough and in general, of the concentrating collectors, is the reduction of heat losses; in fact, this is possible thanks to the limited area at high temperature. The high temperature surface, for these collectors, is the receivers' surface and it has a significant smaller area than the incident area, which is composed by a sheet of reflective material bent into a parabolic shape and it is at relatively low temperature.

Technical improvements found in parabolic trough collectors lead to other advantages [Soteris A. Kalogirou, 2004], listed as follows:

- The working fluid, flowing through the receiver, can achieve higher temperatures in concentrator systems when compared to flat-plate systems of the same solar energy collecting surface. Therefore, higher thermodynamic efficiency can be achieved.
- Reflecting surfaces of parabolic trough collectors require less material and are structurally simpler than flat-plate collectors. Because they only serve as reflective surfaces and the fluid does not flow through their structure as in flat-plate collectors. This simplicity turns out in reduced cost per unit area of the solar collecting surface.
- The receiver area is considerably smaller than the receiving surface of the flat-plate collectors. Hence, selective surface treatment and vacuum insulation, necessary to reduce heat losses and improve the collector efficiency, are economically more viable than in flat-plate collectors, due to reduced costs of materials.

Even though the efficiency of parabolic trough collectors is significantly higher than in flat-plate collectors, some drawbacks arise [Soteris A. Kalogirou, 2004]:

- Diffuse radiation is not widely exploitable and, depending on the concentration ratio, this part of the radiation can be differently employed.
- A form of tracking system is required to follow the sun and to reduce optical losses.
- Maintenance is necessary because, over time, reflecting surfaces may decrease their reflectance characteristic and may require periodic cleaning and refurbishing.

3.3. SAM operating mode

The System Advisor Model (SAM) is a free software made available by the U.S. Department of Energy's National Renewable Energy Laboratory (NREL) and Sandia National Laboratory (USA) [NREL. System Advisor Model 2017.9.5]. It is an open source model oriented to the feasibility assessment of renewable energy projects, providing a detailed simulation of concentrating solar power (CSP) systems, photovoltaic, solar hot-water, and generic fuel-use technologies [Michael J. Wagner et al., 2010].

SAM is based on an hourly simulation engine, integrated with TRNSYS [Transient Simulation Program, 1975], which in the case of CSP calculates the hourly performance of a system including the energy output. The models require input data to describe the performance characteristics of physical equipment in the system. To describe the renewable energy resource and weather conditions at a project location, SAM model requires a weather data file, that can be chosen from a list, downloaded from the Internet or from other software, or created using data.

In this Master Thesis, the Meteonorm software database [www.meteonorm.com, 2018] provides the weather data necessary for the input of the calculation.

3.4. The structure of the solar field

The solar field consists of solar collector assemblies (SCA) that are responsible for heat collecting of the plant. They are combined in one or more parallel loops.
Within each loop, a number of SCA's are used to incrementally heat the thermal fluid to the design outlet temperature. Each SCA is composed of a number of parabolic collectors and their receivers in series. In this model, the SCA serves as the lowest level of discretization, indeed they are considered as a single unit when calculating the model. Each SCA is treated as an independent calculation node within the loop, and the absorbed energy, losses, temperature, pressure drop, and other performance values are calculated independently for each SCA [Michael J. Wagner and Paul Gilman,2011].

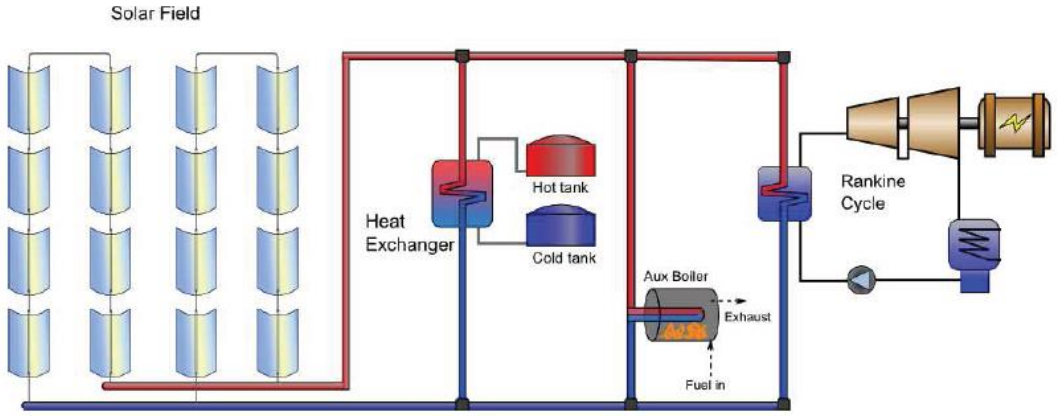

Figure 6: System structure configuration [Michael J. Wagner and Paul Gilman, 2011

3.5. System design

In order to design the collector parabolic field, the model uses the design-point at direct normal irradiance (DNI) value with the Sun position at noon on the summer solstice (June 21 north of the equator, and December 21 south of the equator).
The value of the direct normal irradiance (DNI) available at the design point is chosen as 950 W/m^2. Increasing this value indicates that fewer collectors are needed to achieve the reference condition power, while decreasing this value has the opposite effect. All of the system design inputs are nominal values, or values at the system's design point. SAM calculates actual values during simulation, recalculating the exact values considering the nearest real possible solutions.

The design conditions presented in Figure 7a and in Figure 7b (input data are those in the white boxes, whereas the result data are those which appear in the blue boxes) are the base to calculate the power per surface unit that can be obtained in the loops as heat sink power. In this simulation the power demand that must be satisfied is set as 5MW, which is defined in SAM as the heat sink.
The heat sink represents the thermal input demand that determines the field area that should attend it, and the design of the system. Thus, the heat sink parameters describe the process heat application's thermal load.
For oversizing the receiver design output, a target solar multiple has been defined. This parameter represents the design ratio between the target receiver thermal power and heat sink power.
The heat sink power is the value that is demanded, and it is thought to be set at this time of the calculation, whereas the receiver thermal power directly affects the design of the solar field. Thus, setting a higher value of the target solar multiple leads to a higher oversizing of the solar field.
If the target solar multiple is set as 1, the target receiver thermal power is the same value of the design heat sink power, and the solar field surface has been designed in order to cover the power demand with design-point conditions, that are the most suitable conditions for the power production. The nominal power demand would be, thus, hardly ever satisfied. On the other hand, imposing this

parameter as a value higher than 1, it allows to maintain a reasonable thermal power production during less favourable weather conditions and optical efficiency reduced due to not optimal incident angle. Once set the desired heat sink power (Figure 7a) and set the target solar multiple, the target receiver thermal power can be calculated as follows.

Target Receiver Thermal Power (MWt) = Solar Multiple × Heat Sink Power (MWt)

During the design of the reflective area of the solar field, the model considers the target receiver thermal power as the power which the solar field has to reach in design condition.

Other parameters needed to be set are the temperatures of the heat thermal fluid when it feeds the heat exchanger connected with the secondary loop, and after going through the exchanger, when it returns to the solar field. These can be decided by the user considering the source and the application of the thermal fluid of the solar field.

The SAM model opens up the possibility of integrating thermal storage into the system. Its aim is to increase the stability of the solar field production, i.e. the production time of heat sink power is extended, and the variability in the production is reduced. Both a cold and a hot tank are designed, respectively, to storage the supply and return fluid of the solar loop.
In order to design the thermal storage there is the possibility to define the capacity of the tank expressed in hours at full load. That means the number of hours that the storage system can supply energy at the design point.
Curtailment and availability losses are defined to represent reductions in the system's output or to represent conditions that are not optimal to let the system operate as designed.
Hourly values resulting from the calculation are reduced by the percentage set at this time of the simulation.

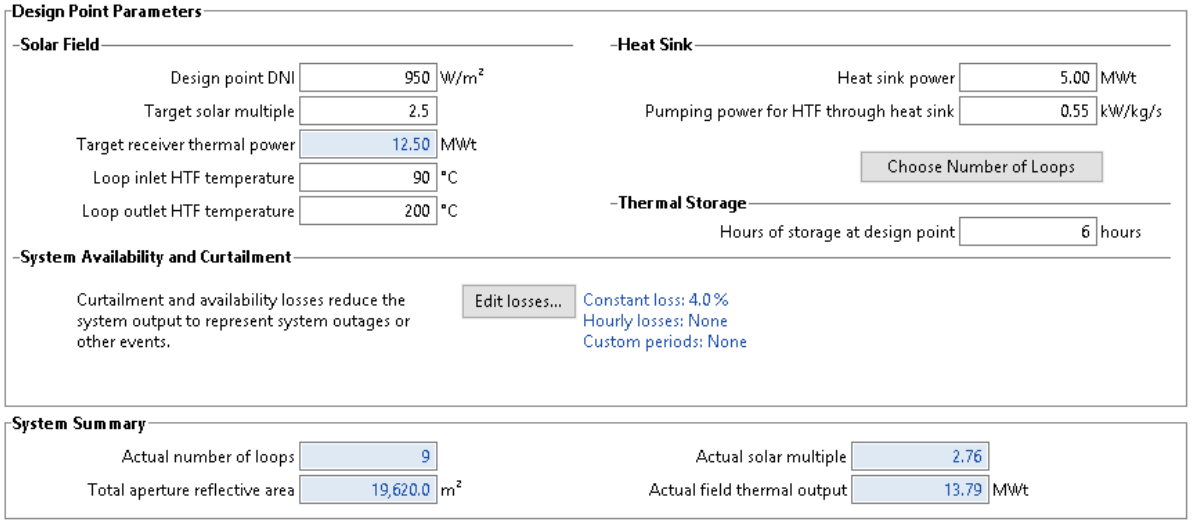

Figure 7a: Design input parameters for sizing the solar field [SAM screenshot, NREL. System Advisor Model 2017.9.5]

The total required aperture and the required number of loops are calculated setting the solar multiple as 1 (SM=1 in the Figure 7b), i.e. considering the receiver thermal power the same value of the heat sink power.
The SAM program calculates the necessary loops, which are equal to the solar multiple times the required number of loops at a solar multiple of 1 (design point conditions). The required number of loops is rounded to the nearest integer to represent a realistic field layout.
The total aperture reflective area, i.e. the aperture of the collector mirrors, is calculated multiplying the actual number of loops in the field for the aperture area corresponding to a single loop.

The actual solar multiple (2.76 in the case of Figure 7b) is recalculated using the ratio between the actual number of loops in the field (9 in the case of Figure 7b) and the required number of loops (3.26 in Figure 7b) with solar multiple equal to 1.
The actual field thermal output (13.79 MWt in Figure 7b) is the thermal power delivered by the solar field under design conditions (5 MWt in Figure 7b) at the actual solar multiple (2.76 in Figure 7b).

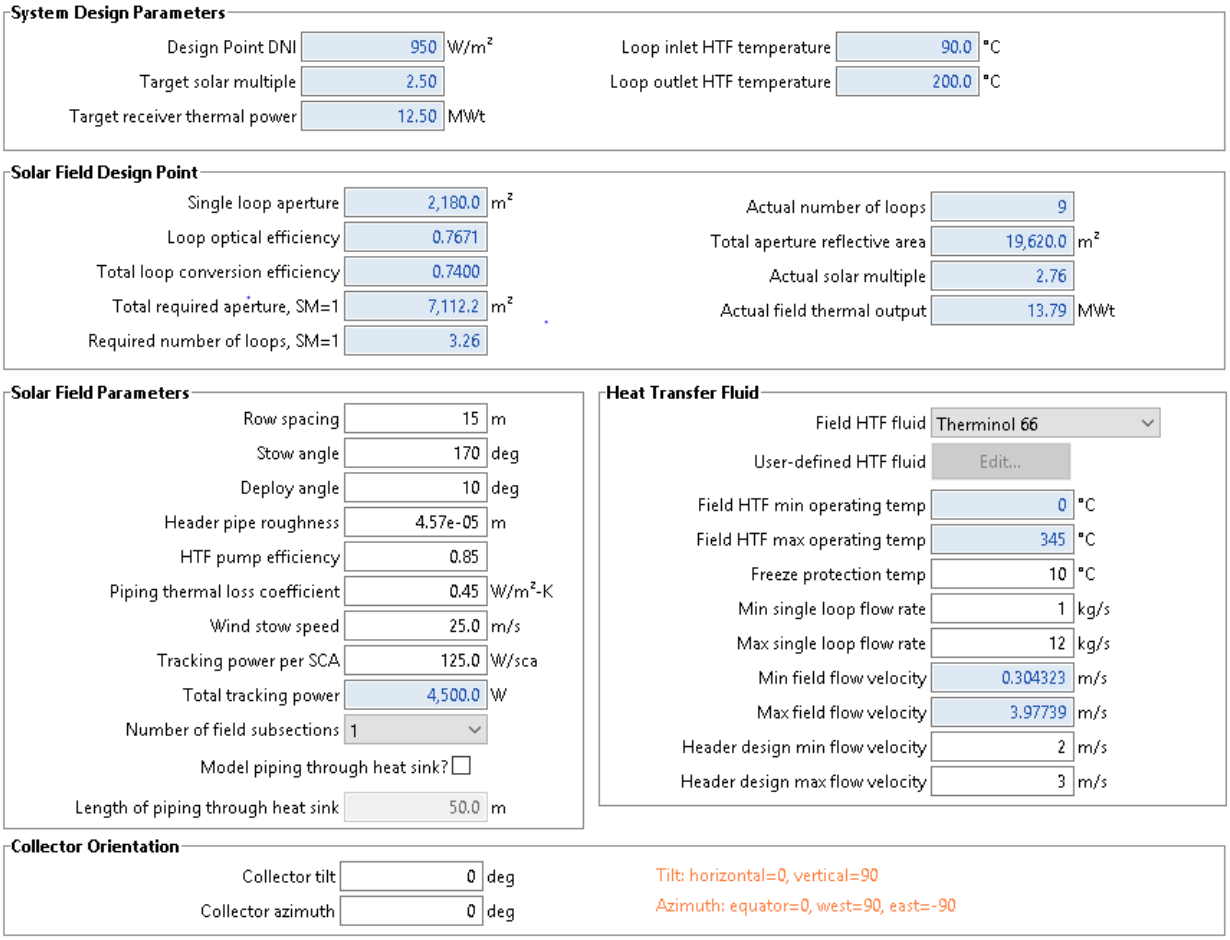

Figure 7b: Solar field parameters and operating constraints [SAM screenshot, NREL. System Advisor Model 2017.9.5]

The collector orientation is north-south direction, i.e. the axis of the collectors is along north-south direction. SAM simulates the system assuming that the collectors are oriented 90 degrees east of the azimuth angle in the morning and tracks the daily movement of the sun from east to west (Figure 8). Throughout the year, a horizontal north-south solar trough field usually collects slightly more energy than a horizontal east-west one. The north-south field collects a lot of energy in summer and much less in winter, whereas the east-west field collects more energy in winter than a north-south field and less in summer, providing a more constant annual output [Liang Hongbo, et al., 2017].
The application of this system aims to cover the cooling demand that is higher in summer and it is useful all year. Therefore, considering that the choice of orientation usually depends on the application, in this case it is right to install collectors in north-south direction.

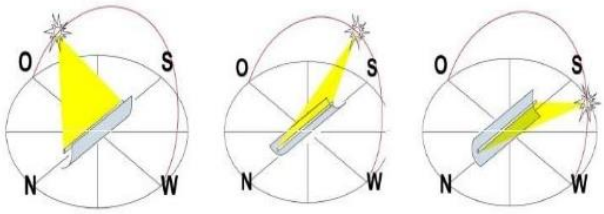

Figure 8: Collector axis oriented north-south, tracking of the sun [AEE INTEC, www.aee-intec.at, 07/2018]

The fluid that flows through the receivers' tube is Therminol 66. It is able to cover an extended operating range, from -85°C to 400°C, and its common applications are heating and cooling processes, exploiting the fluid as a thermal vector for transporting energy [www.therminol.com, 06/2018].

Information is gathered from the manufacturer Eastman [www.eastman.com, 06/2018] and from the Therminol web site, heat transfer fluids from Eastman, [www.therminol.com, 06/2018].

The main properties of Therminol 66

Property	Value
Composition	Hydrogenated terphenyl
Molecular weight	252 kg/mol
Density	1011 kg/m^3
Fire point	216 °C
Boiling point	359 °C

Table 5: www.therminol.com

TEMPERATURE	DENSITY	HEAT CAPACITY	THERMAL CONDUCTIVITY	VISCOSITY	VAPOR PRESSURE
°C	kg/m³	kJ/(kg·K)	W/(m·K)	Pa·s	kPa
90	962	1.803	0.1141	0.00455	0.0299
100	955	1.837	0.1135	0.0036	0.0484
110	948	1.872	0.1128	0.00292	0.0767
120	941	1.908	0.1121	0.00242	0.119
130	934	1.943	0.1114	0.00205	0.181
140	928	1.978	0.1107	0.00175	0.271
150	921	2.014	0.1099	0.00152	0.4
160	914	2.05	0.1091	0.00134	0.579
170	907	2.086	0.1083	0.00118	0.827
180	899	2.122	0.1074	0.00106	1.17
190	892	2.158	0.1065	0.00095	1.62
200	885	2.195	0.1056	0.00086	2.23
210	878	2.231	0.1046	0.000784	3.02
220	870	2.268	0.1036	0.000718	4.06
230	863	2.305	0.1026	0.000661	5.39
240	856	2.342	0.1015	0.000611	7.1
250	848	2.379	0.1004	0.000567	9.25
260	840	2.417	0.0993	0.000529	12
270	832	2.454	0.0982	0.000495	15.3
280	825	2.492	0.097	0.000464	19.5
290	817	2.531	0.0958	0.000437	24.5
300	809	2.569	0.0946	0.000413	30.7

Table 6: Heat transfer fluid calculators [Therminol, https://calculators.therminol.com]

3.6. Collectors

Solar collectors are responsible for reflecting and concentrating the solar radiation to the receivers. Their parabolic shape allows to increment the available incident surface and permits the solar rays to be concentrated on the focus of the parabola. Thus, the receiver, following the geometric rules, is positioned along the structure, where the collector's shape defines the focus.

Figure 9: Siemens collector [www.siemens.com, 07/2018]

When determining the value of the incident radiation onto the receivers, both derate-type losses and variable losses reduce the efficiency of the collector. The incidence angle affects the optical efficiency of the collector, reducing the radiation reflected when not zero. The incidence angle of the incoming solar radiation represents how it differs from the normal to the aperture plane of the collector.

$$\theta = \cos^{-1}\sqrt{1-[\cos(\theta_e-\theta_{col})-\cos(\theta_{col})\cos(\theta_e)(1-\cos(\gamma_s-\gamma_{col}))]^2}$$

θ_e is the solar elevation angle,

θ_{col} is the tilt angle of the collector,

γ_s is the solar azimuth,

γ_{col} is the solar azimuth of the collector.

The optical losses due to the solar position are represented by the following equations.

1. For cosine losses:

   $$\eta_{\cos} = \cos(\theta)$$

2. End losses at the end of each assembly:

   $$\eta_{endLoss} = 1 - L_{f,ave}\tan(\theta) - (\frac{N_{sca}}{2} - 1)\frac{2\cdot(L_{f,ave}\tan(\theta) - L_{spacing})}{N_{sca}L_{col}}$$

   $L_{f,ave}$ is the average focal length,

   N_{sca} is the number of solar collector assemblies per loop,

   $L_{spacing}$ the axis-to-axis distance between collector rows,

   L_{col} collector length.

3. Incidence angle modifier; is a derate factor that accounts for collector aperture foreshortening, glass envelope transmittance, selective surface absorption, and any other losses that area function of solar position.

$$\eta_{IAM} = \alpha_0 + \alpha_1 \frac{\theta}{\cos\theta} + \alpha_2 \frac{\theta^2}{\cos\theta}$$

α_0, α_1, α_2 are coefficients for the polynomial equation defining the incidence angle modifier (IAM).

4. Row-to-row shadowing

$$\eta_{shadow} = \left|\sin(90° - \omega_{col})\right| \frac{L_{spacing}}{w}$$

ω_{col} is the tracking angle

w aperture width of the collector

Fixed losses are applied as constant multipliers. They are tracking error, geometry defects, mirror reflectance, mirror soiling, and general error not captured by the other items.
Total efficiency of the collectors is calculated considering all the efficiency just mentioned.

$$\eta_{tot}(\theta, \omega_{col}) = \eta_{endLoss}(\theta)\eta_{shadow}(\omega_{col})\eta_{IAM}(\theta)\eta_{track}\eta_{geo}\rho_m\eta_{soil}\eta_{gen}$$

Then, the total radiative energy incident on the solar field is calculated as:

$$\dot{q}_{inc,s,f} = I_{bn} A_{ap,tot} \eta_{opt}(\theta, \omega_{col})$$

Where, I_{bn} is the beam normal irradiation

$A_{ap,tot}$ is the total solar field aperture area

[Michael J. Wagner et al., 2010], [Michael J. Wagner and Paul Gilman,2011].

SAM is fitted with a library that includes collectors of well-known brands. The characteristics and coefficients are then used for simulating the production.
The collector type is chosen from the nine technologies presented in the library of SAM. As the images below show (Table 7 and Figure 10), it is chosen a Siemens SunField 6 with the characteristics shown in Table 7.

Siemens SunField 6 characteristic					
Reflective aperture area	**Aperture width total structure**	**Length of collector assembly**	**Number of modules per assembly**	**Average surface to focus path length**	**Piping distance between assemblies**
545 m^2	5.776 m	95.2 m	8	2.17 m^2	0.8 m
IAM F0	**IAM F1**	**IAM F2**	**IAM F3**	**Tracking error**	**Geometry effects**
1	-0.0753	-0.03698	0	0.99	0.968
		Mirror reflectance	**Dirt on mirror**	**General optical error**	
		0.925	0.97	1	

Table 7: Characteristics of the collector [SAM, NREL. System Advisor Model 2017.9.5]

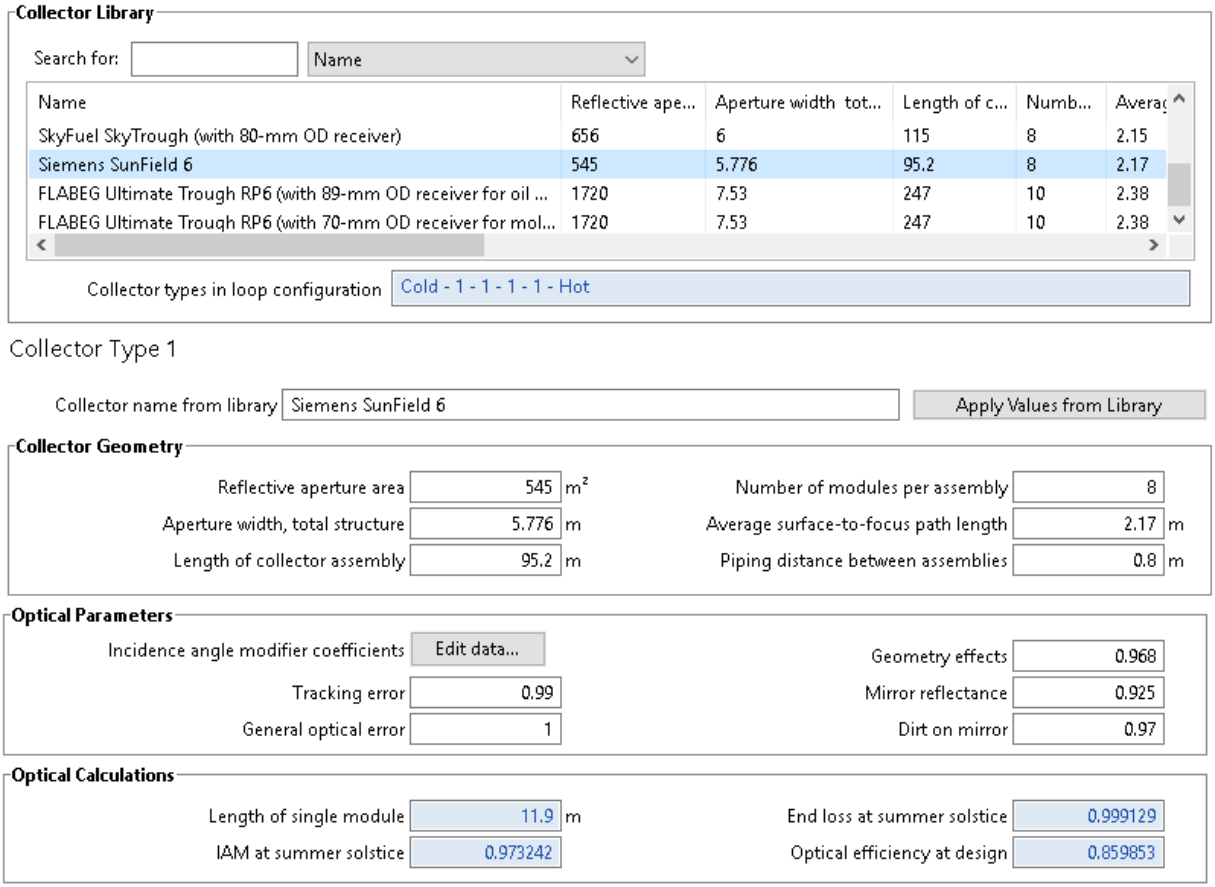

Figure 10: Characteristics of the collector [SAM screenshot, NREL. System Advisor Model 2017.9.5]

The software allows to choose four type collectors, though in this simulation it is only chosen the one whose characteristics are described in Table 7.

The definition of the parameters is clarified in Table 8:

Reflective aperture area (m^2)	The total reflective area of a single collector, used to calculate the loop aperture area of a loop, and number of loops required for a solar field with the aperture area defined with the design process
Aperture width, total structure (m)	The structural width of the collector, including reflective and non-reflective area. SAM uses this value to calculate row-to-row shadowing and blocking effects.
Length of collector assembly (m)	The length of a single collector assembly.
Number of modules per assembly	The number of individual collector-receiver sections in a single collector.
Average surface-to-focus path length (m)	The average distance between the collector surface and the focus of the parabola. This value is not equal to the focal length of the collector. To calculate the value when you know the focal length (a) and aperture width (w), use the following equation, where F_{avg} is the average surface-to-focus path length: $$F_{avg} = w \cdot \sqrt{\frac{\left(4 \cdot a^2 + \left(\frac{w}{2}\right)^2\right)^2}{a^2}} \cdot \frac{12 \cdot a^2 + \left(\frac{w}{2}\right)^2}{12 \cdot w \cdot \left(4 \cdot a^2 + \left(\frac{w}{2}\right)^2\right)}$$
Piping distance between assemblies (m)	Length of pipes and hoses connecting collectors in a single row, not including the length of crossover pipes.
Length of single module (m)	The length of a single collector-receiver module, equal to the collector assembly length divided by the number of modules per assembly.
Incidence angle modifier coefficients	Coefficients for a polynomial equation defining the incidence angle modifier equation.
Tracking error	Accounts for reduction in absorbed radiation error in collectors tracking caused by poor alignment of sun sensor, tracking algorithm error, errors caused by the tracker drive update rate, and twisting of the collector end at the sun sensor mounting location relative to the tracking unit end.
Geometry effects	Accounts for errors in structure geometry caused by misaligned mirrors, mirror contour distortion caused by the support structure, mirror shape errors compared to an ideal parabola, and misaligned or distorted receiver.
Mirror reflectance	The mirror reflectance input is the solar weighted specular reflectance. The solar-weighted specular reflectance is the fraction of incident solar radiation reflected into a given solid angle about the specular reflection direction.
Dirt on mirror	Accounts for reduction in absorbed radiation caused by soiling of the mirror surface.
General optical error	Accounts for reduction in absorbed radiation caused by general optical errors or other unaccounted error sources.

Table 8: Collector's parameters, SAM help page [NREL. System Advisor Model 2017.9.5]

3.7. Receivers

SAM is fitted with a library that includes, in addition to collectors, receivers of well-known brands. The characteristics and coefficients are then used for simulating the production.
The receiver type is chosen from the eight technologies presented in the library of SAM.

Figure 11: Siemens UVAC 2010 receiver [www.siemens.com, 07/2018]

The structure of the receiver is composed basically by a metal pipe contained in a vacuum within glass tube that runs through the focal line of the trough-shaped parabolic collector. Auxiliary structures allow to keep vacuum in each tube. Systems that maximize the absorbing factor of the glass and minimize thermal and optical losses are employed.

The temperature of the heat transfer fluid in each node (the red point in Figure 12) at time t is calculated from the balance between the energy absorbed by the receiver and the mass flow rate of the heat transfer fluid (HTF) through the receiver, and the specific heat of the HTF as follows. The steady state does not represent well the situation due to the thermal mass of the heat transfer fluid that causes transient effect.
Therefore, transient terms are included in the equation representing this situation.

$$T_i = \frac{\dot{q}_{abs,i}}{\dot{m}_{htf} \cdot \dot{c}_{htf,i}} + (T_{0,i} - \frac{\dot{q}_{abs,i}}{\dot{m}_{htf} \cdot \dot{c}_{htf,i}} - T_{i-1}) e^{-\frac{\dot{m}_{htf}}{m_i} \Delta t} + T_{i-1}$$

$\dot{m}_{htf}$ is the HTF mass flow rate,

$\dot{q}_{abs,i}$ is the absorbed thermal energy for the node i,

$\dot{c}_{htf,i}$ is the HTF specific heat for the node i,

$T_{0,i}$ temperature at the end of the previous timestep for the node i,

T_{i-1} is the outlet temperature of the previous node in the loop, equal to the temperature of the incoming heat thermal fluid for the node I,

m_i is the HTF mass in the node i,

Δt is the timestep duration.

This equation is applied to each node i in the loop.

To calculate the boundary conditions of this equation, it is necessary to consider both the inlet temperature of the previous node and the node temperature from the previous timestep.
The time boundary is easy to control: it is the temperature of the node at the previous timestep that is tracked from timestep to timestep.
On the other hand, when considering the loop inlet temperature, it cannot be simply considered the same temperature of the fluid that comes out of the solar field or of the storage loop.
The thermal inertia of the header has to be included, consequently, other equations for loop inlet temperature are required, as follows.

$$T_{sys,c} = (T_{sys,c,0} - T_{in})\, e^{-\frac{\dot{m}_{htf}}{\bar{V}_c \cdot \rho_c}\Delta t} + T_{in}$$

$$T_{sys,h} = (T_{sys,h,0} - T_{out})\, e^{-\frac{\dot{m}_{htf}}{\bar{V}_h \cdot \rho_h + \frac{\dot{m}c_{bal}}{c_h}}\Delta t} + T_{out}$$

$T_{sys,c}$, $T_{sys,h}$ are the cold and hot header temperature,

$T_{sys,c,0}$, $T_{sys,h,0}$ are the cold and hot header temperature from the last timestep,

$\bar{V}_c$, $\bar{V}_h$ are the volume in the cold and hot header and the runner pipe,

ρ_c , ρ_h cold and hot fluid density,

$\dot{m}c_{bal}$ is a term that represents non-HTF thermal inertia, due to pipe walls, insulation, the expansion vessel, heat exchanger mass, and other sources of thermal inertia,

T_{in}, T_{out} are the incoming and outgoing heat thermal fluid temperature,

[Michael J. Wagner et al., 2010].

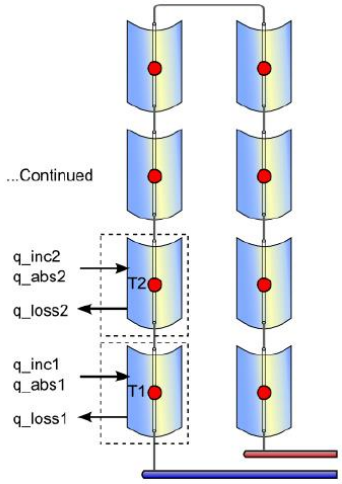

Figure 12: Nodal structure of the loop [Michael J. Wagner et al., 2010]

In the SAM model the behaviour of the receiver is simplified with a 1-dimensional structure, where the temperature changes in the radial direction only of the receiver.
The Figure 13 shows the structure underlying the model calculation.

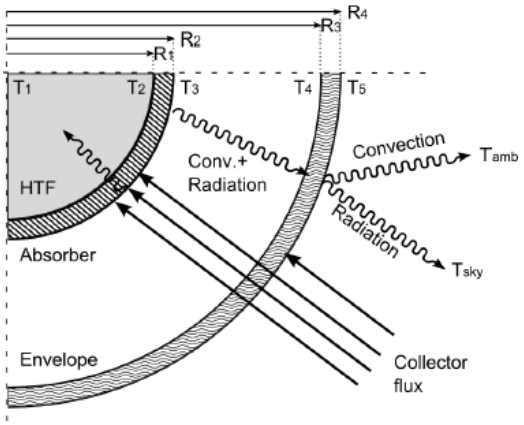

Figure 13: Heat balance for the receiving model [Michael J. Wagner et al., 2010]

Basically, zones of the receiver are separated by layers (the black curves of the Figure 13), in order to calculate the temperature distribution in the receiver, applying the thermal resistance analogy, shown in Figure 14.

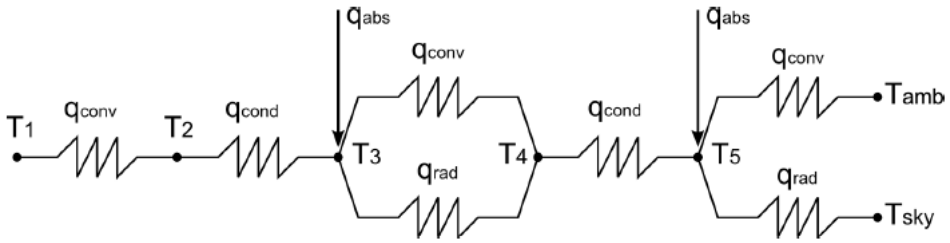

Figure 14: Thermal resistance network for the receiver model [Michael J. Wagner et al., 2010]

This analogy compares the energy balance problem to an electrical resistance network where thermal energy represents current, thermal resistance represents electrical resistance, and temperature drop is equivalent to voltage drop.
Thermal resistances are calculated considering the materials and the thermal and optical coefficients of the structure of the receiver, together with the characteristics of the fluids that flow through the inner zone and the gap between the envelope and the absorber tube of the receiver. From this simulation the total heat loss $\dot{q}_{hl}$ does result.

$$\dot{q}_{hl} = \frac{(T_3 - T_{amb})\hat{R}_{57,rad} + (T_3 - T_{sky})\hat{R}_{56,conv} - \dot{q}_{abs,env}\Omega_{\hat{R}}}{\hat{R}_{34,tot}\hat{R}_{57,rad} + \hat{R}_{34,tot}\hat{R}_{56,conv} + \Omega_{\hat{R}}}$$

Each $\hat{R}_{jk}$ value (in W/K unit) physically represents the thermal resistance of the material to let the heat go through the zone between j and k that represent the points of the network.
$\Omega_{\hat{R}}$ follows from combining resistance values:

$$\Omega_{\hat{R}} = \hat{R}_{56,conv}\hat{R}_{57,rad} + \hat{R}_{45,cond}\hat{R}_{57,rad} + \hat{R}_{45,cond}\hat{R}_{56,conv}$$

[Michael J. Wagner et al., 2010].

The receiver type, in the same way as the collectors, is chosen from the SAM library.
The program allows the users to choose different types of receivers and, for each receiver type, up to four variations can been also specified. The coefficients are presented in Figure 15, taken from the SAM library.

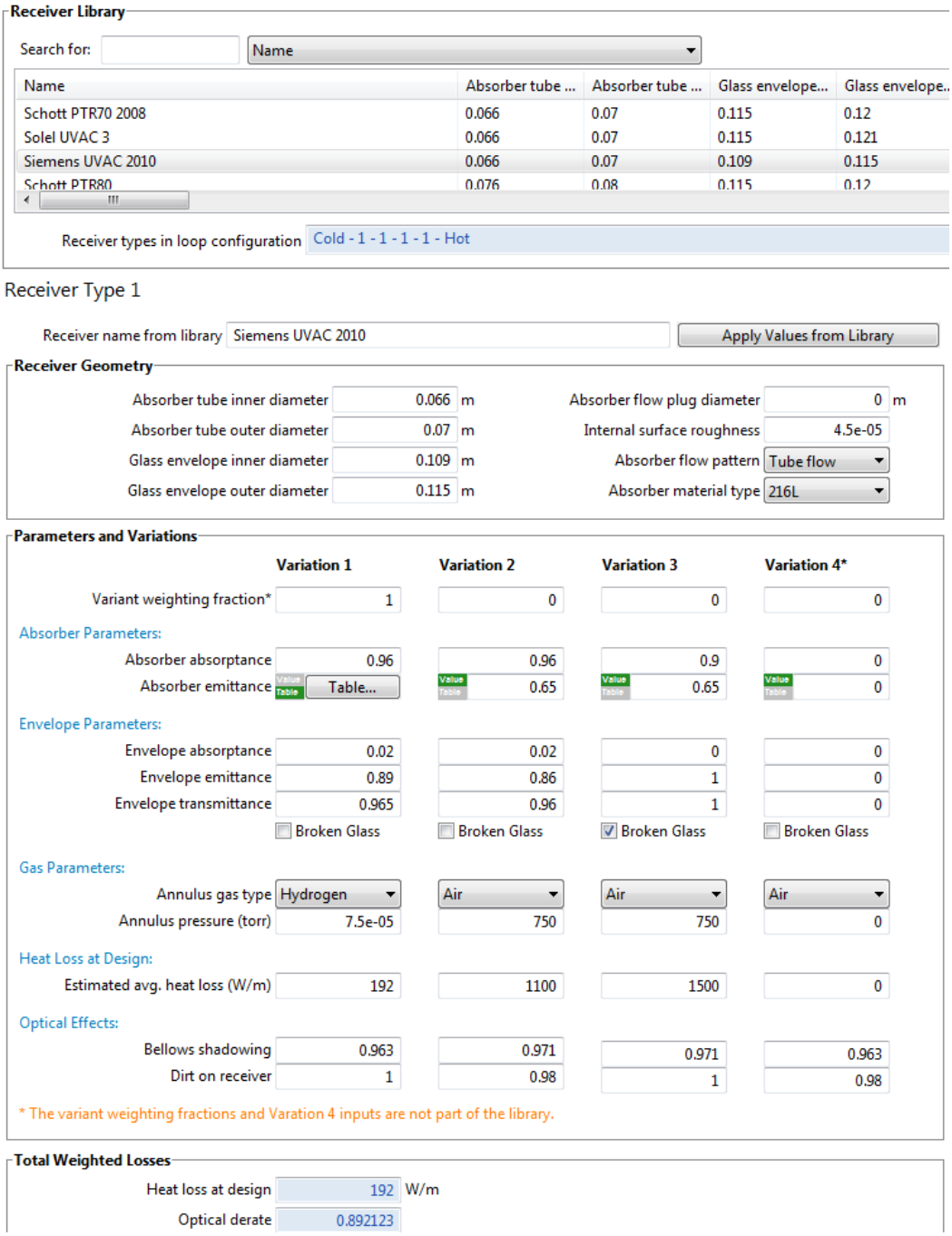

Figure 15: Characteristics of the receiver [SAM screenshot, NREL. System Advisor Model 2017.9.5]

The receivers selected are Siemens UVAC 2010 and only this kind has been chosen for the solar field, Table 9 and Table 10 show its characteristics.

Absorber tube inner diameter	Absorber tube outer diameter	Glass envelope inner diameter	Glass envelope outer diameter	Absorber flow plug diameter	Inner surface roughness	Absorber flow pattern	Absorber material type
0.066 m	0.07 m	0.109 m	0.115 m	0 m	0.000045 m	tube	216L

Absorber absorptance	Envelope absorptance	Envelope emittance	Envelope transmittance	Annulus gas type	Annulus pressure [torr]	Estimated avg heat loss [W/m]	Bellows shadowing	Dirt on receiver
0.96	0.02	0.89	0.965	hydrogen	0.000075	192	0.963	1

Table 9: Characteristics of the receiver [SAM, NREL. System Advisor Model 2017.9.5]

T [°C]	100	150	200	250	300	350	400	450
Absorber emittance	0.0726	0.0778	0.0833	0.089	0.0951	0.1015	0.1082	0.1152

Table 10: Absorber emittance of the receiver [SAM, NREL. System Advisor Model 2017.9.5]

The definition of the less clear parameters is clarified in Table 11.

Absorber absorptance	The ratio of radiation absorbed by the absorber to the radiation incident on the absorber.
Absorber emittance	The energy radiated by the absorber surface as a function of the absorber's temperature. You can either specify a table of emittance and temperature values or specify a single value that applies at all temperatures.
Envelope absorptance	The ratio of radiation absorbed by the envelope to the radiation incident on the envelope, or radiation that is neither transmitted through nor reflected from the envelope. Used to calculate the glass temperature. (Does not affect the amount of radiation that reaches the absorber tube.)
Envelope emittance	The energy radiated by the envelope surface.
Envelope transmittance	The ratio of the radiation transmitted through the glass envelope to the radiation incident on the envelope, or radiation that is neither reflected nor refracted away from the absorber tube.
Annulus gas type	Gas type present in the annulus vacuum. Choose from Hydrogen, air, or Argon.
Annulus pressure	Absolute pressure of the gas in the annulus vacuum, in torr, where 1 torr = 133.32 Pa.
Estimated avg heat loss (W/m)	An estimated value representing the total heat loss from the receiver under design conditions. SAM uses the value to calculate the total loop conversion efficiency and required solar field aperture area for the design point values on the Solar Field page. It does not use the value in simulation calculations.
Bellows shadowing	An optical derate factor accounting for the fraction of radiation lost after striking the mechanical bellows at the ends of the receiver tubes.
Dirt on receiver	An optical derate factor accounting for the fraction of radiation lost due to dirt and soiling on the receiver.

Table 11: Receiver's parameters, SAM help page [NREL. System Advisor Model 2017.9.5]

3.8. Tanks

The SAM model opens up the possibility of integrating thermal storage into the system. Its aim is to increase the stability of the solar field production reducing the fluctuation of the thermal power produced by the solar field. The production time of heat sink power is extended, and the variability in the production is reduced. The power production during the hours of peak are maximized because the exceeding quantity produced is stored and thus, it is not wasted. Both a cold and a hot tank are designed, respectively, to store the supply and return fluid.

Thermal storage capacity is conventionally expressed in SAM in terms of equivalent full-load hours of TES. The magnitude of this value indicates the number of hours that thermal storage can supply energy to operate the power cycle at its full design point output. The realized number of storage hours is usually less than the number specified, since thermal losses and unavailable storage volume are not included in the sizing calculation. The total TES thermal capacity (E_{tes}) is equal to the design-point power cycle thermal requirement (W_{des}) times the total number of desired storage hours (Δt_{tes}) divided by the design-point cycle efficiency ($\eta_{cycle,des}$), which is constant and equal to the value specified when setting the data.

$$E_{tes} = \frac{W_{des} \cdot \Delta t_{tes}}{\eta_{cycle,des}}$$

System Advisor calculates the actual volume of heat thermal fluid ($\bar{V}_{tes}$) required to achieve this energy content, using average material property values for the hot and cold tank design temperatures, where $\rho_{tes,ave}$ is the average density and $c_{tes,ave}$ is the specific capacity of the material.

$$\bar{V}_{tes} = \frac{E_{tes}}{\rho_{tes,ave} c_{tes,ave} f_{hx} (T_{sf,out} - T_{sf,in})}$$

The design temperature difference is equal to the hot solar field outlet temperature ($T_{sf,out}$) minus the cold inlet temperature ($T_{sf,in}$) times the heat exchanger derate factor (f_{hx}). This factor is equal to the ratio of the realised temperature difference on the storage side of the heat exchanger to the solar field temperature difference [Michael J. Wagner and Paul Gilman, 2011].

3.9. Simulation of a solar plant installed in Zaragoza

In this simulation, the number of hours that the storage system can supply energy at the design point is set to 6 hours and the target solar multiple is set to 2.5. This combination allows a right compromise between a feasible oversizing of the solar field (2.5 times larger than the required in design conditions) and the possibility to exploit the energy surplus.
As a matter of fact, the tank stores the energy produced that is not immediately necessary and it allows to expand the operating hours of the power cycle.
If the tank capacity rises, there is the drawback of increasing losses, when the solar multiple and thus the solar field size do not increase, because the production never reaches the maximum capacity of the tank.

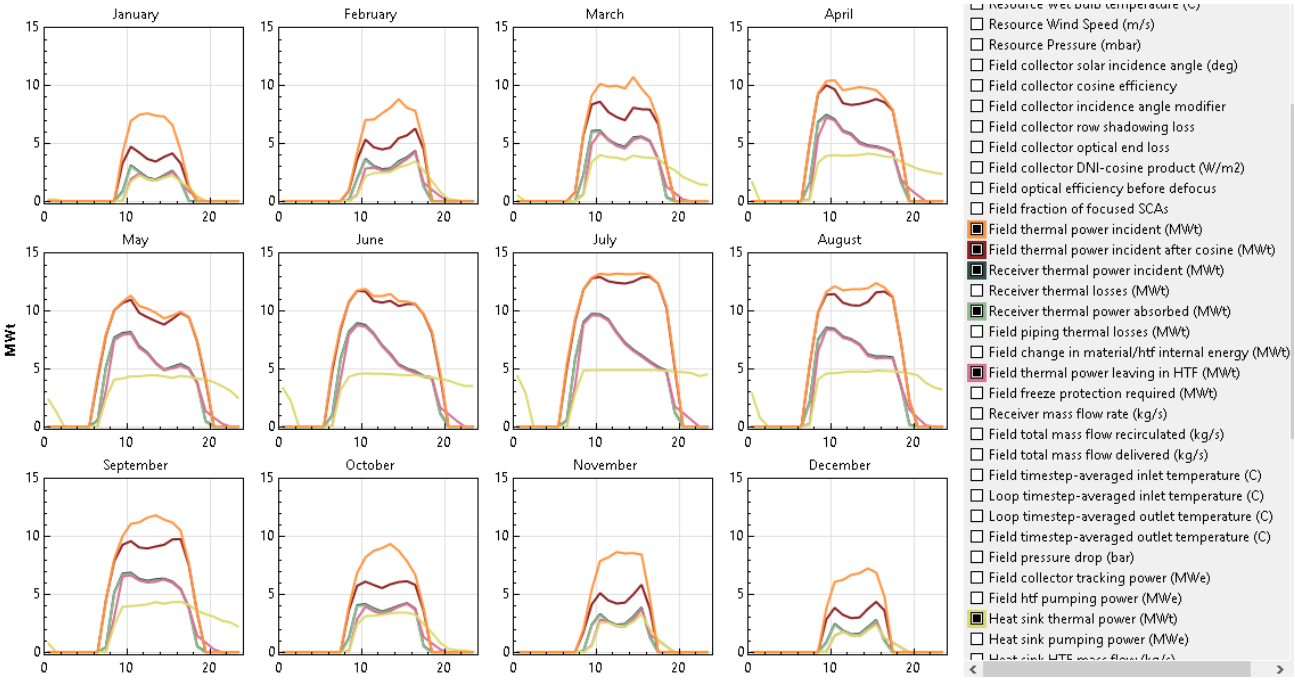

Figure 16: Monthly values of the highlighted values resulting from SAM [SAM screenshot, NREL. System Advisor Model 2017.9.5]

The graphs in Figure 16 present monthly profiles that result from the SAM calculation [SAM screenshot, NREL. System Advisor Model 2017.9.5] of the case analysed.
The representation of the values derives from the annual hourly simulation. The day taken as reference for each month is the average daily profile (hourly values) for each month of the year.
The power values highlighted represent values which are of main concern. As it can be seen from the graphs, the curve of field thermal power leaving in HTF, that is the power transported out from the receiver to the tank or directly to the heat exchanger, is correlated to the profile of field thermal power incident. The latter is obtained from the input weather data, whereas the other power values result from the simulation.
The first difference between these two values is due to the decrease of the power incident on the solar field by the cosine of the incidence angle. This angle defines the angular difference between the normal to the aperture plan of the collector and the incoming solar radiation.
Obviously, the bigger the difference, the less are the cosine angle and the optical efficiency, and as a result the less is the radiation exploitable.
This value is represented in the charts in Figure 16 as the field thermal power incident after cosine.
Analysing the other differences, it is worth to note the reduction of the receiver thermal power incident (Figure 16). The difference between these curves and the field thermal power incident after cosine lies in optical and thermal losses.
As shown in Figure 16, the receiver thermal power absorbed and the field thermal power leaving in HTF diverge slightly from the receiver thermal power incident, the second one decreasing only during the first operating hours and the last few hours before sunset. This effect could depend on the delay of the receiver to rise its temperature when heated by the solar radiation. Indeed, it can be noticed that in winter this difference between the curves is more significant than in summer. Moreover, the fact that the difference occurs the last hours before sunset, is due to the decreasing ambient temperature and consequentially due to increasing thermal losses.
In conclusion, the heat sink thermal power is limited by the set value of 5MW and the availability of the resource, which is influenced by the power leaving in HTF and the discharging of the tank.

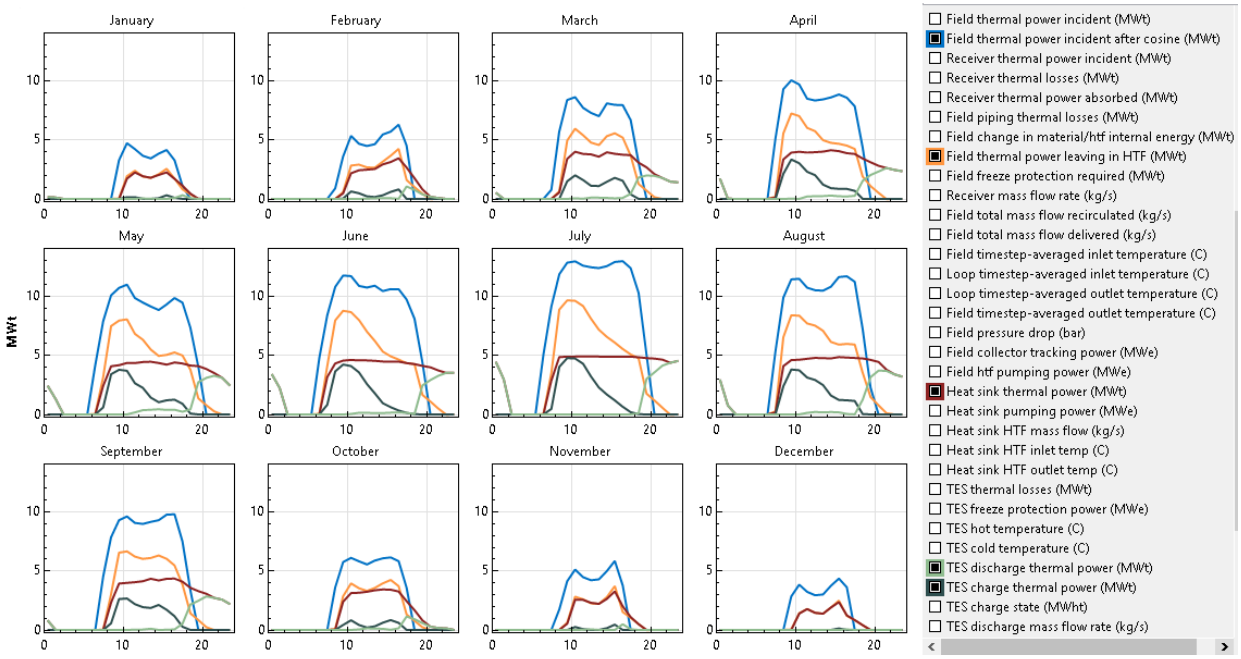

Figure 17: 6h tank capacity – 2.5 solar multiple [SAM screenshot, NREL. System Advisor Model 2017.9.5]

According to the graphs in Figure 17, the heat sink thermal power represented is different each month. In summer, it can almost reach the maximum set (5 MW) for 12 hours, thanks to the high solar radiation and intensive production; whereas in winter it can guarantee a lower value, approximately 2-3 MW, only for 6 hours.

Therefore, these power values show the available hours of production that the solar field is able to guarantee at nominal power (in summer) and at a maximum seasonal reduced value (in winter). It is the aim of this project to exploit the solar field with the maximum efficiency and feasibility, thus it is the solar field itself that imposes the operating hours of the system depending on the solar radiation availability.

This choice results in a better exploitation of the solar field and it assures that the solar source has the main role amongst the sources employed in the system for producing energy.

3.10. Parameters influencing the production

Hereafter, a parametric analysis is conduced to show how the solar field production responds to the change of the tank size and to the oversizing of the reflective surface of the solar field.

3.10.1. Tank size

Several simulations were conducted varying the number of hours during which the storage system can supply energy when fully charged.

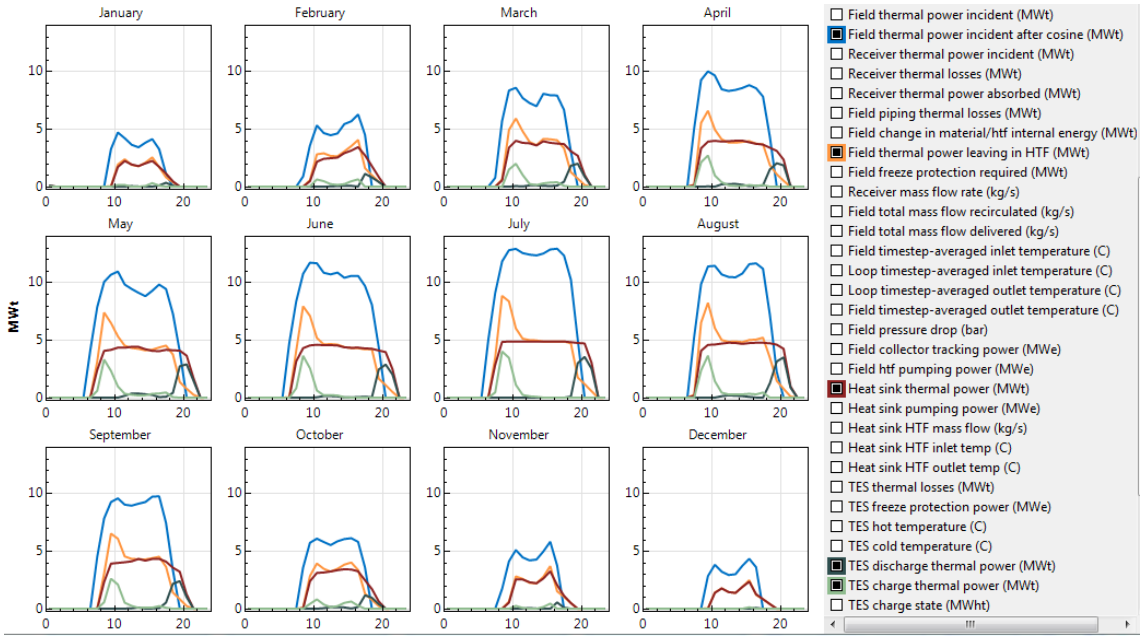

Figure 18: 2h tank capacity – 2.5 solar multiple [SAM screenshot, NREL. System Advisor Model 2017.9.5]

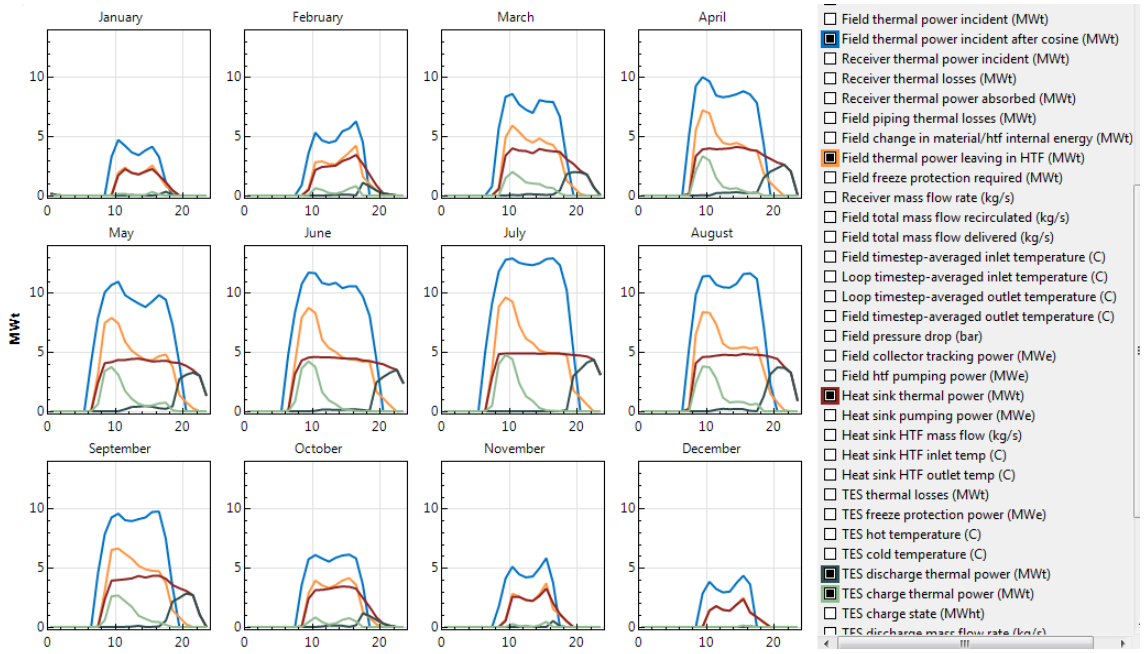

Figure 19: 4h tank capacity – 2.5 solar multiple [SAM screenshot, NREL. System Advisor Model 2017.9.5]

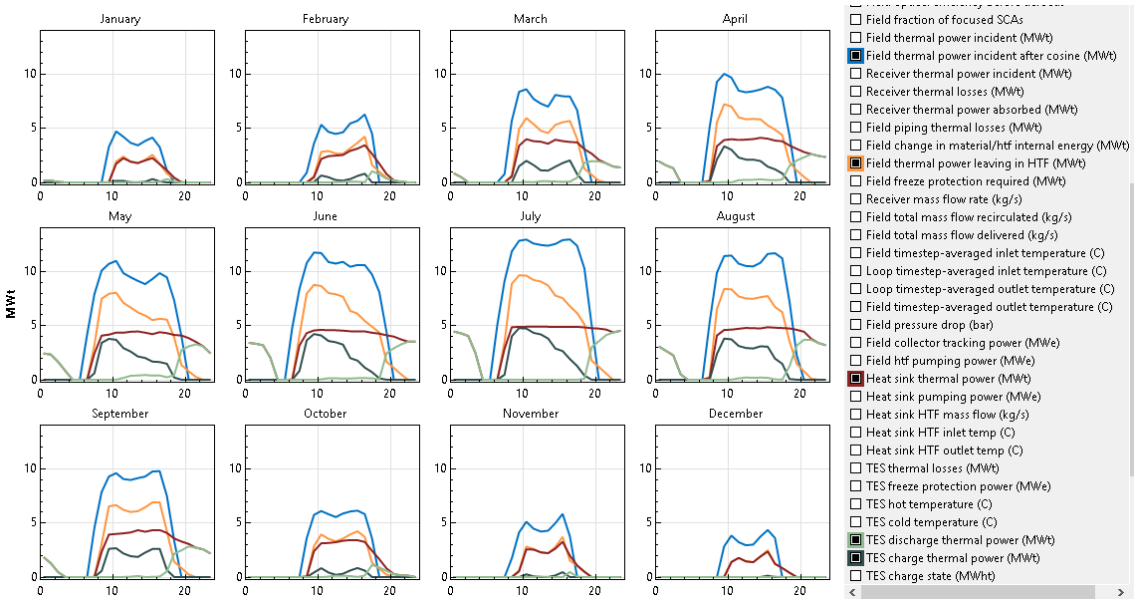

Figure 20: 8h tank capacity - 25 solar multiple [SAM screenshot, NREL. System Advisor Model 2017.9.5]

	2h tank	**4h tank**	**6h tank**	**8 h tank**
Tank diameter [m]	3.9	5.6	6.8	7.9
Storage tank volume [m^3]	184	367	551	734
TES thermal losses [MWh-t]	110.083	162.331	203.917	239.770

Table 12: Tank characteristics with changing capacity [NREL. System Advisor Model 2017.9.5]

Table 12 compares the results of the simulations between models with different capacity tank values and fixed solar multiple equal to 2.5. As it can be seen, increasing the capacity of the tank provokes the increase of thermal losses.

Besides, comparing the charts in Figures 18, 19 and 20 there is a difference between the curves that represent in each figure the field thermal power leaving in HTF, and there is a noticeable difference between the curves of the TES charge thermal power as well. This effect is due to the different exploitation of the energy produced by the solar field. The field thermal power incident after cosine does not change with the tank capacity, because it does not lead to a direct change in the solar field. On the other hand, when rising the tank capacity, more energy can be accumulated in the tank during periods of power production exceeding the nominal value. Thus, when the instant energy produced is not able anymore to cover the demand, the tank discharges the hot fluid stored to reach the design value as long as the remaining charge in the tank is available. Obviously, the availability of the stored hot fluid increases when the tank capacity increases.

The rise of the values in the system with 8 hours of "capacity" is due to the opportunity to use more advantageously the solar irradiation during the time of power surplus.

Drawbacks that appear when rising this parameter are increasing thermal losses and greater investment.

3.10.2. Target solar multiple

This parameter represents the design ratio of the target receiver thermal power and heat sink power. As mentioned before, this value can be used to oversize the receiver surface.

Herein a comparison between solar fields designed using different values of this parameter are presented.

Changing both the tank capacity and the target solar multiple affects the annual net energy. In order to clearly understand how it works and the interaction between the two parameters, the graph in Figure 21 is presented and Table 13 shows the results from SAM using different values of the parameters.

Figure 21 and Table 13 compare the system behaviour varying both the solar multiple and the capacity of the tank.

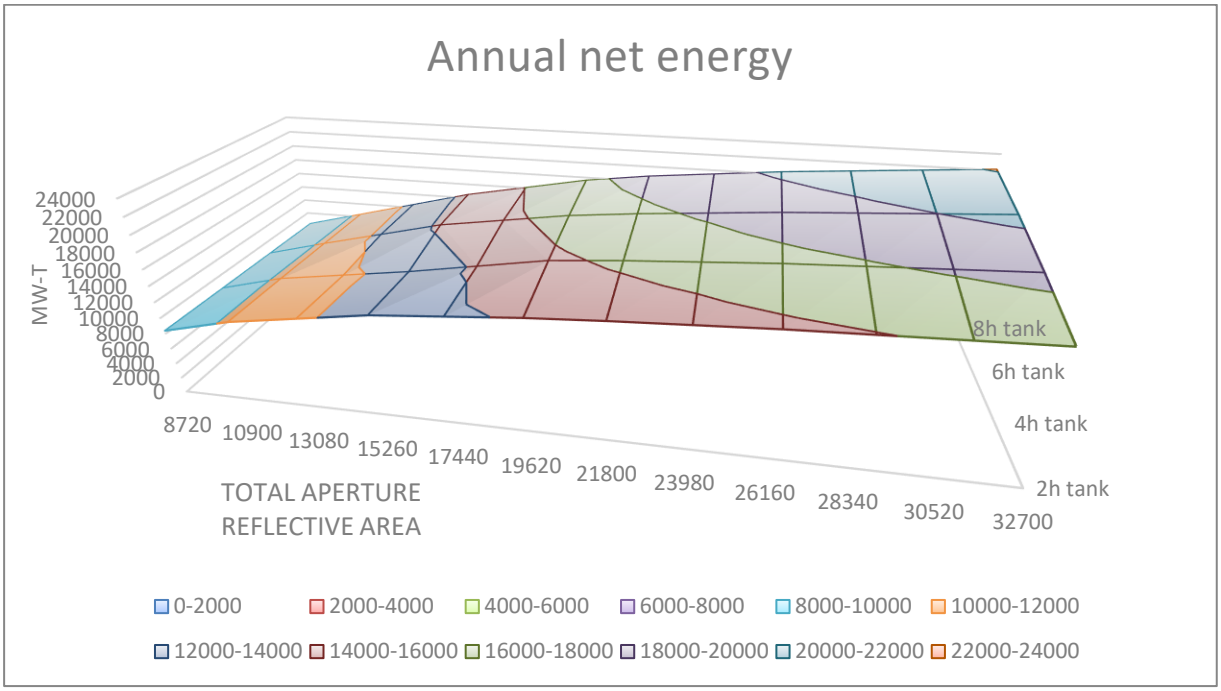

Figure 21: Annual net energy when changing solar multiple and size of thermal storage

	Solar multiple							
	1	**1.5**	**2**	**2.5**	**3**	**3.5**	**4.5**	
Actual number of loops	4	5	7	9	10	12	15	
Total aperture reflective area [m^2]	8720	10900	15260	19620	21800	26160	32700	
Annual net energy [MWh-t]	8351.9	10344.6	12893.5	14285.8	14800.4	15638.9	16529.5	
Annual gross energy [MWh-t]	8410.8	10383.1	12917.6	14299.0	14810.8	15647.0	16536.4	**2h tank**
Annual electricity load [MWh-e]	95.3	88.0	93.1	92.4	95.6	105.6	113.6	
Annual net energy [MWh-t]	8323.5	10399.7	12793.7	15634.6	16335.6	17428.7	18604.2	
Annual gross energy [MWh-t]	8408.0	10452.4	13825.4	15650.5	16347.6	17437.3	18610.9	**4h tank**
Annual electricity load [MWh-e]	120.0	102.4	109.1	107.5	111.1	122.1	131.7	
Annual net energy [MWh-t]	8302.0	10376.5	14286.5	16762.5	17588.9	18962.4	20493.7	
Annual gross energy [MWh-t]	8407.3	10440.1	14323.7	16780.7	17602.3	18971.2	20500.4	**6h tank**
Annual electricity load [MWh-e]	139.8	112.9	119.4	120.0	123.8	136.2	147.8	
Annual net energy [MWh-t]	8284.0	10353.9	14481.6	17599.9	18679.0	20275.0	22107.0	
Annual gross energy [MWh-t]	8407.5	10426.7	14524.1	17620.2	18693.7	20284.1	22113.5	**8h tank**
Annual electricity load [MWh-e]	157.3	121.7	126.5	129.6	134.9	148.2	161.8	

Table 13: Different solar field results when changing solar multiple and size of thermal storage [NREL. System Advisor Model 2017.9.5]

As Figure 21 and Table 13 show, the result of the analysis is that by setting a solar multiple of 1.5 or 1, the annual net energy is higher when using a smaller tank rather than an 8h one. This is due to the fact that the benefit of a bigger tank is not exploitable without oversizing or with a slight oversizing of the collector field. Indeed, a bigger tank leads to a bigger amount of energy losses and it is not fully exploitable. The annual energy produced significantly changes increasing the value of the solar multiple to 2.5. In fact, it grows almost proportionally with the increase of the solar multiple because the aperture area of the collectors and thus the solar field dimension rise.
On the other hand, changing the dimension of the tank for fixed low value of the solar multiple, does not significantly affect the outcome because the system is designed so as to never exceed the limit (with the solar multiple equal to 1) or to rarely exceed the nominal value (with the solar multiple equal to 1.5). This implies that the tank is seldom employed, because no exceeding energy must be stored, causing no improvement in increasing its capacity. As can be seen from Table 13, when the value of the solar multiple is 3.5, only in the case of installing a bigger tank the oversizing of the solar field appears worthwhile. Simulating the system, increasing the solar multiple from 2.5 to 3 results that it does not imply an equally proportional rise in the annual net energy. The ratio between the annual net energy values resulting from the simulation with the parameter set as 3 and 2.5 is less than the ratio between these parameters as well as between the total aperture reflective area. The same result occurs between 3.5 and 3. For each variation of the tank capacity, the effect is the same varying the parameter using these values. This suggests that it is not viable to rise the solar multiple over 2.5. A similar analysis is conducted to determinate if it is more convenient to design the field setting the value as 2.5 or less. Using this analytical approach, it results that the best fit is 2.5. When analysing in the same way the parameter of the tank capacity, it results that the best improvement in the annual energy production of the system is obtainable rising the capacity up to 6h. Therefore, the analysis of the field proceeds with the design parameters of 6 hours that the storage system can supply energy and with the target solar multiple set as 2.5.

MWt	02 am	03 am	04 am	05 am	06 am	07 am	08 am	09 am	10 am	11 am	12 pm	01 pm	02 pm	03 pm	04 pm	05 pm	06 pm	07 pm	08 pm	09 pm	10 pm	11 pm	12 am	01 am
Jan	0	0	0	0	0	0	0	0	1.71	2.23	1.89	1.78	2.02	2.24	1.66	1.11	0.44	0.01	0	0	0	0	0	0
Feb	0	0	0	0	0	0	0	0.47	2.16	2.41	2.46	2.52	2.9	3.11	3.43	2.63	1.71	0.8	0.18	0.07	0	0	0	0
Mar	0	0	0	0	0	0	0.54	3.38	3.98	3.8	3.75	3.56	3.93	3.8	3.72	3.69	3.06	2.66	2.08	1.76	1.45	1.35	0.52	0
Apr	0	0	0	0	0	0.11	3.33	3.9	3.98	3.91	3.94	3.99	4.1	4.03	3.85	3.79	3.4	3.09	2.79	2.61	2.44	2.33	1.72	0.02
May	0	0	0	0	0	2.41	4.06	4.15	4.34	4.33	4.42	4.44	4.33	4.2	4.38	4.29	4.12	4.07	3.83	3.49	3.08	2.58	2.42	1.3
Jun	0	0	0	0	0	3.15	4.29	4.54	4.59	4.55	4.56	4.52	4.46	4.44	4.45	4.33	4.24	4.09	3.97	3.71	3.5	3.5	3.4	2.22
Jul	0	0	0	0	0	2.86	4.83	4.87	4.87	4.87	4.87	4.88	4.86	4.87	4.87	4.87	4.82	4.75	4.71	4.62	4.36	4.36	4.44	2.96
Aug	0	0	0	0	0	0.16	4.07	4.58	4.61	4.69	4.77	4.75	4.72	4.84	4.79	4.76	4.72	4.6	4.42	3.77	3.38	3.18	2.94	0.76
Sep	0	0	0	0	0	0	2.31	3.91	3.97	4.03	4.11	4.32	4.17	4.31	4.33	4.07	3.55	3.27	3.05	2.7	2.55	2.17	0.81	0
Oct	0	0	0	0	0	0	0.03	2.38	3.11	3.13	3.21	3.34	3.41	3.39	3.24	2.42	1.66	0.81	0.27	0.16	0.13	0	0	0
Nov	0	0	0	0	0	0	0	0.52	2.55	2.53	2.28	2.2	2.62	3.25	1.95	1.06	0.49	0	0	0	0	0	0	0
Dec	0	0	0	0	0	0	0	0	1.37	1.76	1.44	1.37	1.89	2.34	1.2	0.83	0.4	0	0	0	0	0	0	0

Table 14: Mean hourly heat sink thermal power for each month (MWt) [NREL. System Advisor Model 2017.9.5]

A minimum value of 0.5 MW of heat sink thermal power obtainable from the solar field is considered as a limit to control the operating time of the system.
In order to illustrate clearly the operating model of the system, Figure 22 represents the mean hourly value of heat sink thermal power in each month, the values below the limit are considered as a power of zero. To obtain a better representation of the problem, the data of 12 am and 1 am are moved in the graphs in Figure 22 and 23 at the end of the day.

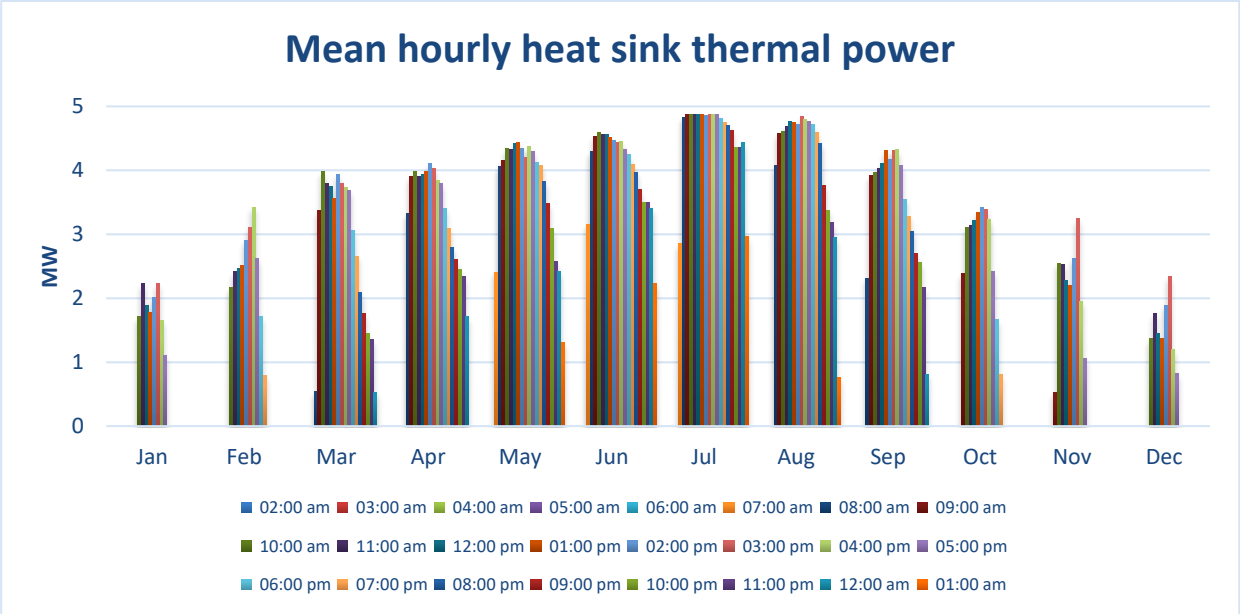

Figure 22: Mean hourly heat sink thermal power for each month

The graphs in Figure 23 (from 23a to 23l) represent the average daily profile of the power production of the solar field for each month of the year. Table 15, as a resume of the graphs later presented, shows the operating hours of the solar field.

	Jan	Feb	Mar	Apr	May	Jun	Jul	Aug	Sep	Oct	Nov	Dec
Operating hours	8	10	17	17	19	19	19	18	17	11	9	8

Table 15: Daily operating hours of the plant for each month

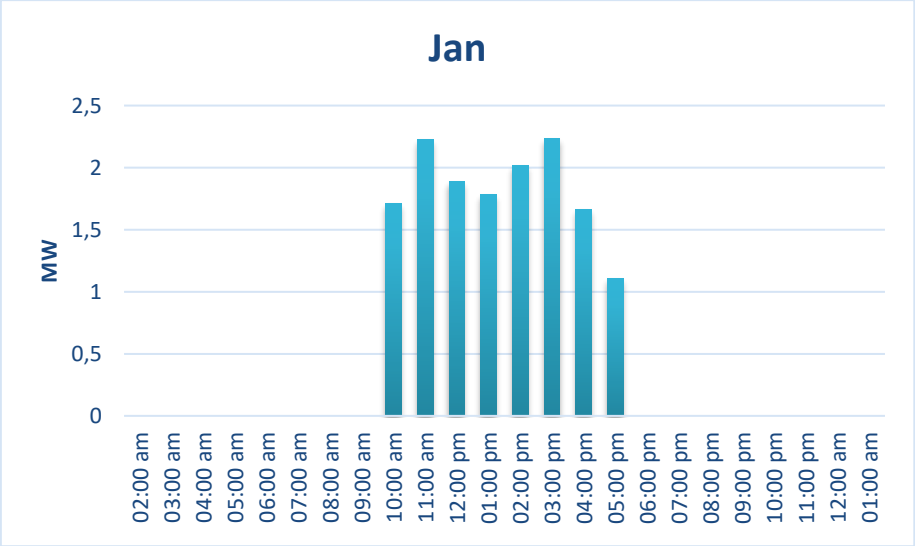

Figure 23a: Mean hourly heat sink thermal power, January

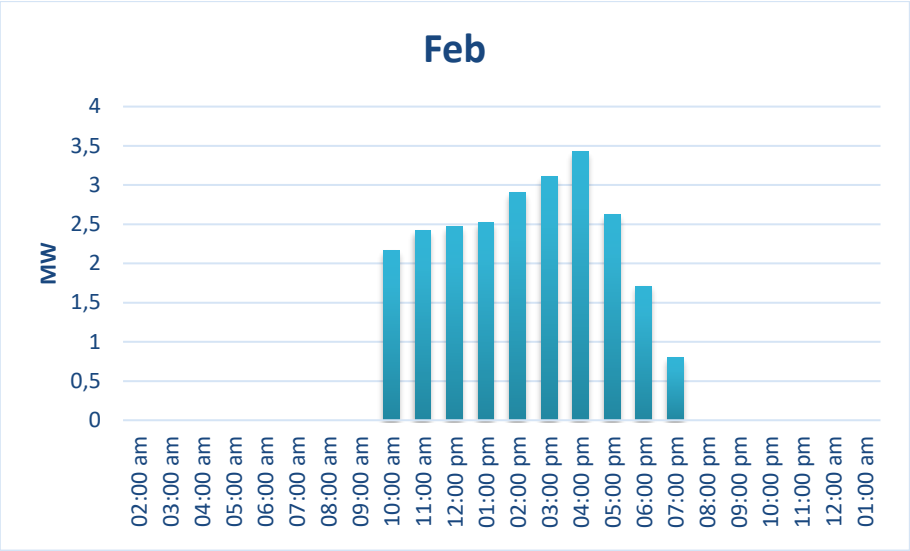

Figure 23b: Mean hourly heat sink thermal power, February

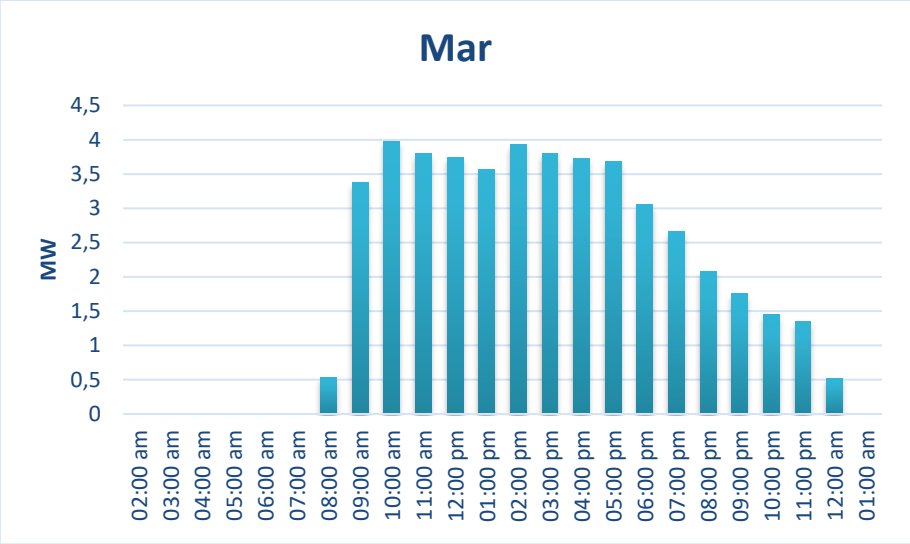

Figure 23c: Mean hourly heat sink thermal power, March

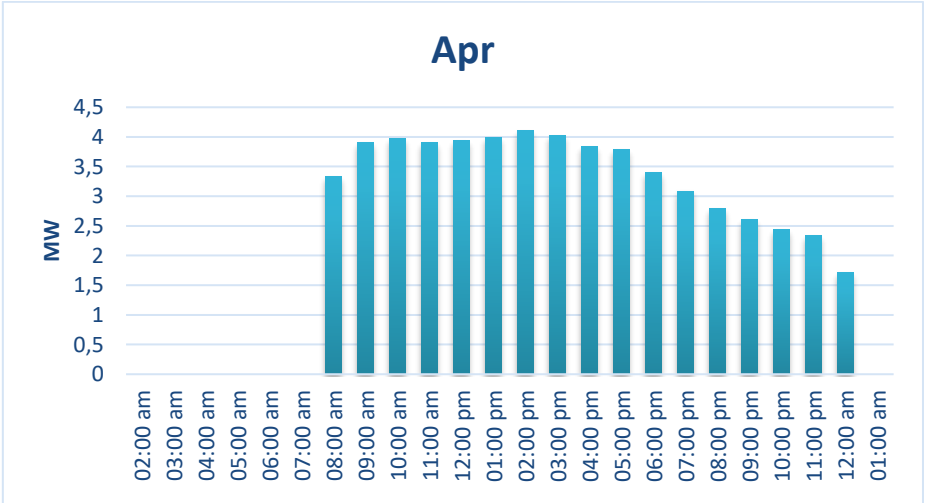

Figure 23d: Mean hourly heat sink thermal power, April

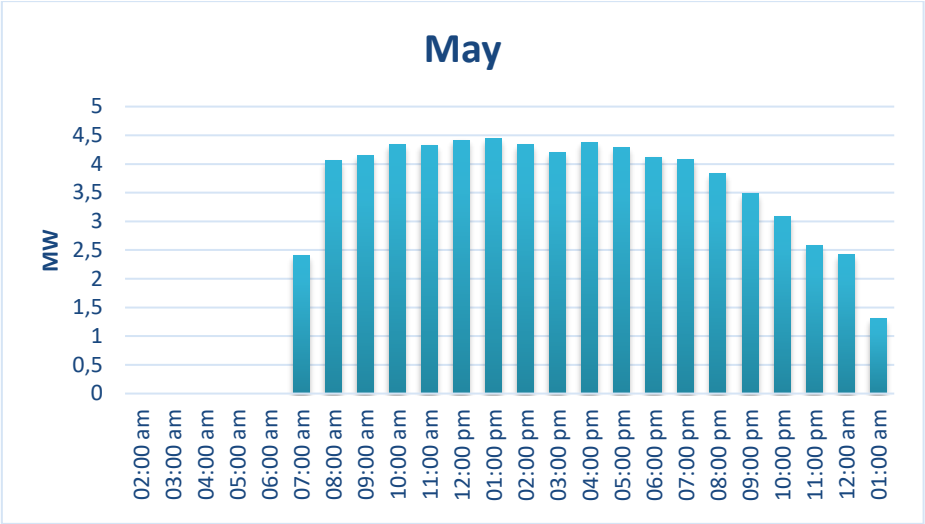

Figure 23e: Mean hourly heat sink thermal power, May

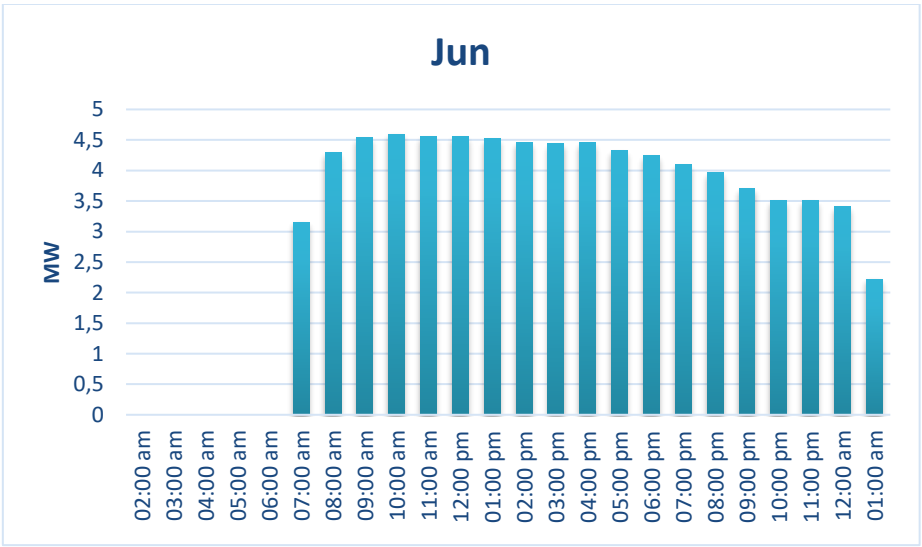

Figure 23f: Mean hourly heat sink thermal power, June

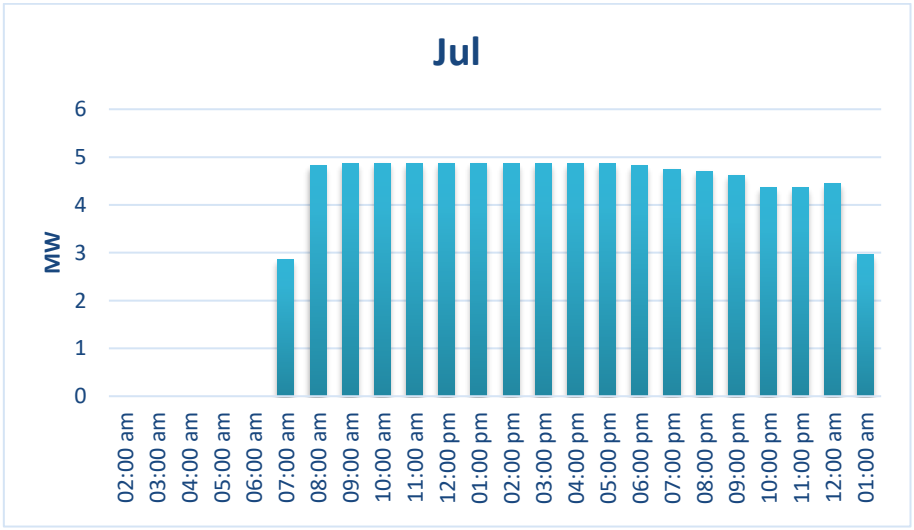

Figure 23g: Mean hourly heat sink thermal power, July

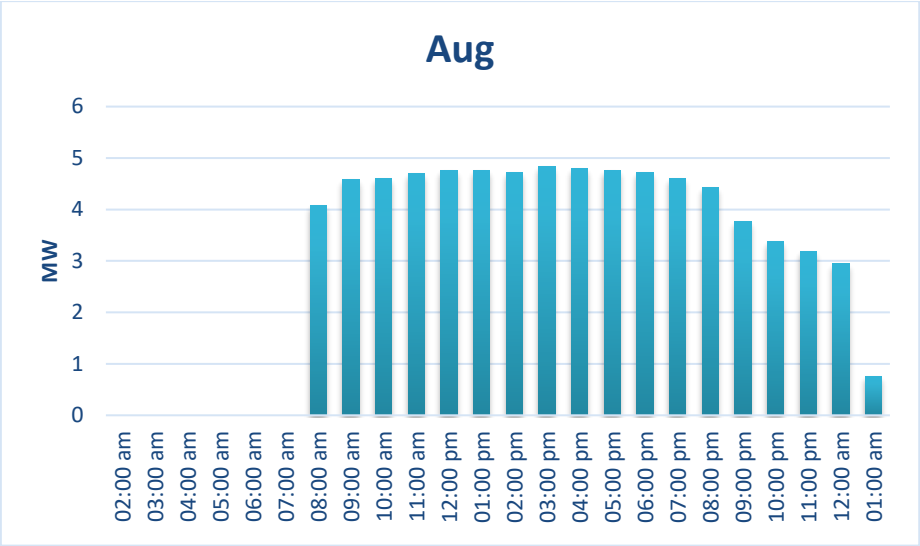

Figure 23h: Mean hourly heat sink thermal power, August

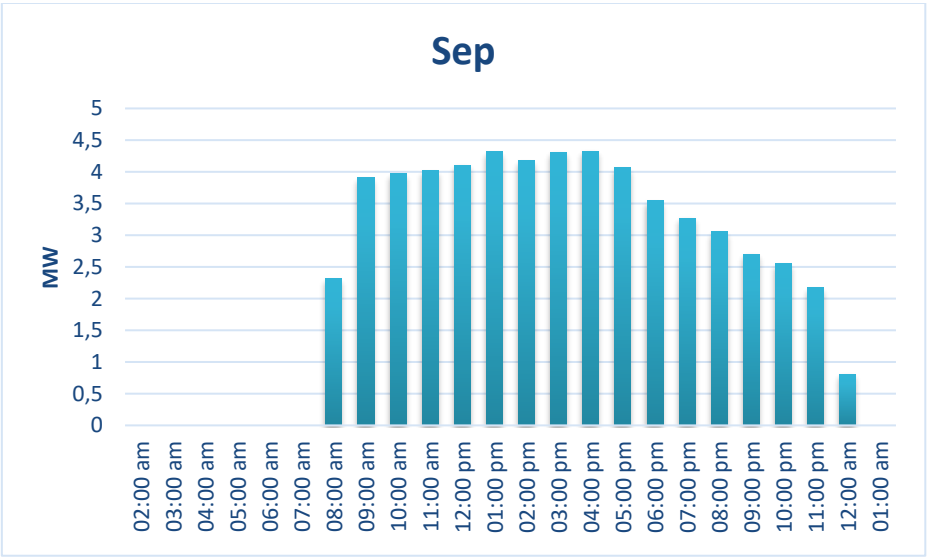

Figure 23i: Mean hourly heat sink thermal power, September

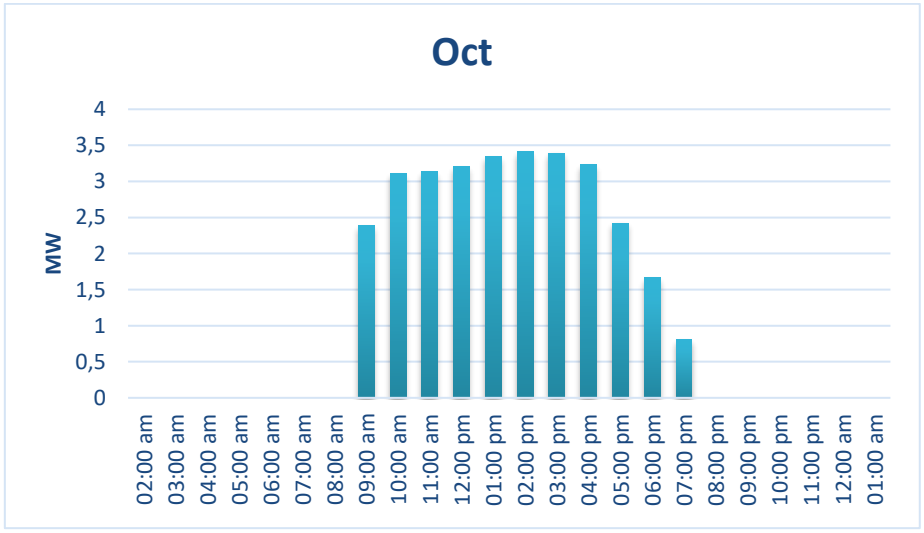

Figure 23j: Mean hourly heat sink thermal power, October

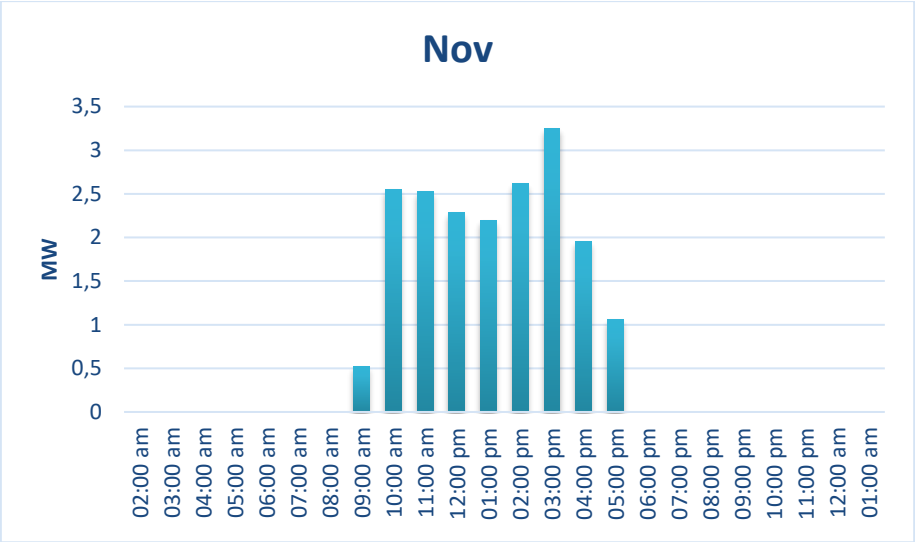

Figure 23k: Mean hourly heat sink thermal power, November

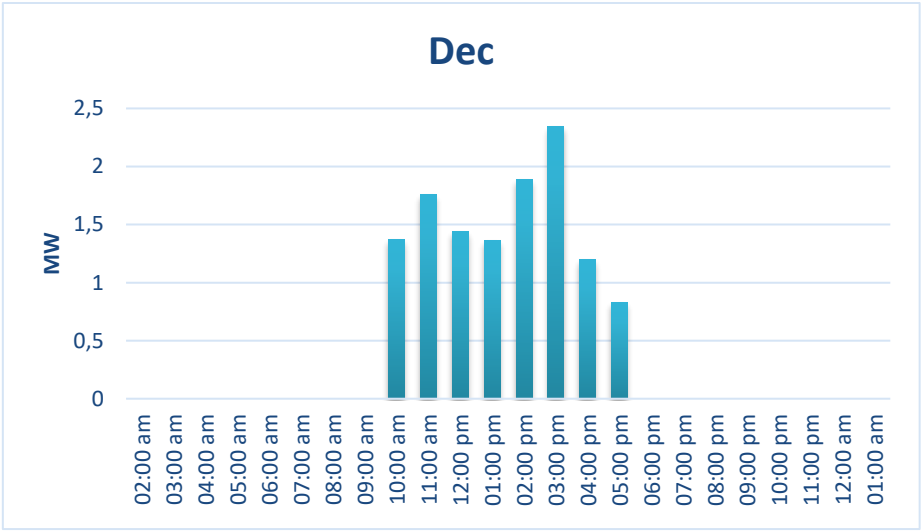

Figure 23l: Mean hourly heat sink thermal power, December

4. Biomass boiler

In order to increase the power from renewable energy of the system, as well as to allow a more stable operation of the power ORC, a biomass boiler supports the solar field. During conditions of cloudiness or in winter or whenever the solar radiation is not able to guarantee the required power of 5 MW, the biomass boiler supplements the solar field production to reach that target.

SAM performs the simulation varying both the inlet temperature and the mass flow of the HTF, trying to adjust the heat sink thermal power to an almost constant value.
When it results impossible, a biomass boiler provides the necessary power to reach the nominal value of the ORC thermal input power. The boiler is installed in parallel with the solar system as shown in Figure 6. The design power of the boiler is 5 MW so as to cover the demand of the ORC and its use is only considered as support of the solar field during the operating hours of the collectors.

Therefore, the mean energy that the boiler should provide to the thermal fluid can be estimated, on average, from the charts in Figure 22 that shows how the collectors exploit the solar source.
The graph in Figure 24 and Table 16 show the mean hourly values of power of the boiler in each month during a year. To obtain a better representation of the problem the data of 12 am and 1 am are moved in Figure 24 at the end of each day.

	JAN	FEB	MAR	APR	MAY	JUN	JUL	AUG	SEP	OCT	NOV	DEC
02:00 AM	0	0	0	0	0	0	0	0	0	0	0	0
03:00 AM	0	0	0	0	0	0	0	0	0	0	0	0
04:00 AM	0	0	0	0	0	0	0	0	0	0	0	0
05:00 AM	0	0	0	0	0	0	0	0	0	0	0	0
06:00 AM	0	0	0	0	0	0	0	0	0	0	0	0
07:00 AM	0	0	0	0	2.59	1.85	2.14	0	0	0	0	0
08:00 AM	0	0	4.46	1.67	0.94	0.71	0.17	0.93	2.69	0	0	0
09:00 AM	0	0	1.62	1.10	0.85	0.46	0.13	0.42	1.09	2.62	4.48	0
10:00 AM	3.29	2.84	1.02	1.02	0.66	0.41	0.13	0.39	1.03	1.89	2.45	3.63
11:00 AM	2.77	2.59	1.20	1.09	0.67	0.45	0.13	0.31	0.97	1.87	2.47	3.24
12:00 PM	3.11	2.54	1.25	1.06	0.58	0.44	0.13	0.23	0.89	1.79	2.72	3.56
01:00 PM	3.22	2.48	1.44	1.01	0.56	0.48	0.12	0.25	0.68	1.66	2.80	3.63
02:00 PM	2.98	2.10	1.07	0.90	0.67	0.54	0.14	0.28	0.83	1.59	2.38	3.11
03:00 PM	2.76	1.89	1.20	0.97	0.80	0.56	0.13	0.16	0.69	1.61	1.75	2.66
04:00 PM	3.34	1.57	1.28	1.15	0.62	0.55	0.13	0.21	0.67	1.76	3.05	3.80
05:00 PM	3.89	2.37	1.31	1.21	0.71	0.67	0.13	0.24	0.93	2.58	3.94	4.17
06:00 PM	0	3.29	1.94	1.60	0.88	0.76	0.18	0.28	1.45	3.34	0	0
07:00 PM	0	4.20	2.34	1.91	0.93	0.91	0.25	0.40	1.73	4.19	0	0
08:00 PM	0	0	2.92	2.21	1.17	1.03	0.29	0.58	1.95	0	0	0
09:00 PM	0	0	3.24	2.39	1.51	1.29	0.38	1.23	2.30	0	0	0
10:00 PM	0	0	3.55	2.56	1.92	1.50	0.64	1.62	2.45	0	0	0
11:00 PM	0	0	3.65	2.67	2.42	1.50	0.64	1.82	2.83	0	0	0
12:00 AM	0	0	4.48	3.28	2.58	1.60	0.56	2.06	4.19	0	0	0
01:00 AM	0	0	0	0	3.70	2.78	2.04	4.24	0	0	0	0

Table 16: Mean hourly values of power of the boiler in each month during a year

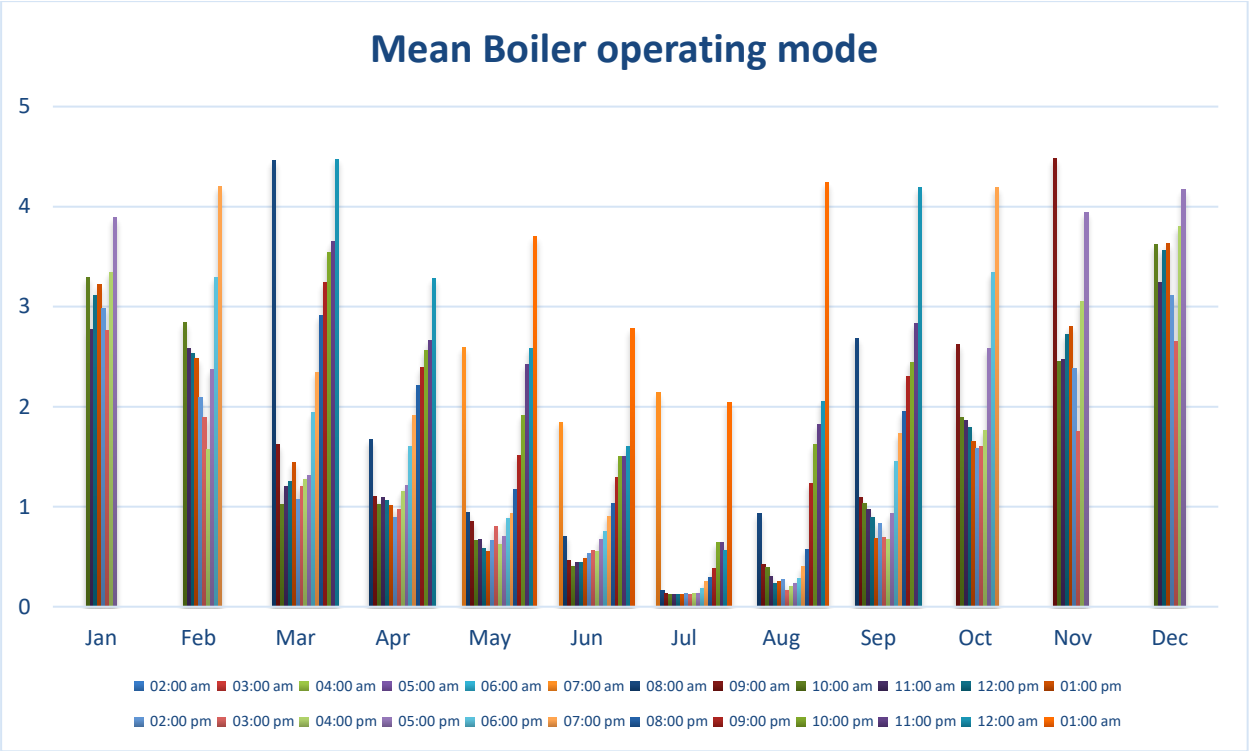

Figure 24 Mean hourly biomass boiler thermal power for each month

The monthly and the total amount of energy provided by the solar field and the boiler along a year are presented in Table 17.

Total energy [MWh]	**Jan**	**Feb**	**Mar**	**Apr**	**May**	**Jun**	**Jul**	**Aug**	**Sep**	**Oct**	**Nov**	**Dec**	**tot**
Solar field Es	453	676	1458	1716	2178	2296	2683	2305	1729	933	569	378	**17374**
Boiler Eb	787	724	1177	834	767	554	262	485	821	772	781	862	**8826**
F_{sol}	37%	48%	55%	67%	74%	81%	91%	83%	68%	55%	42%	30%	**66%**
F_{int}	63%	52%	45%	33%	26%	19%	9%	17%	32%	45%	58%	70%	**34%**

Table 17: Thermal energy production and percentages of solar and biomass production

The solar factor and the integration factor with another source are calculated from the relations:

$$E_{tot} = E_b + E_{sol}$$

$$F_{sol} = \frac{E_{sol}}{E_{tot}} \cdot 100\%$$

$$F_{int} = 1 - \frac{E_{sol}}{E_{tot}} \cdot 100\%$$

Where E_s is the net energy produced by the solar resource and E_{tot} is the total production of the plant.

F_{sol} is the solar factor,

F_{int} is the integration factor of the biomass boiler.

In each month, to calculate the factors it is considered the energy produced by the solar field and by the boiler.

4.1. Biomass technology

Biomass material is defined as carbon-based organic matter available on a renewable basis. Considering the technology, the boiler is similar to the traditional one that uses fossil fuels as energy source, whereas they differ in the fuel. A boiler simply burns the fuel in a chamber, where it has the possibility to transmit the heat released by the combustion to a thermal fluid that rises its temperature, exploiting the calorific value of the energy resource. Common forms of biomass include forest and mill residue, agricultural crops and waste, wood and wood waste, fast-growing trees and plants. Considering the source, the emission of CO_2 during the combustion, does not rise the overall content of carbon dioxide in the atmosphere, because the amount released during the combustion of biomass materials was previously absorbed by the trees or plant products. Thus, biomass fuels are considered carbon free and renewable [www.thegreenage.co.uk, 08/2018].

The boiler considered is a moving grate furnace with a nominal power of 5.9 MWt fed with woodchips (70%), and a small share of wood from sawmills (30%). The feedstock is pre-treated in the drying section till the water content is in the range 15-25% on a wet basis. Woodchips are loaded into the boiler by means of racks moved by hydraulic cylinders that operate at regular time intervals. The output ash from the combustion is collected and properly disposed [Dario Prando et al., 2015]. The characteristics are described in Table 18.

	Power load (%)	
	79	94
Thermal power (kWt)	4160	4709
Input power (kWt)	6300	7143
Biomass consumption (kg/h)	1454	1703
Biomass water content on wet basis (%)	14.4	15.6
Biomass LHV (MJ/kg)	15.6	15.1
Ash production (on dry basis) (kg/h)	11.2	11.5
Thermal efficiency (-)	0.662	0.660

Table 18: Biomass boiler properties [Dario Prando et al., 2015]

The biomass price can vary between 10 and 25 €/MWh [A. Guercio, R. Bini, 2017]. Therefore, based on data shown in Table 18, LHV equal to 15.5 MJ/kg, efficiency equal to 0.66 and 15 €/MWh have been considered in order to continue the analysis [A. Guercio, R. Bini, 2017]. In Table 19 the values of energy produced by the biomass boiler, the biomass consumed and the cost for the raw material are shown.

	Jan	**Feb**	**Mar**	**Apr**	**May**	**Jun**	**Jul**	**Aug**	**Sep**	**Oct**	**Nov**	**Dec**	**Tot annual**
Boiler [MWh]	787	724	1177	834	767	554	262	485	821	772	781	862	**8826**
Biomass [ton]	277	255	414	293	270	195	92	171	289	272	275	303	**3106**
Price [€]	11805	10860	17655	12510	11505	8310	3930	7275	12315	11580	11715	12930	**132390**

Table 19: Energy production of the biomass boiler and cost

5. Organic Rankine Cycle

The ORC is a power cycle that employs an organic fluid as working fluid operating a Rankine cycle. Its purpose is to obtain mechanical energy from a heat source.

When the enthalpy level of the heat source, as well as the temperature, is low the Organic Rankine Cycle is very useful due to its potential industrial applications to medium temperature processes [Mónica Borunda et al., 2015].

Compared to steam at the same pressure levels, organic fluids are characterized by lower evaporation and condensation temperatures. This difference has further substantial implications. The main differences between the traditional steam technology and the ORC are [Sylvain Quoilin et al., 2013]:

- The shape of the organic fluids saturation curve makes the expansion transformation occurs only in the vapour phase. This avoids that liquid-drops fall on the turbine's blades, therefore reducing the risk of corrosion. It is not necessary in a ORC cycle to superheat the fluid after the evaporation process.
- The possibility to choose the most appropriate working fluid depending on the environment and on the available conditions of the heat source.
- The temperature of the source could be at much lower temperature thanks to the lower boiling point of the organic fluid selected, thus the solar field provides energy at a right thermal level.
- In an ORC the high-pressure level generally does not exceed 30 bar, whereas in a steam cycle normally reaches pressures of about 60-70bar. The advantage in lowering the pressure is reducing thermal stress and thus the complexity and the cost of the boiler or the heat exchanger.
- The efficiency of ORCs does not reach efficiency values of the steam Rankine cycles, but complexity of the first ones is typically lower.
- Higher operation flexibility and better performance in different conditions than the nominal values allow electricity production at reduced inputs.
- In steam cycles, turbine with a high number of stages are used, whereas in ORCs the reduced enthalpy-drop and the lower pressure ratio over the turbine allow to employ single or two-stage turbines or other expanders, such as scroll or screw [S. Quoilin et al., 2013]. Lower costs mean a crucial advantage.

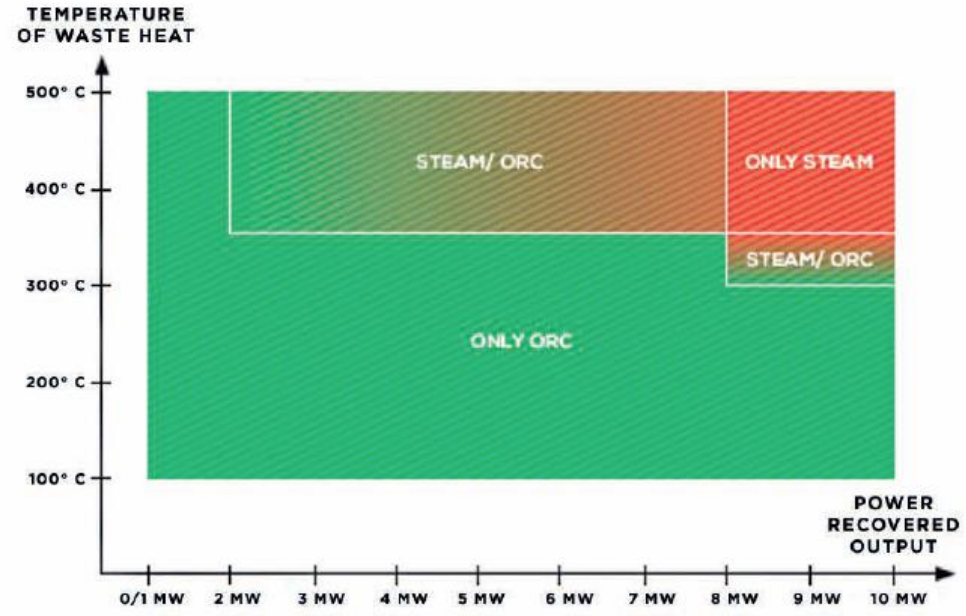

Figure 25: Temperature and power range of application of ORC technologies [www.exergy-orc.com, 07/2018]

5.1. Equipment

In this paragraph the information is gathered from the work of M. Astolfi [2016].

Any ORC cycle mainly consists of four classes of components: the heat exchangers (elements a., c., d., e. and f. in Figure 27), the expander (element g. in Figure 27), the pump (element b. in Figure 27), and the generator unit (element i. in Figure 27). Besides them, some other components are usually required for a safe and stable operation of the system and for its control.

5.1.1. Heat exchangers

These components are used in several points of the system: for connecting the solar field loop with the power cycle and for the heat release to the environment in the condenser, moreover it is added a preheater for recovering the thermal energy coming out of the expander.

5.1.2. The primary heat exchanger

Considering a subcritical cycle, the structure of the primary heat exchanger consists of a economizer, an evaporator and a superheater.

5.1.3. Condensers

The condenser technology considered uses cold water that is previously cooled by ambient air. Vapor that has been previously expanded through a expander, encounters the cold tubes, it condensates and it is eventually subcooled.

5.1.4. The preheater

This piece of equipment increases the efficiency of the cycle and reduces the amount of energy released to the environment. In the case analysed, the preheater handles the fluid outgoing from the expander, which still has high temperature, to preheat the fluid before entering the heat exchanger. This equipment has two positive effect. On one side lowering the enthalpy of the fluid outgoing from the expander, the heat exchanged in the condenser diminishes because it receives a fluid at reduced enthalpy. On the other side, the demand of the primary heat exchanger falls, almost in the same amount of the energy that can be recuperated from the fluid outgoing from the expander. As a disadvantage the work of the expander falls but the total efficiency of the cycle is increased.

5.1.5. The expander and generator

The expander is the key component of an ORC. It converts the energy contained in the fluid as pressure and temperature (enthalpy) to mechanical energy that will be consequentially converted into electricity in the generator.

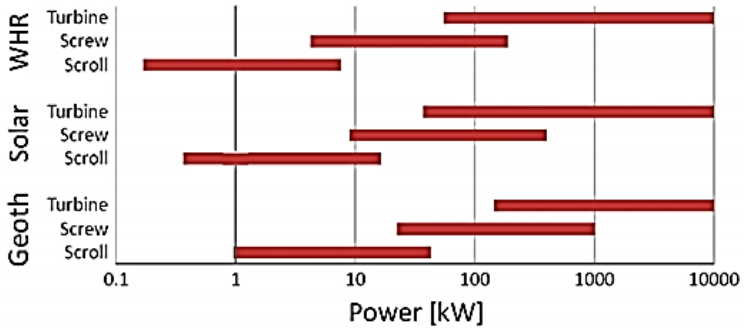

Figure 26: Optimum operating map for 3 expander technologies and 3 targets [S. Quoilin et al., 2013];

Considering the variety of turbomachines commercially available, the best fit for the system studied for medium/large power plants, with typical power output between 500 kW and 15 MW and integrated in an ORC application are axial turbines which are able to support applications with low grade heat sources.

Screw and scroll expanders are volumetric expanders, the work they produce depends on the pressure variations due to the changing volume of the chamber where the fluid is contained. The velocity of the fluid flowing through the expander is quite small whereas the pressures are extremely higher than in turbines.
Turbines are dynamic expanders, that convert the high internal energy of the fluid in mechanical energy, besides, the velocity of the fluid flowing through the turbine is significantly high [Andreas P. Weiß, 2015].
Axial turbines are less affected than radial turbines by ambient temperature variations, allowing almost constant efficiency when varying the operating conditions [www.turboden.eu]. In fact, in the ORC Turboden technology [www.turboden.eu] the turbine is axial, which is the most in use turbine configuration in the power industry, and it will be then considered as reference for the case studied.

In ORC cycles are usually employed single or two-stage turbines. Two stages-turbines can achieve a higher efficiency exploiting the repartition of the whole volume flow variation on two or more stages [E. Macchi, M. Astolfi, 2017].

5.1.6. Pumps

The technology usually employed in the ORC cycle is usually a centrifugal pump. It employs the effect of centrifugal force of its impeller, which rotating converts the mechanical energy of its engine into kinetical energy, then transfers its kinetical energy into to the fluid rising the fluid's pressure.

5.1.7. The plant

In Figure 27, the plant layout of the ORC cycle considered is shown. The heat source, represented by the assembly of the solar field and the biomass boiler, heats the thermal fluid. The temperature goes up from c4 to c1 condition. The thermal fluid that comes out of the heat source flows throughout the primary heat exchanger (PrHE) and warms the working fluid of the power cycle in three stages: superheater (f), evaporator (e) and economizer (d). The outlet working fluid at maximum temperature of the ORC (6) is then expanded in a turbine (g) until condition (7). Mechanical work is converted into electricity by the generator (i). The temperature of the fluid in this condition is still high therefore it can pass throughout a recuperator (c) to preheat the cold fluid entering the PrHE to (3) condition.

The cooled fluid (8) then flows through the condenser and then into a pump to rise its pressure to the higher-pressure level of the cycle.

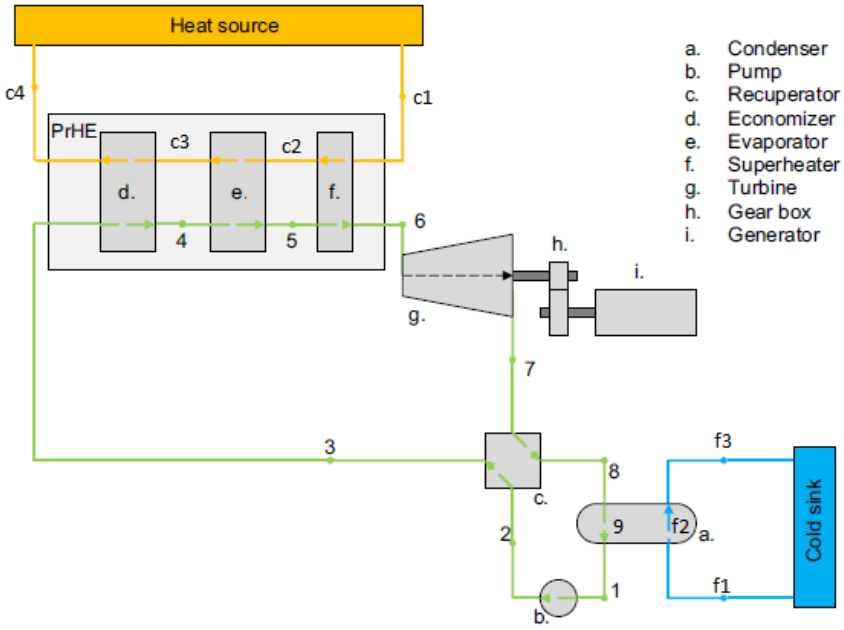

Figure 27: Plant layout for a single pressure level cycle [M.Astolfi, 2016]

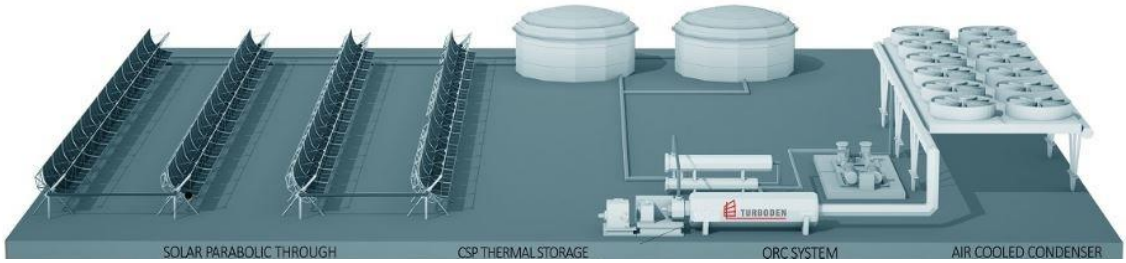

Figure 28: Turboden [www.turboden.eu]

5.2. Model

The Organic Rankine Cycle is modelled within the EES environment [EES, S.A. Klein and G. Nellis, 2018].
The large data bank of thermodynamic and transport properties built into EES is helpful in solving problems in thermodynamics, fluid mechanics, and heat transfer. EES can be used for many engineering applications.
To solve the model presented as follows, the equations of state of the fluid analysed have been employed, it has been possible to use data provided by the EES library.
EES calculates the thermodynamic properties of the fluid R245fa using the equation of state developed by Eric W. Lemmon and Roland Span [2006].
It calculates the thermodynamic properties of the fluid R141b using the equation of state provided by Martin-Hou [1995].
Whereas for the fluid R123, the equation of state developed by Reiner Tillner-Roth [1998] provides the properties.
At first, the design condition of the solar field is being considered to estimate the power produced and design equipment.
Moreover, the values set for the heat exchanger are:

Tcal = 130 ºC, organic fluid temperature during the phase change in the evaporator;
iTrec = 50 K, superheating temperature difference;
dTecal = 20 K, temperature difference between the incoming thermal hot oil and the organic fluid;
dTpcal = 10 K, pinch point, minimum temperature difference between the thermal hot oil and the organic fluid inside the heat exchanger.

In the same way, some values in the condenser are set as follows.

Tcon = 40 ºC, organic fluid temperature during the phase change in the condenser;
dTecon = 10 K, temperature difference between the incoming cooling and the organic fluid;
dTpcon = 5 K, pinch point, minimum temperature difference between the cooling fluid and the organic fluid inside the condenser.

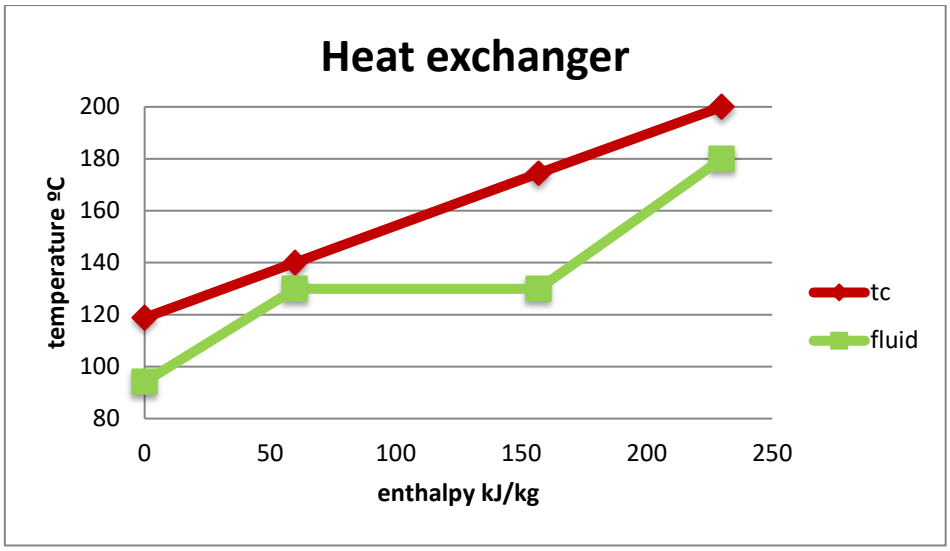

Figure 29: Pinch point condition in the heat exchanger

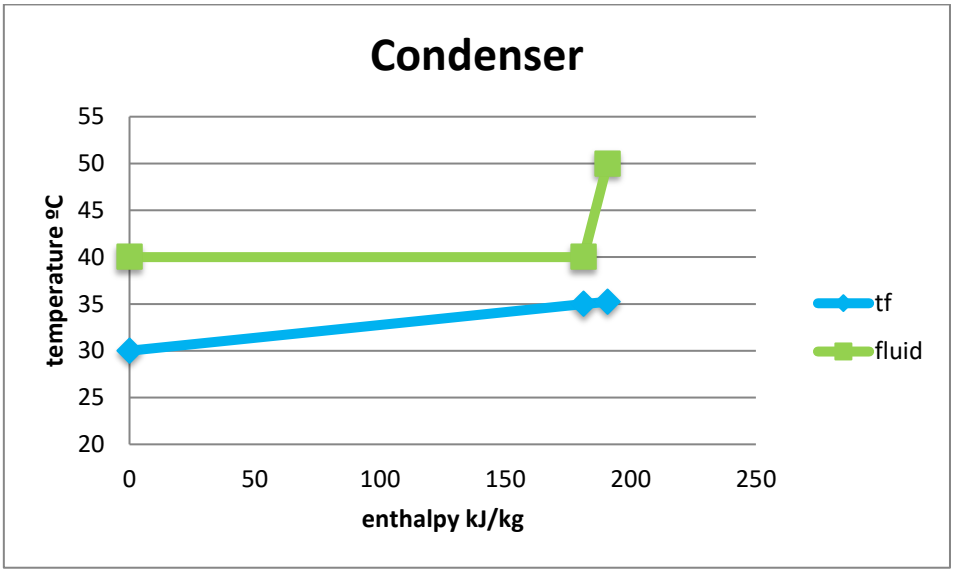

Figure 30: Pinch point condition in the condenser

5.3. Fluids

5.3.1. Criteria for selecting organic working fluids

The selection of working fluid for the ORC is critical, the fluid must have physical and thermodynamic properties that match the conditions of the cycle. Moreover, it must meet safety requirements and economic costs.

Thus, the main parameters to consider in the selection of working fluids are [Tchanche BF et al.,2011]:

1. Environmental: low environmental impacts (low ODP, low GWP and low atmospheric lifetime).
    - The selected working fluids should be not phased out by relevant national regulations
2. Safety: good safety characteristics (non-toxic and non-flammable). Non-flammable fluids avoid explosions.
3. Chemical stability: good thermal and chemical stability (stable at high temperature), and good compatibility with materials (non-corrosive).

4. Physical properties:
    - Vapour saturation curve with zero or positive slope (ds/dT) (isentropic or dry fluids);
    - High latent heat of vaporization;
    - High density (liquid/vapor phase);
    - High specific heat;
    - Moderate critical parameters (temperature, pressure);
    - Acceptable condensing and evaporating pressures (>1 bar and <25 bar resp.);
    - Good heat transfer properties (low viscosity, high thermal conductivity);
    - High thermodynamic performance (high energetic/exergetic efficiency);
5. Thermodynamic properties:
    - Positive slope of the vapour saturation curve on T-S diagram to assure that all expansion states exist on the superheat region;
    - Critical temperature above the evaporation temperature of the cycle;
    - Low specific volume ratio over the turbine in order to reduce volumes;
    - Even though working fluid cost is a small part of the entire investment because the fluid is enclosed in ORC without the leaking loss, low cost and good availability is requested.
    - The working fluid should be known in state-of-the-art ORC applications or in the scientific literature.
    - A determining factor in the choice of the fluid to adopt in a cycle, are the critical temperature and pressure. Furthermore, in addition to the thermodynamic properties, legislative requests are very important conditions to be observed. The protection of the ozone layer and the reduction of emissions of greenhouse gases are at the root of various regulations and understandings as the Montreal Protocol which is the most important agreement on substances [Montreal Protocol, 2006].

5.3.2. Analysis

A comparison between three fluids flowing through the power cycle as possible different options is presented in the analysis. The same input variables of temperature and pinch point values are used to model the cycle analysing how three different fluids behave throughout the cycle. The efficiency of the ORC and the electrical power that result from the cycle for each fluid, are indexes of the thermodynamic behaviour of the fluids. As it can be seen from the Tables 20, 21 and 22, the efficiencies do not considerably deviate from each other. Therefore the fluids behave almost in the same way when working at these temperature levels. The latter are generally considered for ORC application when the source is a solar source such as parabolic trough collector technology [Mónica Borunda et al., 2015].

The input variables are the values set for the heat exchanger proposed above and the heat power, 5MW, provided by the solar field.

R123	Ti	pi	si	xi	hi
	[°C]	[bar]	[kJ/(kg·K)]	[-]	[kJ/kg]
1	40	1.55	241.89	1.1425	0
2	40.9	14.61	243.2	1.1437	-100
3	92.3	14.61	299.64	1.3093	-100
4	130	14.61	345.37	1.4275	0
5	130	14.61	457.71	1.7062	1
6	180	14.61	508.26	1.8233	100
7	121	1.55	470.19	1.8476	100
8	48.9	1.55	413.75	1.6909	100
9	40	1.55	407.15	1.6702	1
10	40	1.55	241.89	1.1425	0

ηglob	**0.17**	**[-]**
Wnet	**850**	**[kW]**

Table 20: Results of the power cycle with R123, EES

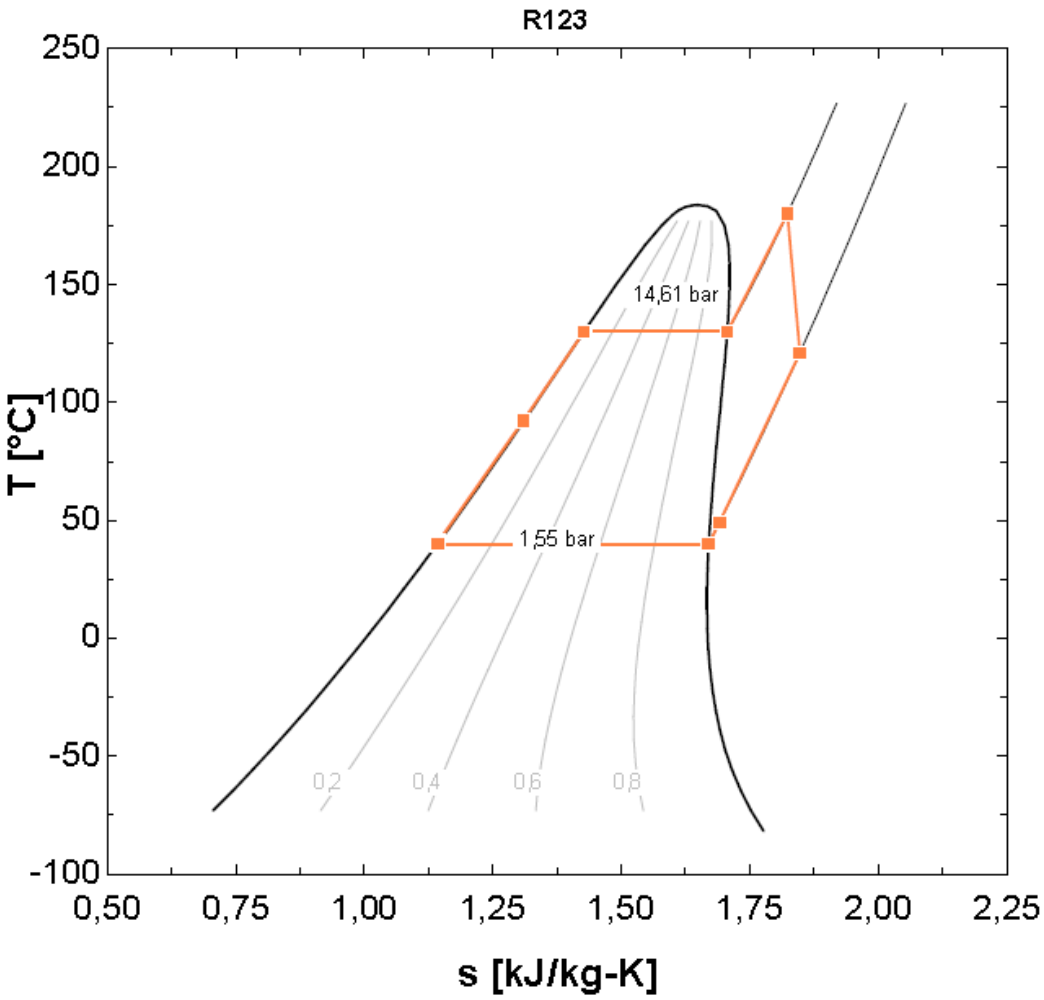

Figure 31: Graph of the power cycle with R123, EES[1]

[1] The comma is the decimal separator in the figures that directly derive from EES data.

R141b	Ti [°C]	pi [bar]	si [kJ/(kg·K)]	xi [-]	hi [kJ/kg]
1	40	1.33	0.3114	0	85.06
2	41.4	12.51	0.3166	-100	86.7
3	85.1	12.51	0.4796	-100	141.78
4	130	12.51	0.6375	0	202.59
5	130	12.51	1.0328	1	361.98
6	180	12.51	1.1579	100	415.47
7	113.1	1.33	1.1901	100	366.61
8	48.5	1.33	1.0343	100	311.54
9	40	1.33	1.0127	1	304.66
10	40	1.33	0.3114	0	85.06

ηglob	**0.166**	**[-]**
Wnet	**832.5**	**[kW]**

Table 21: Results of the power cycle with R141b, EES

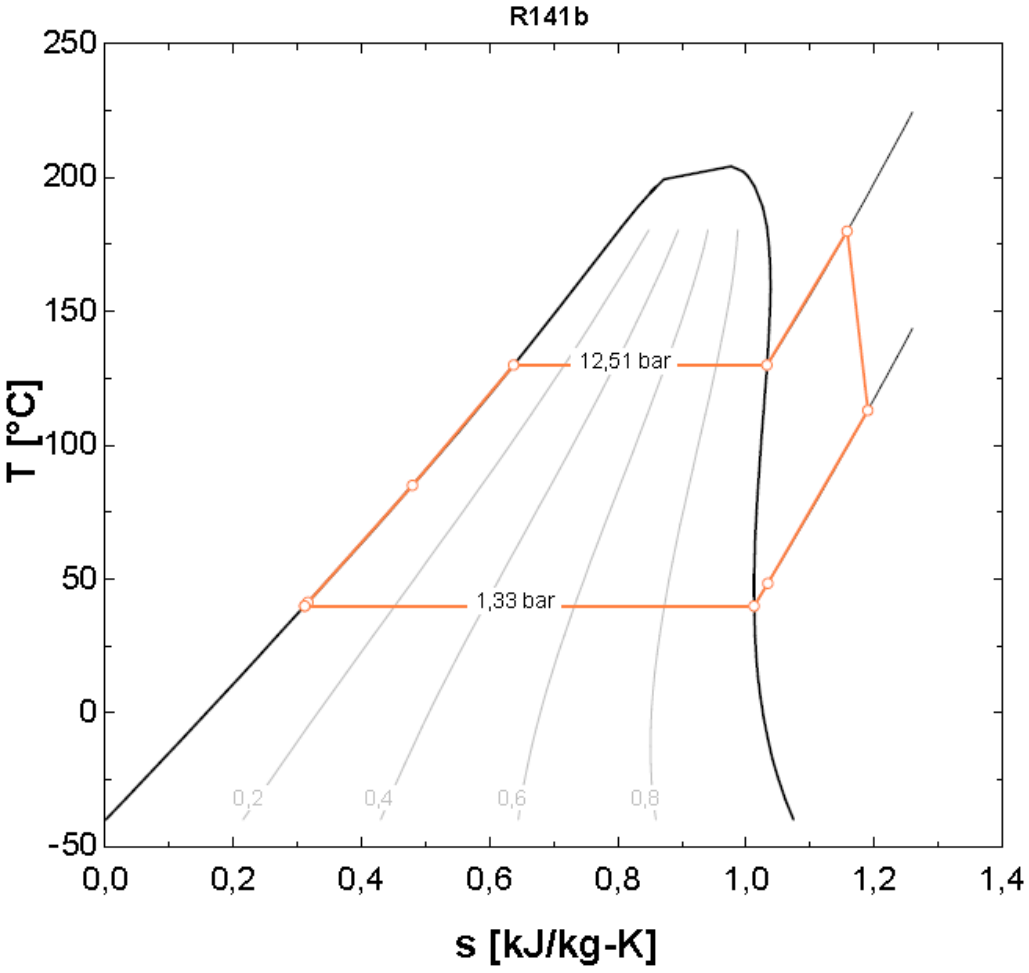

Figure 32: Graph of the power cycle with R141b, EES[1]

R245fa	Ti	pi	si	xi	hi
	[°C]	[bar]	[kJ/(kg·K)]	[-]	[kJ/kg]
1	40	2.5	1.179	0	252.57
2	41.3	23.39	1.1812	-100	254.87
3	94.1	23.39	1.4022	-100	330.17
4	130	23.39	1.5584	0	390.4
5	130	23.39	1.8003	1	487.88
6	180	23.39	1.971	100	560.66
7	123.5	2.5	1.9978	100	518.64
8	49.5	2.5	1.7879	100	443.34
9	40	2.5	1.7577	1	433.74
10	40	2.5	1.179	0	252.57

ηglob	**0.166**	**[-]**
Wnet	**828.8**	**[kW]**

Table 22: Results of the power cycle with R245fa, EES

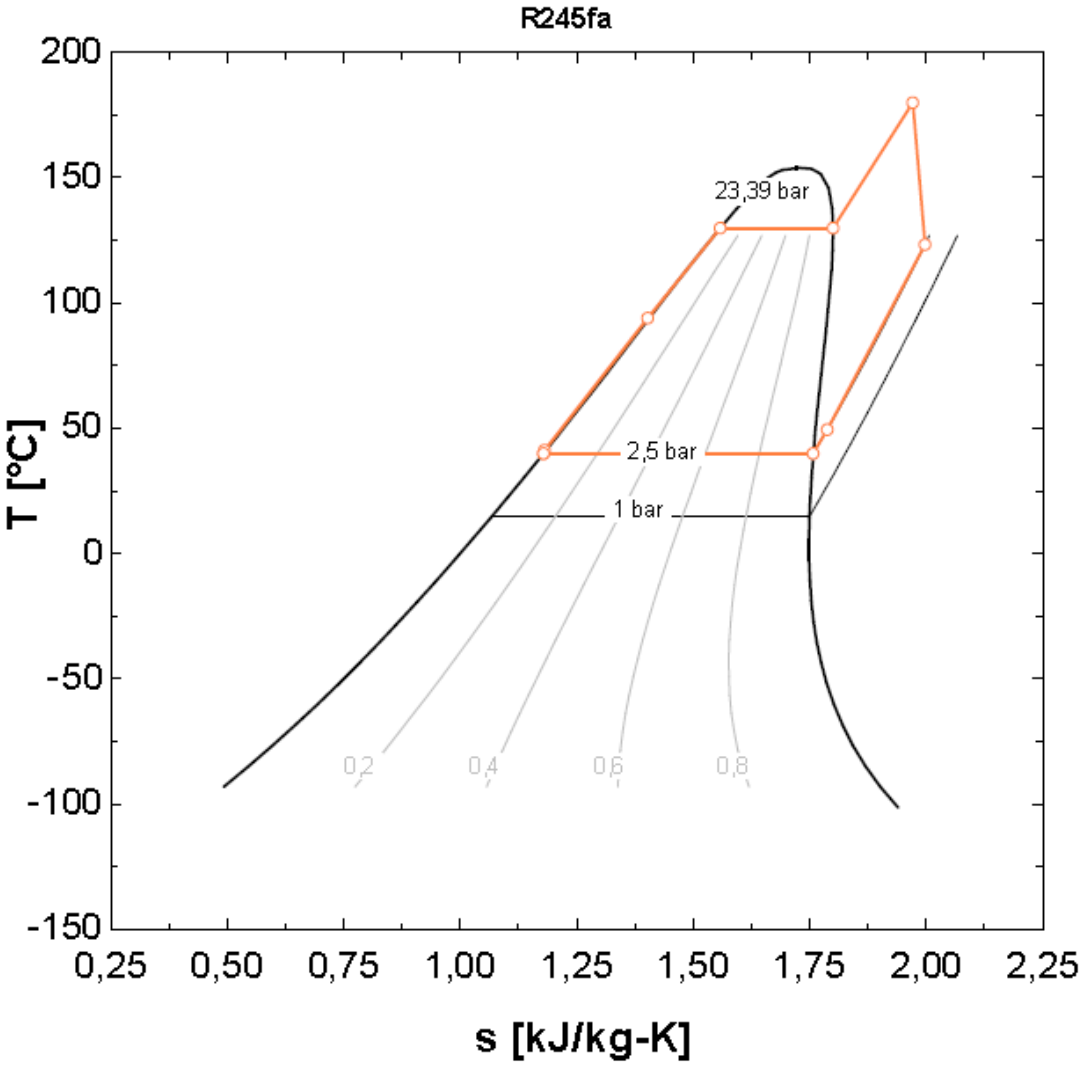

Figure 33: Graph of the power cycle with R245fa, EES[1]

Name of working fluids	chemical formula	group name	ingredient name	Tc [ª C]	Pc [bar]	ODP	GWP
R123	$C_2HF_3Cl_2$	HCFC	2,2-Dichloro-1,1,1-trifluoroethane	183.68	36.62	0.02	77
R141b	$C_2H_3FCl_2$	HCFC	1,1-Dichloro-1-fluoroethane	204.20	42.50	0.11	725
R245fa	$C_3H_3F_5$	HFC	1,1,1,3,3-Pentafluoropropane	154.05	36.40	0	1030

Table 23: fluids specifics [ASHRAE, www.ashrae.org]

As HCFCs contribute both to ozone depletion and global warming, the use of HCFCs is being phased out as part of global legislation [Montreal Protocol, 2006].

Even though some HCFCs can still be used, under the Montreal Protocol, it was agreed that ozone-depleting substances, including CFCs and HCFCs, would be phased out globally.

Nowadays, when considering the most employed refrigerants in this kind of applications, CFCs are viewed as the largest contributor refrigerants to ozone depletion. Nevertheless, HCFCs are considerably less damaging to the ozone layer than the CFCs. The Montreal Protocol has imposed the complete phase-out of HCFCs globally by 2040. On the other hand, HFCs are categorised as having zero ODP (Ozone Depleting Potential) and medium to high GWP (Global Warming Potential). Thus, they are considered more environmentally friendly alternative to CFCs and HCFCs [www.linde-gas.com, 07/2018].

The Global Warming Potential is an index that compares the characteristic of capturing the solar energy radiation of the substance considered to the CO2's global warming ability as a reference index. Moreover, the higher the index the more is the global warming potential and the more the considered substance leads to an increasing global warming.

The Ozone Depleting Potential is a relative index that compares the depletion of the ozone caused by the substance considered as a reference, which is the R11 (that is fixed as 1.0). The depletion of the ozone layer is caused by substances (such as CFCs, halocarbons, methyl bromide, methyl chloroform) that reach the stratosphere, thanks to their long atmospheric lifetime. There, ultraviolet light breaks their chemical bonds, thus chlorine and bromine can be freed and react with the ozone layer, leading to its degradation.
The effect of this degradation is the so-called *ozone hole.* This condition allows the most damaging wavelengths of the ultraviolet light (UVB) to reach the Earth's surface. UVB-wavelengths cause risk of cancer, cataract and inhibition of the immune system.

R245fa has an ODP value of zero, it is non-toxic and non-flammable, moreover it has high heat exchanger efficiency that leads to favourable heat transfer properties.

For this kind of technologies, such as stationary equipment, the Regulation No. 517/2014 [Official Journal of the European Union,2014] claims that HFCs with GWP values higher than 2500 will be banned from 1 January 2020. This is not the case of the R245fa that has a GWP of 1030 and therefore it is below the limit.

This paper considers analysing the cycle proceeding with the R245fa refrigerant, that is one of the main HFCs used in low-temperature solar ORC applications. R245fa has a lower pressure critical level compared to other refrigerants, this leads to the use of cheaper equipment, such as heat exchanger and

pump, in the power cycle [Bruno et al., 2008]. Besides, R245fa has a high molecular weight (134.05g/mole), that is a great advantage considering the turbine technology. In fact, the rotational speed or the number of turbine stages can be lowered, and it guarantees a not elevated mass flow rate and a reasonable turbine nozzle area. [X.D. Wang et al., 2010].

5.4. Condenser

When the condenser of the power cycle is designed, two options can be considered.

5.4.1. Groundwater

In the first case, the organic fluid can be cooled by groundwater from the phreatic layer.
In the area of Zaragoza, the temperature of the groundwater is 10°C in winter and in summer it is 17°C. Therefore, the cycle with the condenser characterized by these temperature levels is analysed. The available cold water Tf1 (see Figure 27), has been changed maintaining the temperature of the evaporator (Table 24) and then, Tf1 has been fixed and the temperature of the evaporator has been changed (Table 25).

Tev=130°C	**R245fa**			
tf1 [°C]	**ηglob**	**Wnet [kW]**	**pcond [bar]**	**Tcond[°C]**
10	0.199	994.2	1.22	20
15	0.191	953.1	1.48	25
17	0.187	936.6	1.59	27

Table 24: Results of the power cycle changing the available cold temperature of the condenser

Tf1=15°C	**R245fa**			
Tev [°C]	**ηglob**	**Wnet [kW]**	**pev [bar]**	**Tc1[°C]**
150	0.209	1045	33.81	220
140	0.2	1001	28.15	210
130	0.191	953.1	23.39	200
120	0.18	899.9	19.29	190
110	0.168	841.1	15.74	180
100	0.155	776	12.69	170
90	0.141	704	10.09	160

Table 25: Results of the power cycle changing the temperature of the evaporator

5.4.2. Ambient air

In the second case, water passes through the condenser and cools down the organic fluid. Then, it is cooled by an air-cooled condenser.

Different ambient conditions lead to different available temperatures of the cooling fluid. Varying condenser conditions allows giving an idea of how different external conditions or other temperature values change the power output and the global efficiency; more possible options are considered.
By setting different values of the available temperature of the cooling fluid (Tf1) the results presented in Tables 26 and 27 are obtained.

Tev=130°C	**R245fa**			
Tf1 [°C]	**ηglob**	**Wnet [kW]**	**pcond [bar]**	**Tcond[°C]**
30	0.166	828.8	2.5	40
35	0.157	787	2.94	45
40	0.149	745.1	3.43	50
45	0.141	702.8	3.99	55
50	0.132	660.4	4.62	60
55	0.124	617.6	5.32	65
60	0.115	574.5	6.1	70

Table 26: Results of the power cycle changing the available cold temperature of the condenser

Tf1=30°C	**R245fa**			
Tev [°C]	**ηglob**	**Wnet [kW]**	**pev [bar]**	**Tc1[°C]**
150	0.186	928.1	33.81	220
140	0.176	880.9	28.15	210
130	0.166	828.8	23.39	200
120	0.154	771	19.29	190
110	0.141	706.8	15.74	180
100	0.127	635.3	12.69	170
90	0.111	555.8	10.09	160

Table 27: Results of the power cycle changing the temperature of the evaporator

5.5. Operating conditions

To analyse the operating condition of the cycle during different situations, herein the characteristic of ORC commercial equipment and data's performance are presented (Figure 34).
The technology chosen to present the problem is a Turboden ORC [www.turboden.eu].

		TURBODEN 6/7 HR DE		TURBODEN 10 to 14 HR DE		TURBODEN 18 to 24 HR DE		TURBODEN 27 to 40 HR DE		TURBODEN 50 to 100 HR DE	
		Range of Operation	Reference Case TD 6 HR	Range of Operation	Reference Case TD 10 HR	Range of Operation	Reference Case TD 22 HR SPLIT	Range of Operation	Reference Case TD 40 HR SPLIT	Range of Operation	Reference Case TD 70 HR
INPUT* - Thermal Oil											
Thermal Oil inlet temperature	°C	240-300	270	240-310	290	240-310	285	250-315	315	240-310	290
Thermal Oil outlet temperature	°C	170-120	140	170-120	145	170-120	120	170-120	130	150-110	115
Thermal power input	MW	2.5-4.0	3.0	5.0-7.0	5.54	8.0-12.0	11.21	13.0-22.0	21.40	24.0-50.0	32.00
Thermal Oil inlet temperature	*°F*	*464-572*	*518*	*464-590*	*554*	*464-590*	*545*	*482-599*	*599*	*464-590*	*554*
Thermal Oil outlet temperature	*°F*	*338-248*	*284*	*338-248*	*293*	*338-248*	*248*	*338-248*	*266*	*302-230*	*239*
Thermal power input	*MMBtu/hr*	*8.53-13.65*	*10.24*	*17.06-23.88*	*18.90*	*27.30-40.95*	*38.25*	*44.36-75.07*	*73.02*	*81.89-170.61*	*109.00*
OUTPUT - Cooling Water**											
Typical cooling water temperature (in/out)	°C	25/35	25/35	25/35	26/38	25/40	22/40	20/45	22/54	25/40	20/27
Thermal power to condenser	MW	2.0-3.5	2.4	4.0-5.0	4.4	6.0-9.5	9.0	10.0-17.5	17.2	19.2-40.0	25.2
Typical cooling water temperature (in/out)	*°F*	*77/95*	*77/95*	*77/95*	*79/100*	*77/104*	*72/104*	*68/113*	*72/129*	*77/104*	*68/81*
Thermal power to condenser	*MMBtu/hr*	*6.82-11.94*	*8.19*	*13.65-17.06*	*15.01*	*20.47-32.42*	*30.71*	*34.12-59.71*	*58.69*	*65.51-136.49*	*86.00*
PERFORMANCES											
Gross electric power	kW	500-800	600	900-1600	1108	1700-2500	2120	2600-4500	4000	4800-10500	6800
Gross electric efficiency***		17%-20%	20%	17%-22%	20%	17%-22%	19%	17%-21%	19%	17%-22%	21%
Captive power consumption	kW	18-36	25	36-70	46	60-100	80	100-200	200	200-800	465
Net active electric power output	kW	480-760	575	850-1550	1062	1650-2400	2040	2500-4000	3800	4500-9800	6335
Net electric efficiency***		16%-19%	19%	16%-21%	19%	16%-21%	18%	16%-20%	18%	16%-21%	20%
Electric generator****		50Hz, 400V 60Hz, 480V	50Hz, 400V 60Hz, 480V	50Hz, 400V 60Hz, 480V	50Hz, 400V 60Hz, 480V	50Hz, 660V 60Hz, 4160V	50Hz, 660V 60Hz, 4160V	50Hz, 6kV 60Hz, 4160V	50Hz, 6kV 60Hz, 4160V	50Hz, 6kV 60Hz, 4160V	60Hz, 4160V
Cooling systems		closed loop water cooling or wet tower		closed loop water cooling or wet tower		closed loop water cooling or wet tower		closed loop water cooling or wet tower		wet tower or air condenser	
Typical delivery time (EXW)	Months	9-11		9-11		9-11		11-13		12-14	

Figure 34: Characteristic of the Turboden ORCs [www.turboden.eu]

According to the graph in Figure 35, it can provide part load operation down to 10% of nominal load maintaining 90% of the cycle efficiency down to 50% load.

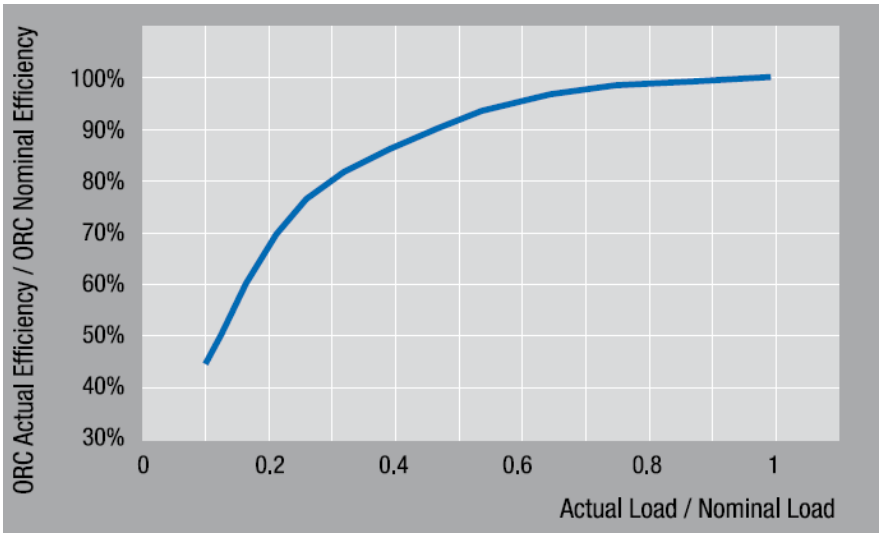

Figure 35: Efficiency reduction due to part load operations of the Turboden ORC [www.turboden.eu].

The power obtainable from the turbine is almost 1MW for all the analysed options. In order to proceed with this case study, the power produced is thought to be used in a mechanical chiller to meet the cooling demand of a shopping centre in Zaragoza, Spain.

6. Cooling technology – Chiller

6.1. Mechanical chiller

The mechanical chiller is a machine that has the aim to cover a cooling demand of a site, consuming electricity. It is based on a reverse Rankine cycle that exploits the evaporation of the working fluid to provide the cooling demand.

The basic elements of a mechanical chiller machine are:

1. A compressor, which elevates the pressure and the temperature of the refrigerant, through an adiabatic process, consuming electricity.
2. A condenser, that extracts heat from the refrigerant fluid, which experiments a condensation process, while releasing it to the environment (hot source).
3. A throttling valve, whose purpose is to reduce the temperature and the pressure of the working fluid, thus, reaching the conditions needed in the evaporator.
4. An evaporator, which is the responsible of the cooling effect of the machine. The working fluid absorbs the heat from an ambient to be cooled (cold source) while evaporating through an almost isobaric process.

To obtain a more complete picture of the system, a commercial chiller has been selected. A Swegon mechanical chiller is the one chosen for the analysis [www.swegon.com].

TECHNICAL DATA COBALT W

Unit size			95.2	100.2	105.2	110.2	117.2	124.2	130.3	137.3	143.3	147.3	153.3
Cooling (Gross values)													
Nominal cooling capacity	(1)	kW	946	993	1049	1091	1171	1225	1282	1369	1424	1464	1527
Total power input for cooling	(1)	kW	199	218	221	239	254	267	281	297	311	318	326
EER	(1)		4,74	4,55	4,74	4,56	4,62	4,59	4,56	4,61	4,58	4,60	4,68
ESEER			5,56	5,40	5,60	5,39	5,41	5,52	5,46	5,49	5,47	5,49	5,60
Efficiency class			B	C	B	C	C	C	C	C	C	C	B
Cooling (EN 14511 values)													
Nominal cooling capacity	(1),(5)	kW	942	989	1044	1087	1167	1221	1278	1364	1418	1457	1520
EER	(1),(5)		4,55	4,35	4,52	4,40	4,44	4,41	4,39	4,43	4,39	4,40	4,47
ESEER	(5)		4,73	4,56	4,71	4,65	4,62	4,68	4,67	4,68	4,61	4,62	4,76
Efficiency class			C	C	C	C	C	C	C	C	C	C	C
Compressors													
Type			Screw										
Quantity/Cooling circuits		n°/n°	2	2	2	2	2	2	3	3	3	3	3
Capacity steps		n°	Continue										
Total oil load		l	40	51	56	56	56	56	74	79	84	84	84
Refrigerant total load		kg	160	180	190	195	220	230	225	250	270	280	290
Evaporator													
Water flow	(1)	l/h	134.136	142.906	151.055	162.683	201.431	210.711	220.546	235.409	244.911	251.752	262.622
Pressure drop	(2)	kPa	41	46	48	54	50	55	53	58	69	72	75
Condenser													
Water flow	(1)	l/h	162.081	174.033	184.141	196.973	245.059	256.592	268.904	286.450	298.359	306.438	318.684
Pressure drop		kPa	32	31	51	54	54	57	50	50	54	54	54
Noise levels													
Noise power level	(3)	dB(A)	98	100	100	100	101	101	101	101	101	101	101
Noise pressure level	(4)	dB(A)	79	81	81	81	81	81	81	81	81	81	81
Noise power level (LN version)	(3)	dB(A)	93	95	95	95	96	96	96	96	96	97	97
Noise pressure level (LN version)	(4)	dB(A)	74	76	76	76	76	76	76	76	76	77	77
Noise power level (SLN version)	(3)	dB(A)	86	88	89	89	90	91	91	91	91	91	91
Noise pressure level (SLN version)	(4)	dB(A)	67	69	70	70	70	71	71	71	71	71	71
Basic version dimensions and weights													
Length		mm	4.060	4.060	4.770	4.770	4.770	4.770	4.450	4.450	4.450	4.450	4.450
Depth		mm	1.280	1.280	1.460	1.460	1.420	1.420	2.130	2.130	2.130	2.130	2.130
Height		mm	1.950	1.950	2.150	2.150	2.220	2.220	2.300	2.300	2.300	2.300	2.300
Operating weight		kg	3.365	3.354	3.975	4.080	4.772	4.810	6.192	6.297	6.402	6.492	6.581

Figure 36: Technical data of the chiller, Swegon Group [www.swegon.com]

(1) Water temperature at condenser inlet-outlet 30-35°C;
(2) Water temperature at evaporator inlet-outlet 12-7°C
(3) Calculated according to ISO 3744 under nominal operating conditions.
(4) Sound pressure levels measured at 1 metres from the unit in free field under nominal working conditions, according to ISO 3744.
(5) Values in compliance with EN 14511-3:2011.

The model chosen is COBALT W 153.3. In order to guarantee the demand three chillers have been considered to be installed. Therefore, the nominal cooling capacity is 4581 kW. Sleeve tube bundle type with dry expansion evaporator; optimized for operation with R134a, enhance the COP value of the unit, reducing the refrigerant load and the overall dimensions.

Mechanical chillers belong to the category of *stationary refrigeration equipment,* considering the Regulation No. 517/2014 [Official Journal of the European Union,2014]. As mentioned before, it claims that HFCs with GWP values higher than 2500 will be banned from 1 January 2020. This statement does not affect the refrigerant R134a, whose GWP index is 1430 [www.ashrae.org]. What affects the use of these fluids, however, is the regular leak checking depending on the number of CO_2 emitted that must be fulfilled. Thus, the use of fluid with high GWP value is discouraged. Moreover, the cost of these refrigerants has risen. These conditions are encouraging the market to find other refrigerants with a lower GWP.

These could be hydrocarbons, ammonia, R-1234yf, R-1234ze, R-32, R-452B, R-450A, R-513A and others. On the other hand, they have worse characteristic when considering the flammability, toxicity or thermodynamic characteristics [www.carel.com, 08/2018].

Therefore, the chiller applied for this simulation has been considered to operate with R134a fluid, being a mature technology and with high performances, not excluding the possibility of working with more environmental friendly fluids.

In Figure 37 are presented the performance changing both the outlet water temperature of the condenser and evaporator. It takes into account, therefore, variations in ambient conditions and different request of outlet temperature.

In Figure 38 are presented operating limits of the chiller with different temperature values both considering the user and source variations.

COOLING CAPACITY - COBALT W

Model	To	Condenser outgoing water temperature [°C]														
	[°C]	30			35			40			45			50		
		Pf	Pe	Pr	Pf	Pe	Pr	Pf	Pe	Pr	Pf	Pe	Pr	Pf	Pe	Pr
95.2	6	971	185	1156	920	198	1117	865	215	1079	800	239	1039	736	268	1004
	7	999	187	1186	**946**	**199**	**1145**	887	218	1104	823	242	1065	759	271	1030
	8	1031	188	1219	973	202	1175	915	220	1135	850	245	1095	784	274	1058
	9	1059	191	1250	1003	205	1207	943	223	1166	877	248	1124	809	277	1086
	10	1092	193	1285	1034	207	1241	972	225	1198	903	250	1154	834	281	1114
100.2	6	1020	203	1223	965	216	1182	908	235	1143	847	259	1106	781	289	1070
	7	1049	204	1254	**993**	**218**	**1212**	935	237	1172	872	261	1133	804	292	1097
	8	1084	206	1290	1026	221	1247	966	240	1205	901	264	1165	831	296	1127
	9	1119	208	1327	1059	223	1282	997	242	1240	931	268	1198	859	299	1158
	10	1155	210	1365	1094	225	1319	1030	245	1275	961	271	1232	888	303	1191
105.2	6	1077	206	1283	1020	219	1239	959	238	1197	894	262	1156	824	293	1117
	7	1108	207	1316	**1049**	**221**	**1271**	987	240	1227	920	265	1185	849	296	1145
	8	1145	209	1354	1084	224	1308	1020	243	1263	952	268	1220	878	299	1178
	9	1182	211	1394	1120	226	1346	1054	246	1299	983	271	1254	908	303	1211
	10	1220	213	1434	1156	228	1384	1088	248	1336	1016	274	1290	938	307	1245
110.2	6	1116	222	1338	1056	237	1293	992	257	1250	925	284	1208	852	318	1169
	7	1152	224	1376	**1091**	**239**	**1330**	1026	260	1286	956	287	1243	881	321	1202
	8	1190	226	1416	1126	242	1368	1059	263	1322	988	291	1278	911	325	1236
	9	1228	228	1456	1162	245	1407	1093	266	1359	1020	294	1314	941	329	1270
	10	1266	230	1496	1198	247	1445	1128	269	1397	1052	297	1350	971	333	1304
117.2	6	1199	235	1434	1135	251	1386	1067	273	1340	992	302	1294	913	338	1251
	7	1238	237	1475	**1171**	**254**	**1425**	1101	276	1377	1025	305	1330	944	342	1286
	8	1278	240	1517	1209	256	1466	1137	279	1416	1058	309	1368	976	346	1322
	9	1318	242	1560	1248	259	1507	1174	282	1456	1093	313	1406	1008	350	1358
	10	1360	244	1604	1287	262	1549	1211	286	1497	1128	317	1444	1040	355	1395
124.2	6	1255	247	1502	1187	264	1451	1116	287	1403	1036	318	1354	953	357	1310
	7	1295	249	1544	**1225**	**267**	**1492**	1152	290	1442	1069	322	1392	985	361	1346
	8	1337	252	1588	1265	270	1535	1189	294	1483	1105	326	1431	1018	365	1383
	9	1379	254	1633	1305	273	1578	1227	297	1524	1140	330	1470	1051	370	1421
	10	1422	257	1679	1346	276	1621	1266	300	1566	1176	334	1510	1085	374	1459
130.3	6	1313	261	1574	1243	278	1521	1169	302	1471	1091	333	1424	1006	372	1378
	7	1354	263	1618	**1282**	**281**	**1564**	1206	306	1512	1126	337	1463	1039	376	1415
	8	1398	266	1664	1324	284	1608	1245	309	1554	1163	340	1504	1074	381	1454
	9	1442	268	1710	1366	287	1653	1285	312	1597	1201	344	1545	1109	385	1494
	10	1487	271	1757	1408	290	1698	1325	316	1641	1239	348	1587	1144	389	1534
137.3	6	1401	276	1677	1327	294	1621	1248	319	1567	1165	351	1516	1074	393	1467
	7	1446	278	1724	**1369**	**297**	**1666**	1288	322	1611	1202	355	1558	1109	397	1506
	8	1492	281	1773	1413	300	1713	1330	326	1656	1242	359	1601	1147	402	1548
	9	1539	283	1822	1458	303	1761	1373	329	1702	1282	363	1645	1184	406	1590
	10	1587	286	1873	1503	306	1809	1416	333	1748	1323	367	1690	1222	411	1633
143.3	6	1459	288	1747	1381	308	1689	1300	334	1634	1213	368	1581	1118	411	1530
	7	1504	291	1795	**1424**	**311**	**1735**	1341	337	1678	1251	372	1623	1155	416	1570
	8	1553	294	1847	1471	314	1785	1386	341	1727	1293	376	1670	1194	421	1615
	9	1603	297	1900	1519	317	1836	1431	345	1776	1336	381	1717	1234	426	1660
	10	1654	299	1953	1567	321	1888	1477	349	1825	1379	385	1765	1275	431	1706
147.3	6	1499	295	1795	1420	315	1735	1336	342	1678	1246	377	1623	1149	421	1571
	7	1546	298	1844	**1464**	**318**	**1782**	1378	345	1723	1286	381	1667	1186	426	1612
	8	1596	301	1897	1512	321	1833	1424	349	1773	1329	385	1714	1227	431	1658
	9	1648	303	1951	1561	325	1886	1470	353	1823	1373	390	1763	1268	436	1704
	10	1700	306	2007	1611	328	1939	1517	357	1874	1417	394	1812	1310	441	1751
153.3	6	1564	303	1867	1481	323	1804	1394	350	1744	1300	386	1686	1199	432	1631
	7	1613	305	1918	**1527**	**326**	**1853**	1437	354	1791	1341	390	1731	1237	436	1674
	8	1665	308	1974	1577	329	1907	1485	358	1843	1386	395	1781	1280	442	1721
	9	1719	311	2030	1628	333	1961	1533	362	1895	1432	399	1831	1323	447	1769
	10	1773	314	2087	1680	336	2016	1582	366	1948	1478	404	1882	1366	452	1818

Figure 37: Power values with variations in the outlet water temperature of the chiller's condenser [www.swegon.com]

Pf: cooling capacity [kW]
Pe: electrical power absorbed by the compressors [kW]
Pr: condenser heating capacity [kW]
T0: evaporator outlet water temperature [°C] Evaporator thermal gap = 5°C

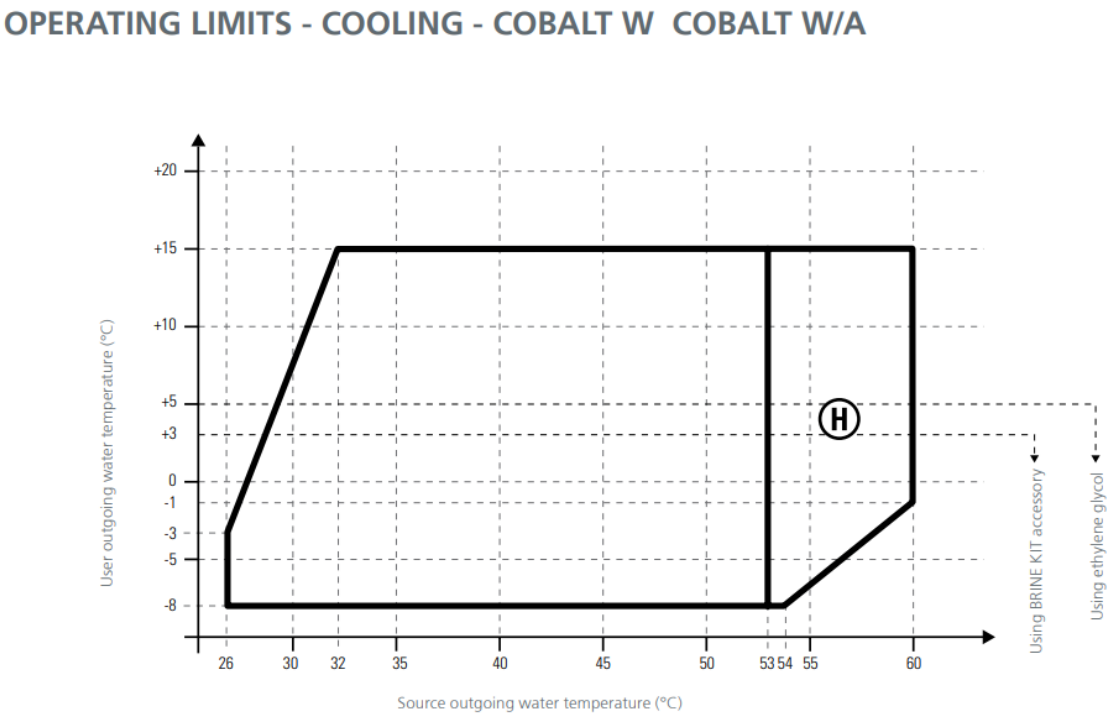

Figure 38: Temperature range for user/source outlet water temperature of the chiller [www.swegon.com]

6.2. Absorber refrigerators

Another possible technology to be included in this system, as alternative to the mechanical chillers, could be absorber refrigerators. They are driven by thermal energy instead of electrical energy, thus they could exploit waste heat from other processes, solar thermal energy or other heat sources. In the system studied, one option to integrate this technology could be to use the thermal energy of the organic fluid that flows from the turbine, after the expansion, as heat source. It would be necessary to install a heat exchanger connecting the organic fluid of the Rankine cycle with the fluid of the absorber refrigerator. Therefore, the power cycle would be able to produce both electrical and thermal energy. A problem to be analysed, would be how to divide the product of the turbine in electricity and thermal energy, considering the electrical and thermal demand respectively.

In this thesis the focus is on the integration of solar parabolic trough with the ORC technology and this option has not been investigated, thus, a mechanical chiller, in particular the model COBALT W 153.3 has been chosen.

7. Demand of the shopping centre

Considering the demand profile of a shopping centre, as the one described below, allows the system to have an application throughout the year.

7.1. Electrical demand for cooling

This demand has been estimated in a shopping centre of Madrid by Daikin [Daikin, www.daikin.eu, 07/2018]. The same percentage values presented in the diagrams (Figure 39 and Figure 40) can be considered for Zaragoza, because the weather conditions are similar to Madrid. In fact, both cities have a continental climate and they lie within the same climatic zone (D3) [Gobierno de España, Ministerio de Fomento, 2017], characterized by scorching summers, bitter winters and moderate temperatures in months in Spring and Fall seasons. Moreover, the data is highly dependent on the occupation more than on the site location and therefore is not so relevant whether the location is exactly Madrid or a city close to it.

The data is employed to develop the demand profile of cooling considering the occupational indexes in weekdays (Figure 39) and in holidays (Figure 40), as well as in each month (Figure 41). Thus, for the typical day of each month, a 24 hours profile of cooling demand is estimated. The percentage values refer to the total nominal power of the three chillers in Figure 39 and in Figure 40.

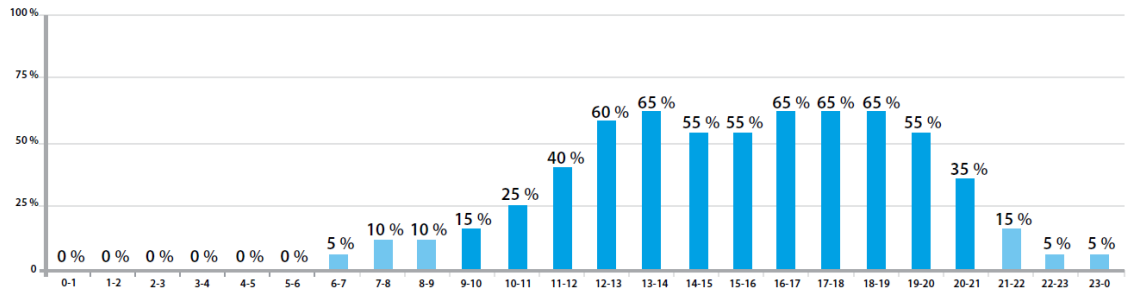

Figure 39: Occupational index in weekdays, cooling demand (Daikin)

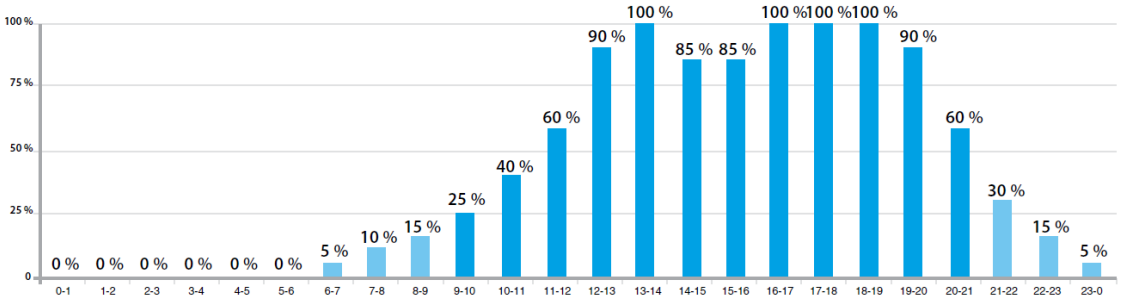

Figure 40: Occupational index in holidays, cooling demand (Daikin)

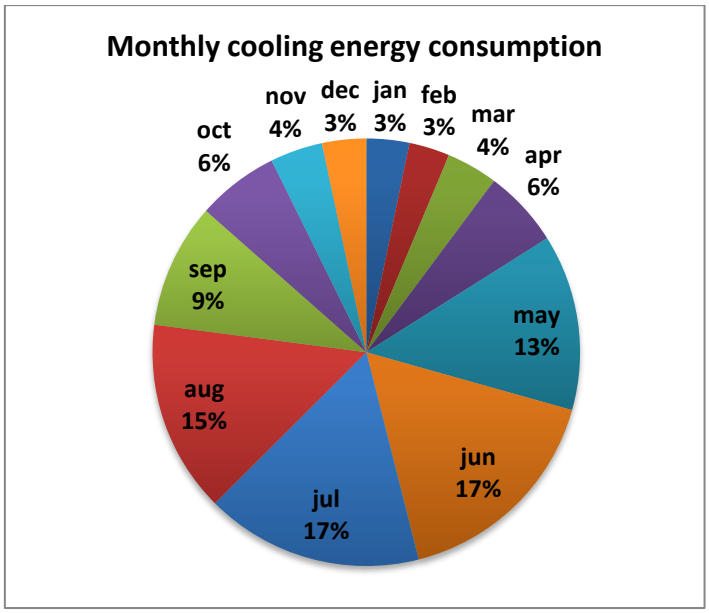

Figure 41: Monthly cooling energy consumption in percentage

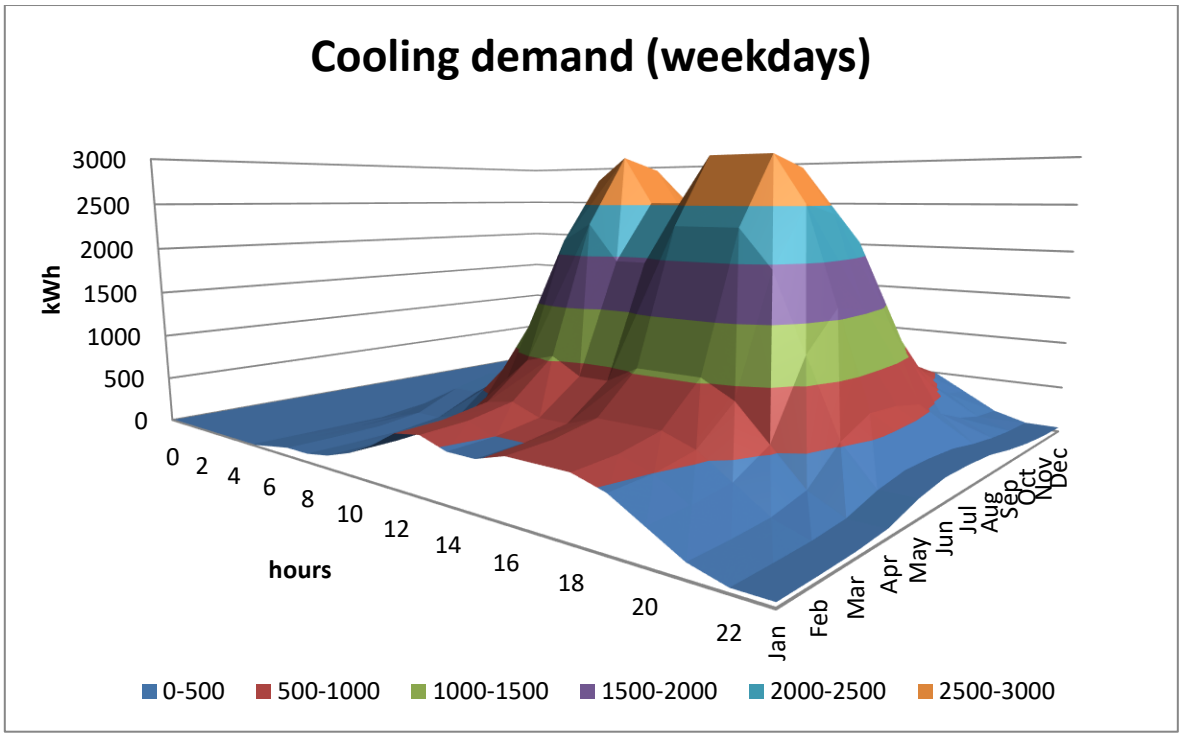

Figure 42: Cooling demand during weekdays

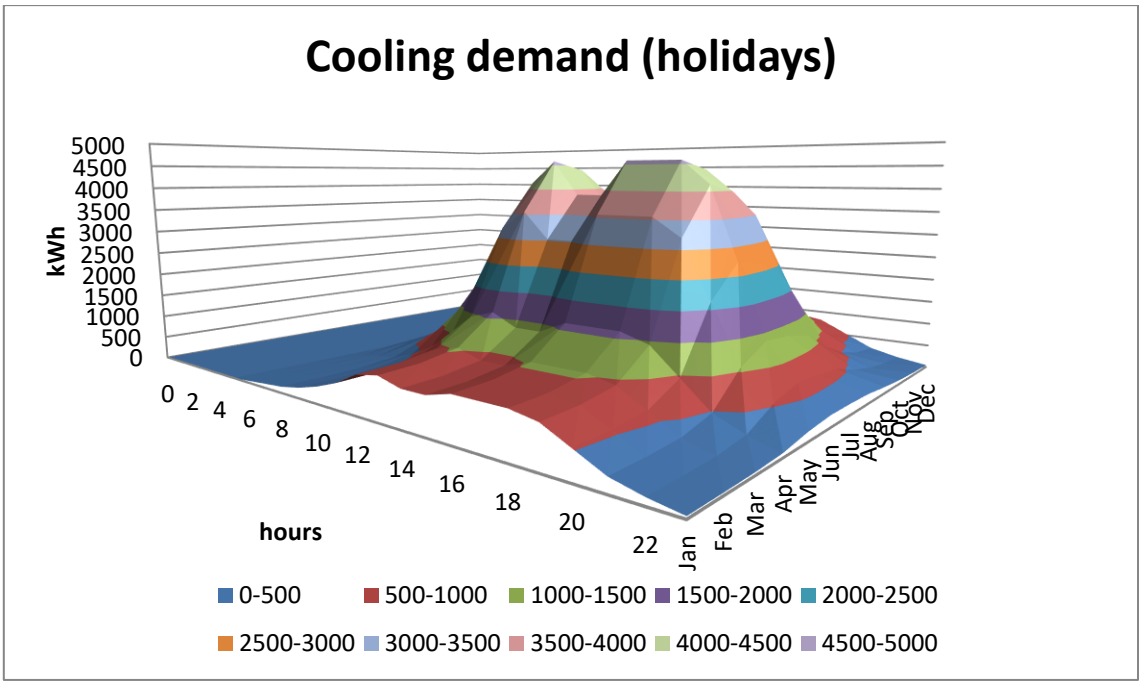

Figure 43: Cooling demand during holidays

From the cooling demand (Figure 42 and Figure 43), the calculation is carried on finding the electrical hourly demand, needed to the chiller (Figure 44 and Figure 45).

The COP considered for calculating these values varies with the external temperature, since environmental conditions affect the condenser and consequentially the operating conditions of the chillers. The results are presented in the graphs in Figure 44 and Figure 45.

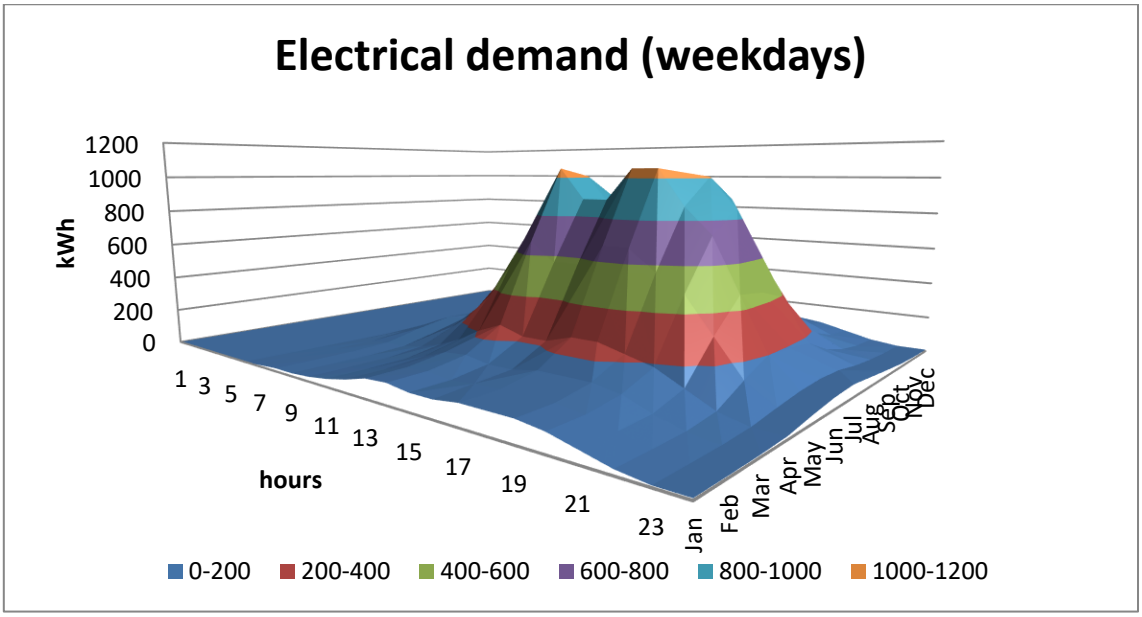

Figure 44: Electrical demand during weekdays

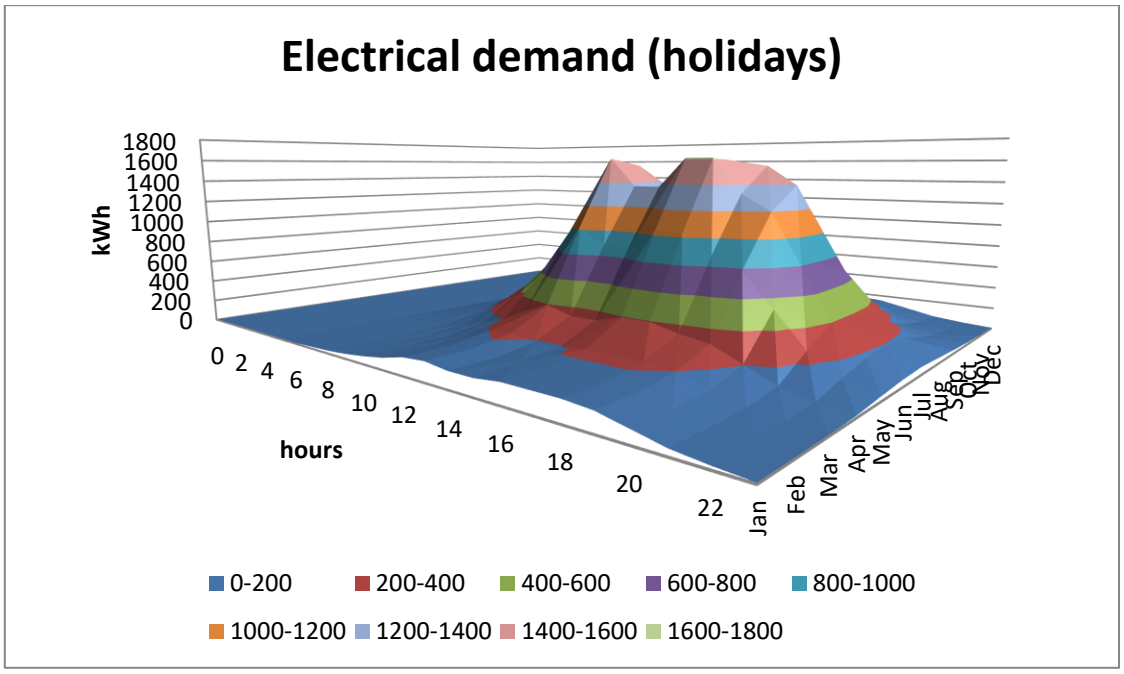

Figure 45: Electrical demand during holidays

It results that during holidays the electrical demand is higher than in weekdays because of the occupation that is strikingly greater in these days.

7.2. Electricity consumption

Moreover, to fully exploit the electrical production of the system, it is thought to cover also the electrical demand due to the lighting and supply electrical devices.

Therefore, it is studied the electrical hourly demand profile throughout the year, considering that the electrical total annual demand is almost the same value of the cooling demand. All days are considered to consume the same value during each month, the demand only changes depending on if it is weekday rather than holiday (Figure 46). In Figure 46 it is shown the daily electrical demand profile in percentages referred to the maximum daily demand.

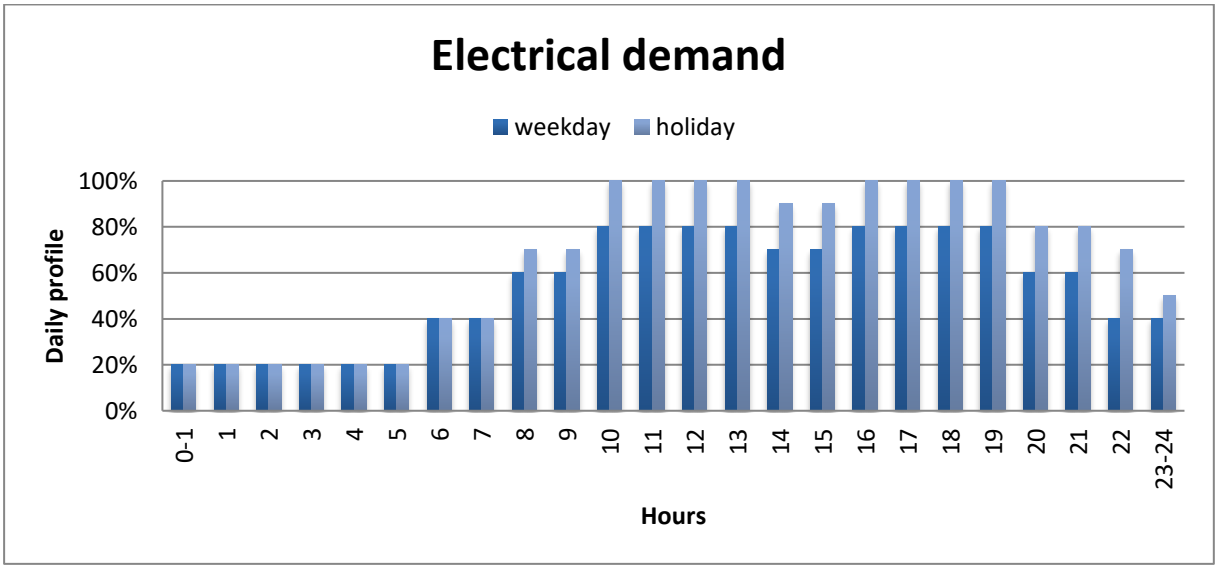

Figure 46: Hourly profile of the electrical demand

8. Design of the power cycle

Covering the cooling demand is the criterion chosen to design the ORC cycle. This choice is a compromise between trying to cover, at least, the cooling demand and not oversizing the whole system. In order to provide the necessary electricity to cover the entire electrical demand of the shopping centre, a connection to the grid will be afterwards considered.

The model chosen to cover the demand is COBALT W 153.3. In order to guarantee the demand three chillers have been considered to be installed with an overall nominal cooling capacity of 4581 kW.

The choice of installing more chillers allows to work with only one or two chillers when the demand is lower than the nominal power. Thus, the chillers in operation can work almost at the same level of the nominal power, maintaining a high level of efficiency.

The electrical nominal demand of the chiller is 326kW for each one of the three machines that are used, therefore the electrical output that the power cycle has to provide is:

Wnt=978kW.

Another condition that has to be set is the temperature of the condenser inlet water (Tf1) to the same value of the design condition of the refrigeration water of the chiller.

To analyse the possible design of the field, the model of the ORC cycle has been defined in EES [EES, S.A. Klein and G. Nellis, 2018].

The solar field with the integration of the biomass boiler provides the thermal input power of the cycle (Qct) with certain thermal conditions of the thermal oil (Tc1).

Therefore, setting Qct as the value to be minimized, and Tc1 as the independent variable, the software EES calculates the best value as Table 28 shows.

Wnt [kW]	Tfi [°C]	ηtoc [-]	Qct [kW]	Tc1 [°C]
978	30	0.189	5170	174.0

Table 28: Results of the Qct minimization problem, EES

When computing the problem in order to find the maximum efficiency, the same results of Table 28 are obtained.

The cycle results a critical cycle, the thermodynamic values are presented below, resulting from the EES model.

	t_i [°C]	p_i [bar]	s_i [kJ/(kg·K)]	x_i	h_i [kJ/kg]
1	40,0	2,50	1,1790	0	252,57
2	42,1	36,50	1,1825	-100	256,30
3	100,0	36,50	1,4227	-100	338,91
4	154,0	36,50	1,7217	0	460,32
5	154,0	36,50	1,7324	1	464,89
6	204,0	36,50	1,9880	100	578,52
7	131,8	2,50	2,0200	100	527,52
8	51,1	2,50	1,7928	100	444,91
9	40,0	2,50	1,7577	1	433,74
10	40,0	2,50	1,1790	0	252,57

Table 29: Thermodynamic properties of the working fluid in each point of the critical cycle, EES[1]

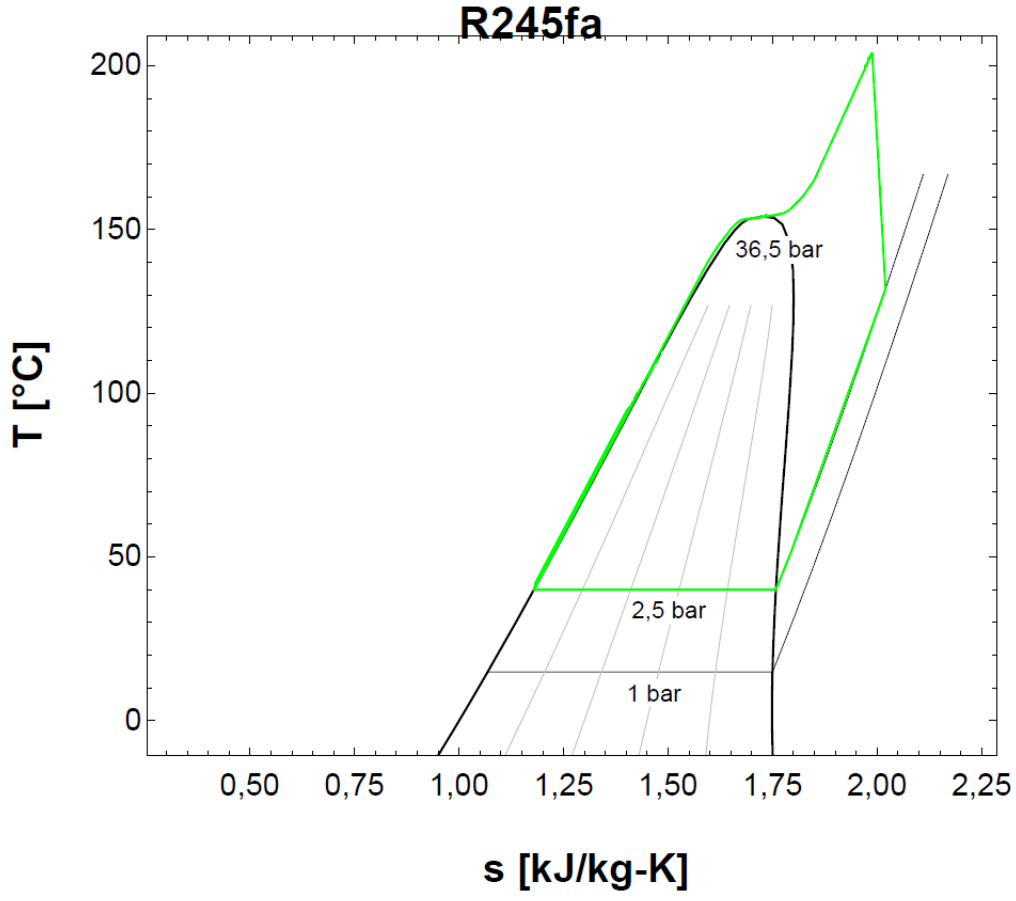

Figure 47: Graph of the critical power cycle with R245fa, EES[1]

Reaching critical conditions leads to higher turbine inlet temperatures and therefore it results in increasing the thermal efficiency.

As it can be seen in the Figure 48, the research conducted by S. Quoilin et al. [2011] led to a comparison between more fluids setting different evaporation temperatures. According to this graph, increasing the evaporation temperature of the fluid R245fa, always leads to a rising in overall efficiency, until the critical value has been reached.

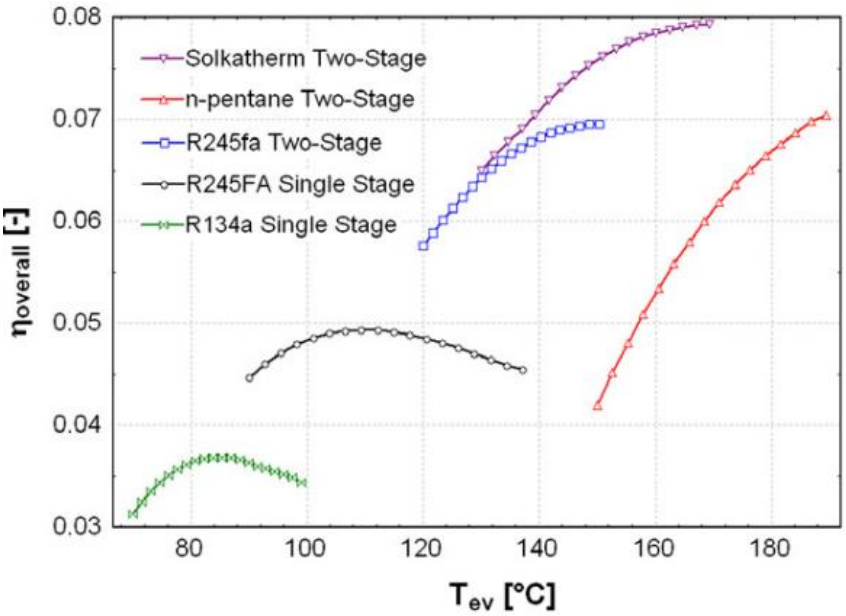

Figure 48: Overall efficiency for different working fluids of a low-cost solar ORC [S. Quoilin et al., 2011]

Even though the critical cycle results as a better solution regarding efficiency and minimizing thermal power demand, it leads to stability problems [Giorgio Bonvicini,2014].
In a subcritical cycle, the evaporation temperature of the ORC is limited by the critical temperature of the fluid. The upper limit of the maximum process temperature is the fluid stability and material compatibility.
Decreasing the evaporation temperature from the critical temperature by 10-15°C, seems reasonable to guarantee the stability [Xiaojun Zhang et al., 2016], [Giorgio Bonvicini,2014].
It is a right compromise between reducing the temperature below the critical value and still getting good efficiency value, compared to the cycle in critical conditions.
The thermodynamic values are presented below, resulting from the model setting the evaporation temperature to 144°C.

	t_i [°C]	p_i [bar]	s_i [kJ/(kg·K)]	x_i	h_i [kJ/kg]
1	40,0	2,50	1,1790	0	252,57
2	41,8	30,28	1,1819	-100	255,62
3	97,7	30,28	1,4152	-100	335,59
4	144,0	30,28	1,6251	0	418,55
5	144,0	30,28	1,7933	1	488,66
6	194,0	30,28	1,9820	100	571,51
7	128,7	2,50	2,0118	100	524,22
8	50,5	2,50	1,7907	100	444,25
9	40,0	2,50	1,7577	1	433,74
10	40,0	2,50	1,1790	0	252,57

Table 30: Thermodynamic properties of the working fluid in each point of the design cycle, EES [1]

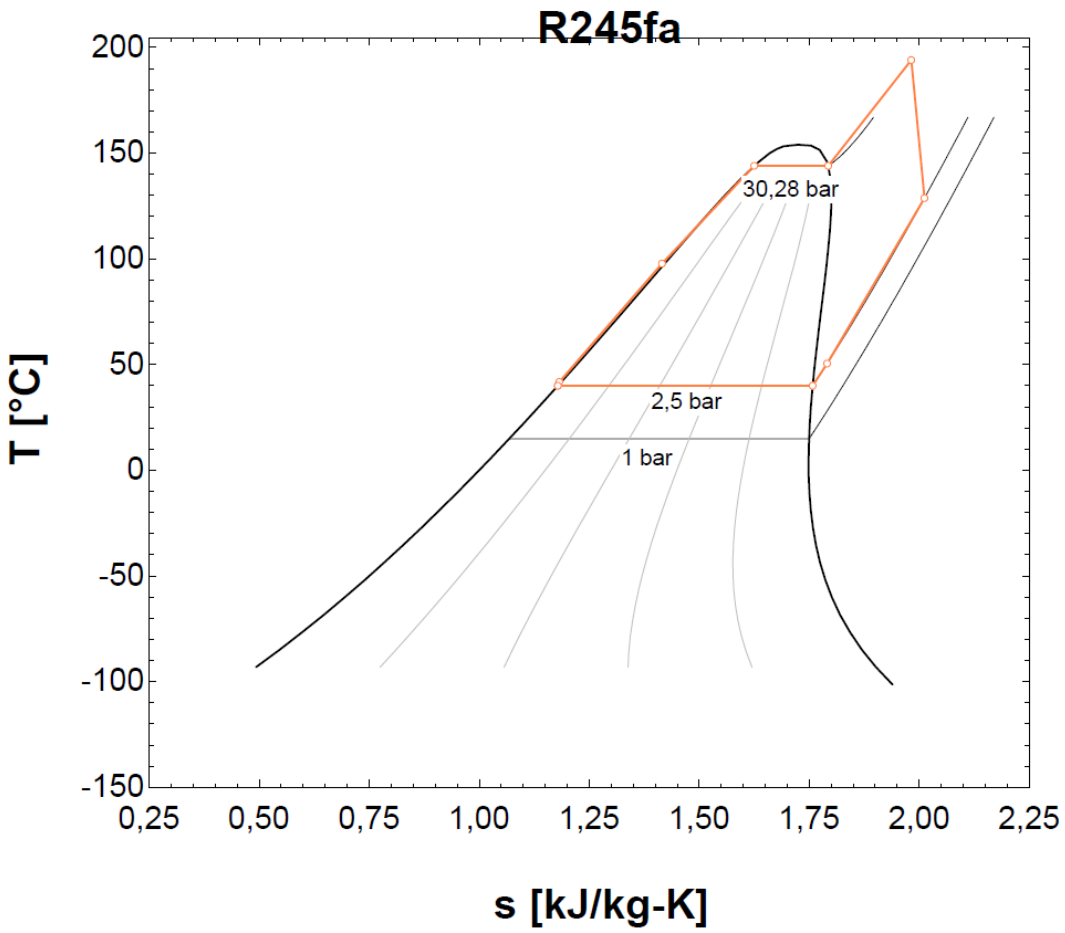

Figure 49: Graph of the design power cycle with R245fa, EES[1]

The significant characteristics of the cycle are presented in Table 31.

Wnt [kW]	Tfi [°C]	ηtoc [-]	Qct [kW]	Tc1 [°C]	Tc4 [°C]
978	30	0.180	5431	214.0	121.5

Table 31: Result of the design cycle, EES

As a consequence of the temperature needed in the cycle as thermal source, the solar field must be designed according to the value of Qct, Tc1 and Tc4 (Table 32).

Solar field	
Hours of storage [h]	6
Actual number of loops	9
Total aperture reflective area [m2]	19620
Actual solar multiple	2.54
Actual field thermal output [MW-t]	13.79
Annual net energy [MWh-t]	17190.322
Annual gross energy [MWh-t]	17212.374
Annual electricity load [MWh-e]	129.923

Table 32: Main characteristics of the solar field

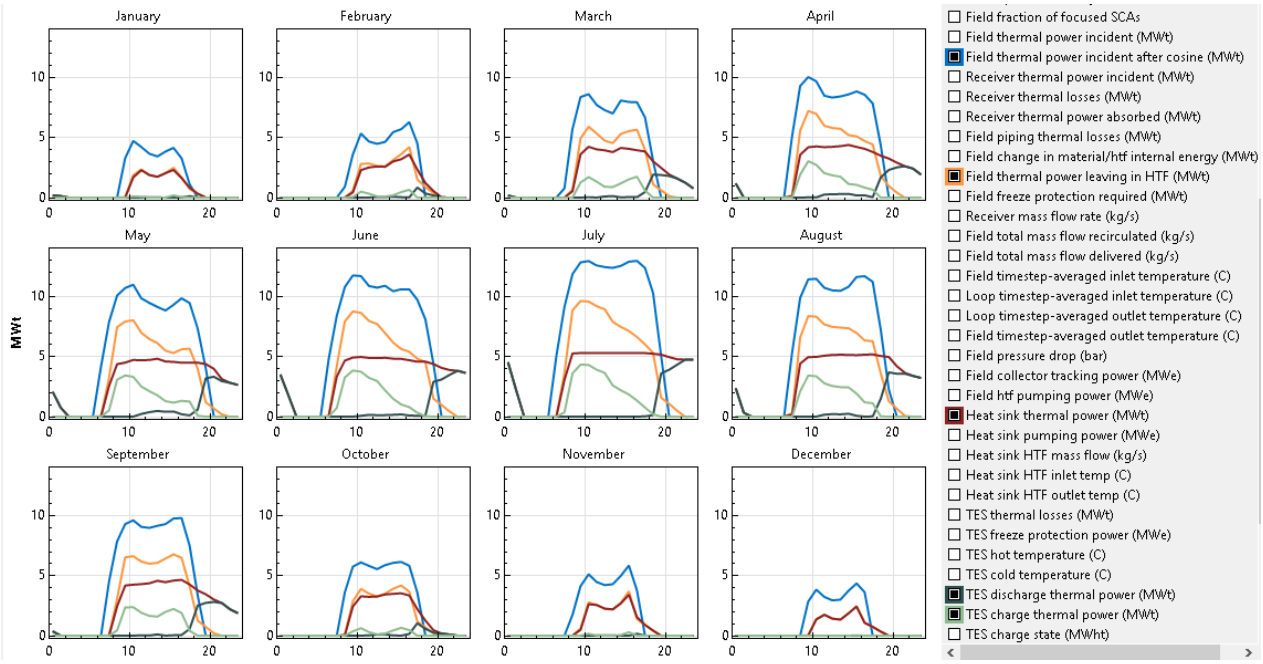

Figure 50: Monthly values of the highlighted values resulting from SAM [SAM screenshot, NREL. System Advisor Model 2017.9.5]

Power values lower than 0.5MW are not included, considering the production not worth to let the solar field and the power cycle work in these conditions. The daily operating hours of the system differ in each month, depending on the solar field production, they are represented in Table 33. The mean hourly thermal power per month provided by the solar field is shown in Table 34.

	Jan	**Feb**	**Mar**	**Apr**	**May**	**Jun**	**Jul**	**Aug**	**Sep**	**Oct**	**Nov**	**Dec**
Operating hours	8	10	16	17	19	19	19	17	16	10	8	8

Table 33: Daily operating hours of the system for each month

Solar field	Jan	Feb	Mar	Apr	May	Jun	Jul	Aug	Sep	Oct	Nov	Dec
02:00 am	0	0	0	0	0	0	0	0	0	0	0	0
03:00 am	0	0	0	0	0	0	0	0	0	0	0	0
04:00 am	0	0	0	0	0	0	0	0	0	0	0	0
05:00 am	0	0	0	0	0	0	0	0	0	0	0	0
06:00 am	0	0	0	0	0	0	0	0	0	0	0	0
07:00 am	0	0	0	0	2.54	3.31	3.04	0	0	0	0	0
08:00 am	0	0	0.52	3.55	4.35	4.64	5.24	4.39	2.43	0	0	0
09:00 am	0	0	3.58	4.17	4.48	4.9	5.28	4.94	4.16	2.41	0	0
10:00 am	1.67	2.28	4.22	4.25	4.7	4.95	5.27	4.95	4.23	3.26	2.6	1.33
11:00 am	2.27	2.5	4	4.18	4.68	4.87	5.27	5.05	4.27	3.21	2.54	1.73
12:00 pm	1.87	2.58	3.92	4.21	4.7	4.85	5.27	5.11	4.34	3.24	2.25	1.41
01:00 pm	1.73	2.55	3.77	4.27	4.8	4.88	5.28	5.13	4.55	3.42	2.18	1.33
02:00 pm	2.02	3	4.12	4.36	4.57	4.81	5.26	5.12	4.43	3.47	2.67	1.85
03:00 pm	2.3	3.18	4.04	4.2	4.54	4.79	5.27	5.1	4.57	3.51	3.39	2.41
04:00 pm	1.62	3.57	3.93	4.05	4.47	4.68	5.27	5.14	4.63	3.33	1.53	1.06
05:00 pm	0.82	2.33	3.83	3.78	4.49	4.55	5.27	5.16	4.24	2.19	0.89	0.73
06:00 pm	0	1.22	3	3.47	4.47	4.56	5.21	5.03	3.74	1.25	0	0
07:00 pm	0	0.54	2.47	3.24	4.36	4.37	5.14	4.95	3.43	0	0	0
08:00 pm	0	0	1.91	2.9	3.96	4.04	4.93	4.18	2.99	0	0	0
09:00 pm	0	0	1.58	2.6	3.11	3.86	4.75	3.63	2.7	0	0	0
10:00 pm	0	0	1.23	2.4	2.8	3.8	4.73	3.38	2.19	0	0	0
11:00 pm	0	0	0.73	1.9	2.8	3.45	4.72	3.21	1.86	0	0	0
12:00 am	0	0	0	1.17	2.06	3.5	4.52	2.36	0	0	0	0
01:00 am	0	0	0	0	0.74	1.76	2.21	0	0	0	0	0

Table 34: Mean hourly thermal power per month provided by the solar field

The Figure 51 represents more clearly the power profile of the values of Table 34.

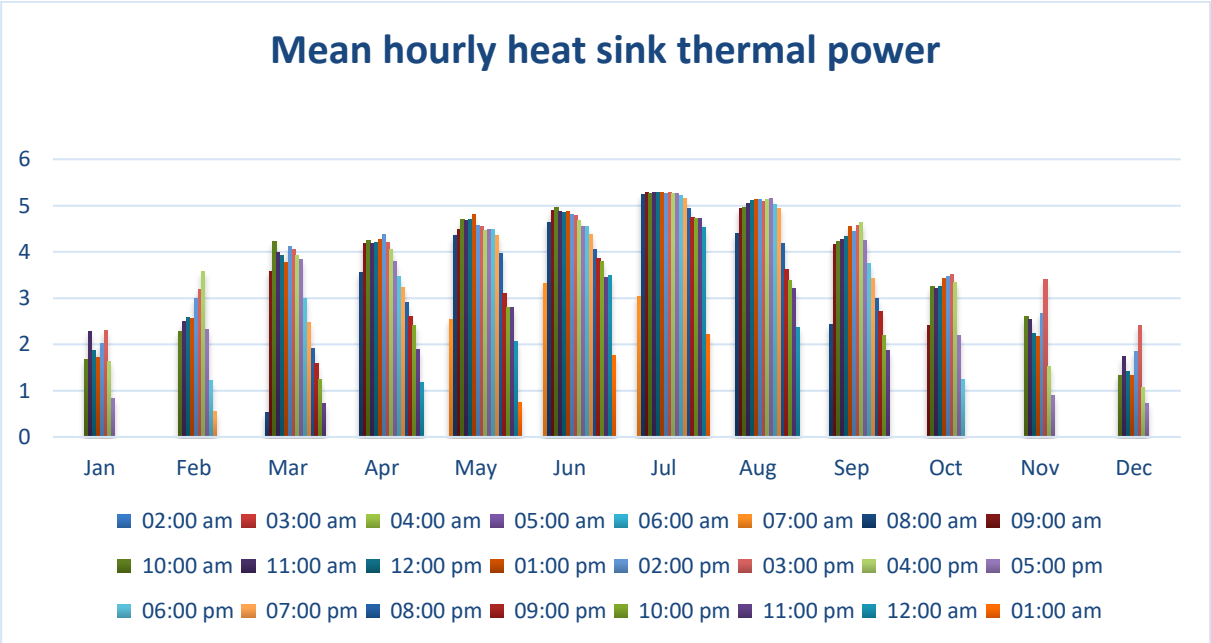

Figure 51: Mean hourly heat sink thermal power for each month

In Table 35 are presented the hourly power values that the boiler must guarantee, in order to reach the input nominal thermal power of the ORC cycle.

Boiler	Jan	Feb	Mar	Apr	May	Jun	Jul	Aug	Sep	Oct	Nov	Dec
02:00 am	0	0	0	0	0	0	0	0	0	0	0	0
03:00 am	0	0	0	0	0	0	0	0	0	0	0	0
04:00 am	0	0	0	0	0	0	0	0	0	0	0	0
05:00 am	0	0	0	0	0	0	0	0	0	0	0	0
06:00 am	0	0	0	0	0	0	0	0	0	0	0	0
07:00 am	0	0	0	0	2.89	2.12	2.39	0	0	0	0	0
08:00 am	0	0	4.91	1.88	1.08	0.79	0.19	1.04	3	0	0	0
09:00 am	0	0	1.85	1.26	0.95	0.53	0.15	0.49	1.27	3.02	0	0
10:00 am	3.77	3.15	1.22	1.19	0.73	0.48	0.16	0.48	1.2	2.17	2.83	4.1
11:00 am	3.16	2.93	1.43	1.25	0.75	0.56	0.16	0.38	1.16	2.22	2.89	3.7
12:00 pm	3.56	2.85	1.51	1.22	0.73	0.58	0.16	0.32	1.09	2.19	3.19	4.02
01:00 pm	3.71	2.88	1.66	1.17	0.63	0.55	0.16	0.3	0.88	2.02	3.25	4.1
02:00 pm	3.41	2.43	1.31	1.07	0.86	0.62	0.17	0.31	1	1.96	2.76	3.58
03:00 pm	3.13	2.25	1.39	1.23	0.89	0.64	0.16	0.33	0.86	1.92	2.04	3.02
04:00 pm	3.81	1.86	1.5	1.39	0.96	0.75	0.16	0.29	0.8	2.1	3.9	4.37
05:00 pm	4.61	3.1	1.61	1.65	0.94	0.88	0.16	0.27	1.19	3.24	4.54	4.7
06:00 pm	0	4.21	2.43	1.96	0.96	0.87	0.22	0.4	1.69	4.18	0	0
07:00 pm	0	4.89	2.97	2.19	1.07	1.06	0.29	0.48	2	0	0	0
08:00 pm	0	0	3.52	2.53	1.47	1.39	0.5	1.25	2.44	0	0	0
09:00 pm	0	0	3.85	2.83	2.32	1.57	0.68	1.8	2.73	0	0	0
10:00 pm	0	0	4.2	3.03	2.63	1.63	0.7	2.05	3.24	0	0	0
11:00 pm	0	0	4.7	3.53	2.63	1.98	0.71	2.22	3.57	0	0	0
12:00 am	0	0	0	4.26	3.37	1.94	0.91	3.07	0	0	0	0
01:00 am	0	0	0	0	4.69	3.67	3.22	0	0	0	0	0

Table 35: Mean hourly thermal power per month provided by the biomass boiler

In Figure 52 the annual power profile of the biomass boiler is presented. As it can be seen, in the summer months the contribute of the boiler is greatly reduced compared to the winter ones, due to the wider availability of the solar radiation in summer and thus, the higher productivity of the solar field.

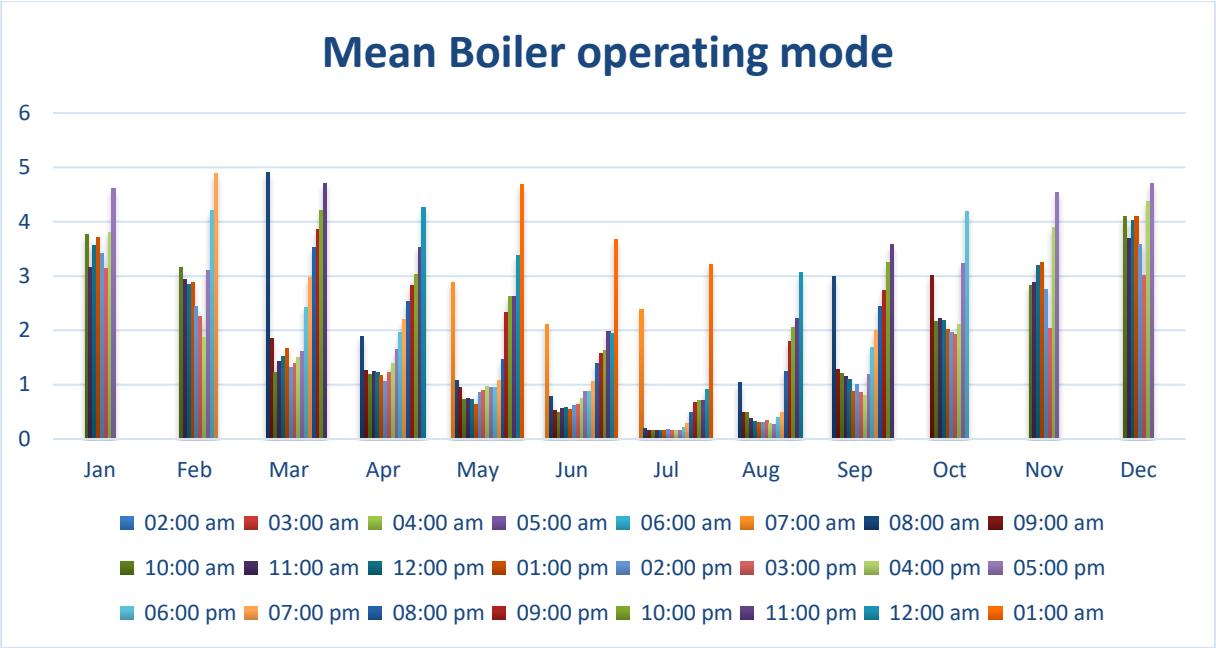

Figure 52: Mean hourly biomass boiler thermal power for each month

The biomass price can vary between 10 and 25 €/MWh. Therefore, LHV equal to 15.5 MJ/kg and 15 €/MWh have been considered in order to continue the analysis [A. Guercio, R. Bini, 2017].

	Jan	Feb	Mar	Apr	May	Jun	Jul	Aug	Sep	Oct	Nov	Dec	Annual
Boiler [MWh]	904	856	1242	1009	947	678	348	480	844	775	762	979	9825
Biomass [ton]	318	301	437	355	333	239	123	169	297	273	268	345	3457
Price [€]	13554	12841	18627	15136	14206	10174	5225	7207	12654	11630	11427	14687	147368
Solar field [MWh]	443	665	1452	1761	2252	2417	2851	2382	1763	908	542	368	17803
Solar field [%]	32.9	43.7	53.9	63.6	70.4	78.1	89.1	83.2	67.6	53.9	41.6	27.3	64
Boiler [%]	67.1	56.3	46.1	36.4	29.6	21.9	10.9	16.8	32.4	46.1	58.4	72.7	36

Table 36: Overview of the energy production throughout the year

Table 36 shows both the energy production of the biomass boiler, with the consume and the cost of its fuel, and the energy production due to the solar field. Besides, the percentages of the total energy produced respectively by the solar field and by the boiler are represented. The result shows that throughout the year the percentages vary considerably: in spring and summer the solar field energy production exceeds the 50% of the total production, reaching almost the 90% in July. On the other hand, in autumn and winter the biomass boiler production is more than the energy produced by the solar field. The annual value shows that the 64% of the energy is produced by the solar field.

9. Electricity production and connection to the grid

During the operating hours of the cycle it provides, neglecting variations for climatic conditions, almost the same nominal power as output. The graph in Figure 53 represents the electrical energy produced by the ORC in each hour of the typical day in each month. The profile shape is conditioned by the solar field production that has set the operating hours of the system.

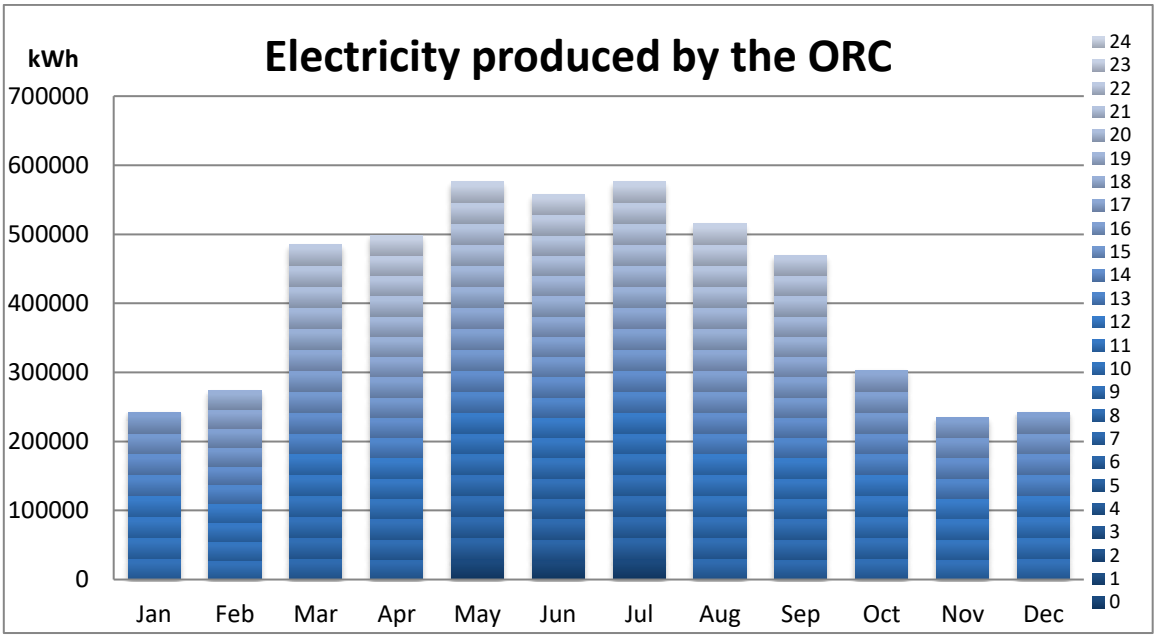

Figure 53: Total electricity produced by the ORC in each month

To better exploit the ORC electrical production, it is thought to use the electricity produced by the power cycle to cover this demand.

In order to provide the electricity that the whole system needs, it can be considered to buy the amount that the ORC system is not able to produce whilst the demand is not fully covered.

Thus, buying electricity from the grid assures a constant supply.

The estimated values are presented in the Figure 54. Figure 55 shows the percentages in which the electricity has been bought in each month.

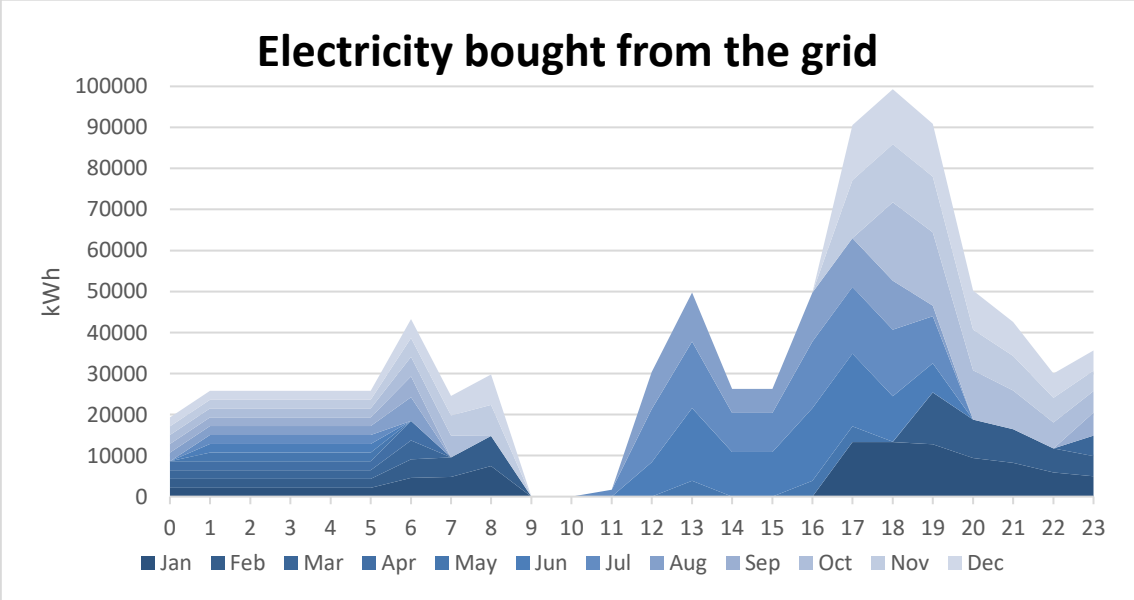

Figure 54: Total monthly electricity both from the grid highlighting the hour considered

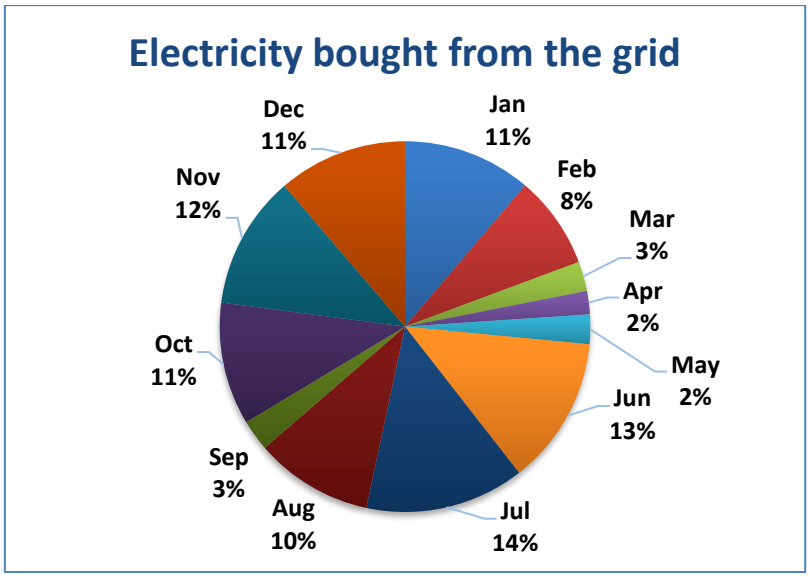

Figure 55: Percentage of the electricity bought from the grid in each month

Whereas there are hours when the electricity produced is not sufficient, there are as well hours when the electricity exceeds. Then, it is possible to sell the exceeding electricity to the grid, the values are estimated as shown in Figure 56. Figure 57 shows the percentages in which the electricity has been sold in each month.Selling to the grid gives the chance to have an economic return of the investment, even when the production exceeds the demand of the shopping centre.

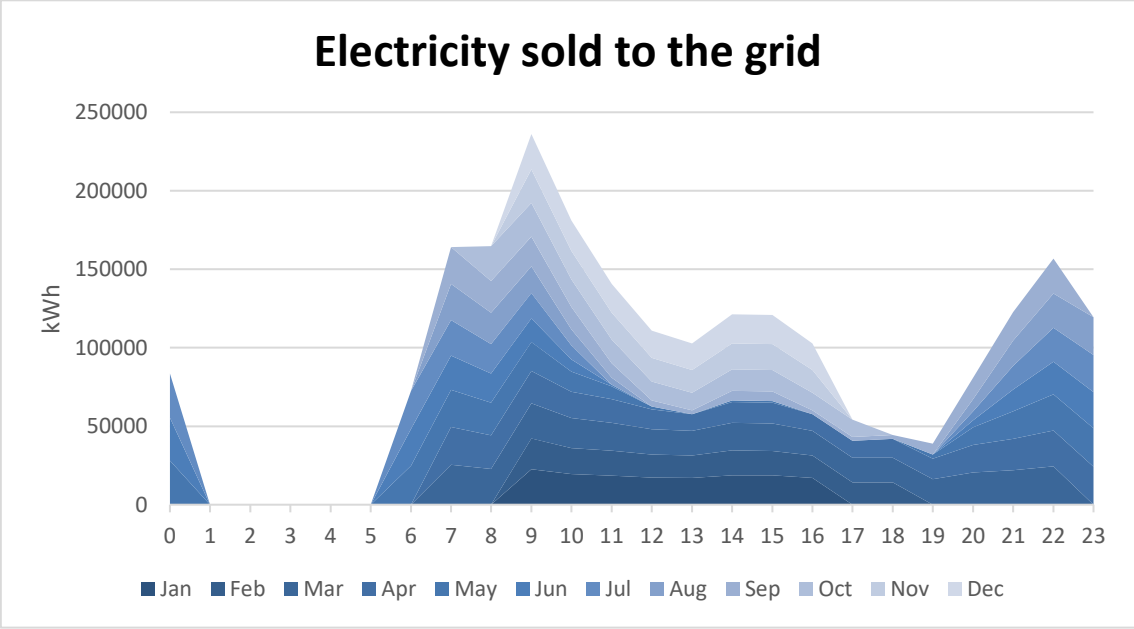

Figure 56: Total monthly electricity sold to the grid highlighting the hour considered

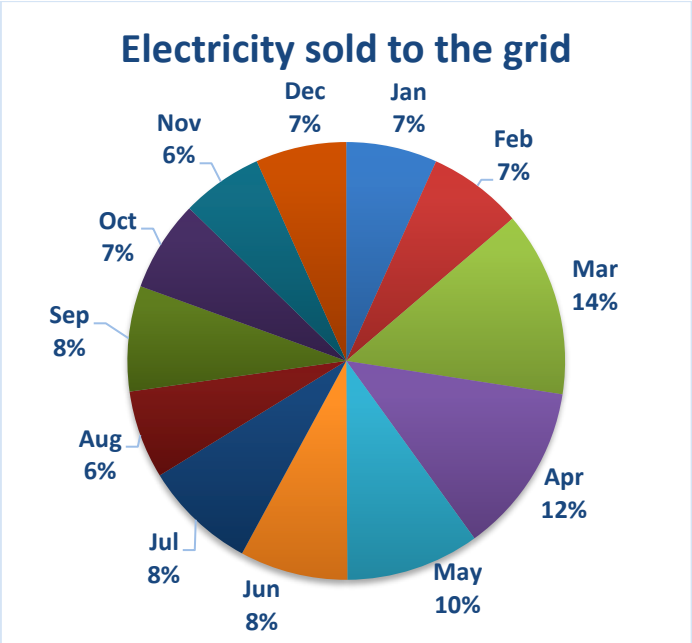

Figure 57: Percentage of the electricity sold to the grid in each month

Table 37 represents in which percentages the different technologies affect the electricity production and in which percentages the production is divided into the demand and the electricity sold to the grid. The total of the solar field plus the biomass boiler productions, in percentage, is equal to the ORC production in Table 37.

	Jan	Feb	Mar	Apr	May	Jun	Jul	Aug	Sep	Oct	Nov	Dec	Annual
Solar field	23.5	34.8	51.5	61.4	67.8	65.0	73.7	70.9	64.4	41.3	29.0	19.4	54.9
Biomass boiler	47.8	44.8	44.1	35.2	28.5	18.2	9.0	14.3	30.8	35.2	40.8	51.8	30.3
ORC	71.3	79.5	95.6	96.6	96.3	83.2	82.7	85.2	95.2	76.5	69.9	71.2	85.1
Electricity bought	28.7	20.5	4.4	3.4	3.7	16.8	17.3	14.8	4.8	23.5	30.1	28.8	14.9
Electricity sold	43.9	45.1	59.9	54.1	36.6	26.4	26.6	23.9	35.0	37.7	39.8	43.7	38.0
Demand	56.1	54.9	40.1	45.9	63.4	73.6	73.4	76.1	65.0	62.3	60.2	56.3	62.0

Table 37: Overview of the energy production throughout the year, values in percentage

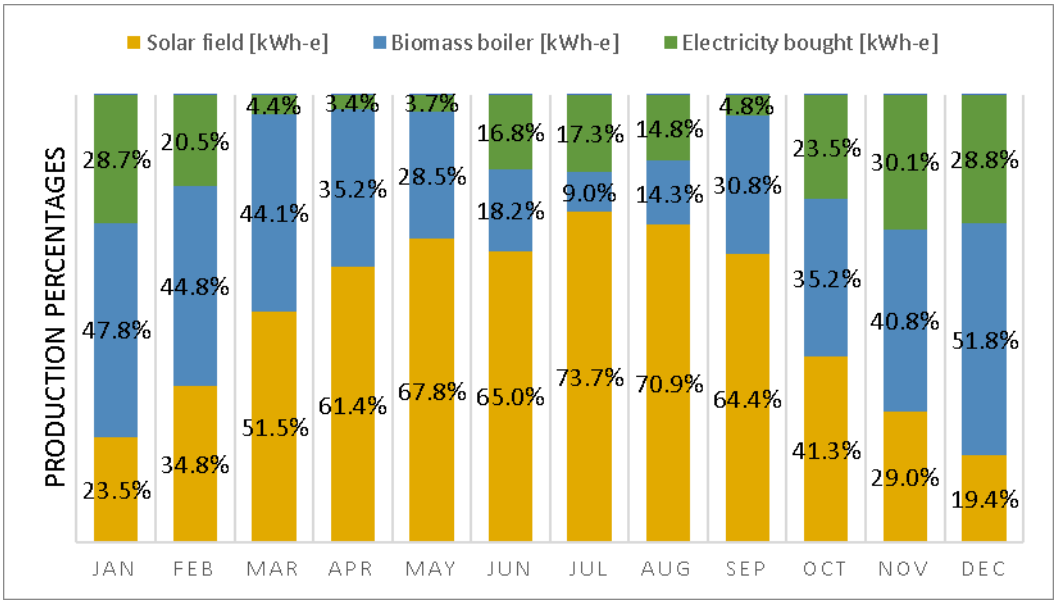

Figure 58: Percentages of production of the total electricity (used and sold) from the various sources

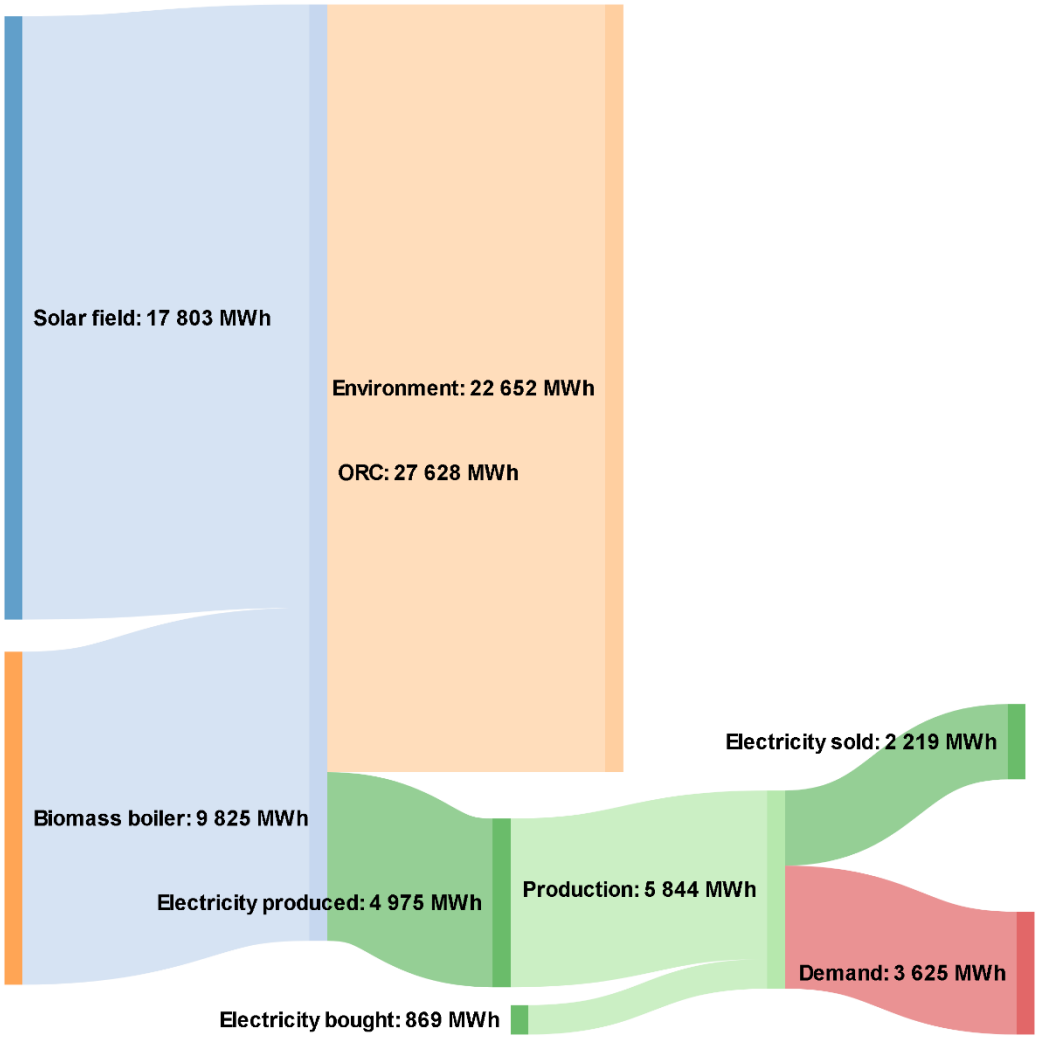

Figure 59: Annual energy (GWh) distribution of sources and outcome

10. Conclusion

The aim of the analysis hereby conducted is to prove the technological feasibility of a solar cogeneration plant of electricity and cooling based on solar parabolic trough combined with ORC and biomass applied to a shopping centre.

Firstly, this paper has given some valuable insights into the use of the SAM software and some suggestions about how varying the design parameters affects the production results of the solar field. The study proceeds with the ORC examination of possible configurations and presenting a model option.

Then, the chillers, whose data have been presented, are taken as starting point to design a case study with a realistic application of the system. The demand, both cooling and electrical demand, of a shopping centre is what the system aims to cover.

According to the analysis, the whole system is able to provide yearly 4975MWh of electrical energy, of which almost 64% of the electrical production is carried out by the solar field and 36% by the biomass boiler. Because the design of the system was based on covering the nominal power of the chillers, with the purpose of not oversizing it, it was not considered the electrical demand of the site. When the cooling demand is considerably lower than the nominal power of the chillers, it results that the system is capable to partially or completely cover the electrical demand too, besides, a certain amount could exceed.

However, when the cooling demand is equal or higher than the power production of the system, it is necessary to integrate another option to cover the electrical demand. Therefore, the integration into the electrical grid results indispensable to allow to buy the electricity when needed, and thus to supply the whole demand of the shopping centre. The estimated yearly value of 869MWh of electricity bought is reached. The total electrical production of the system plus the electricity proceeding from the grid reach the yearly value of 5844MWh, of which the 62% (3625MWh) is used to cover the demand of the shopping centre and the remaining 38% (2219MWh) is sold to the grid, following the request of the profile of cooling and electrical demand. Figure 59 highlights how the source and the end-user are linked through the electrical production and demand.

In drawing some conclusions, the results clearly show how it would be possible to cover a significant percentage of the demand throughout the year, although with variations in each month, considering exclusively the use of the solar source (Figure 58). The analysis includes another renewable technology to cover an additional percentage of electrical demand, a biomass boiler. Thus, the assembly, through the ORC power production, lets only a few percentage points uncovered with different values each month (Figure 58), that the grid must supply.

It is of prime importance given the contemporary challenges facing our societies with regards to climate change and energy consumption. New self-sustainable ideas such as the one presented in this paper would certainly have a positive impact and prompt ground-breaking innovation in the sector.

A possible analysis that could be conducted following the data presented in this thesis could be an economical study of the technologies employed and of the operating costs. Such recommendations have the potential of complementing this research with a more comprehensive overview of these technologies alongside concrete applicability.

11. References

A. Guercio, R. Bini. *Chapter 15. Biomass-fired Organic Rankine Cycle combined heat and power Systems,* in Organic Rankine Cycle (ORC) Power Systems: Technologies and Applications, Woodhead Publishing Series in Energy, 2016.

A. Temraz, A. Rashad, A. Elweteedy and K. Elshazly. *Thermal analysis of the ISCC power plant in Kuraymat*, Egypt, AMME Conference, 2018.

Aalborg CSP: www.aalborgcsp.dk, 07/2018.

ACCIONA Energy of Spain: www.acciona-energia.com, 07/2018.

AEE INTEC: www.aee-intec.at, 07/2018

Andreas P. Weiß, "*VOLUMETRIC EXPANDER VERSUS TURBINE–WHICH IS THE BETTER CHOICE FOR SMALL ORC PLANTS*", 3rd International Seminar on ORC Power Systems, October 12-14, 2015, Brussels, Belgium, 1(2015), PAPER ID:22, p. 1

ASHRAE: www.ashrae.org, 06/2018.

Brønderslev Forsyning: www.bronderslevforsyning.dk,07/2018.

Bruno, J.C., López-Villada, J., Letelier, E., Romera, S., Coronas, A., *Modelling and optimisation of solar organic rankine cycle engines for reverse osmosis desalination*. Applied Thermal Engineering, 2008.

Buket Boz, Alvaro Diez, *Comparative Study of Sub-Critical and Supercritical ORC Applications for Exhaust Waste Heat Recovery*, World Academy of Science, Engineering and Technology International Journal of Energy and Power Engineering, Vol:12, No:2, 2018.

Carel: www.carel.com, 08/2018.

Daikin: www.daikin.eu, *Optimización del Sistema en aplicaciones de enfriadoras condensadas por aire*, 07/2018.

Daniele Fiaschi, Giampaolo Manfrida, Francesco Maraschiello. *Thermo-fluid dynamics preliminary design of turbo-expanders for ORC cycles*, Firenze, Italy, 2012.

Dario Prando, Massimiliano Renzi, Andrea Gasparella, Marco Baratieri. *Monitoring of the energy performance of a district heating CHP plant based on biomass boiler and ORC generator*, Bolzano, Italy, 2015.

E. Macchi, M. Astolfi, *Chapter 9. Axial flow turbines for Organic Rankine Cycle applications*, in Organic Rankine Cycle (ORC) Power Systems: Technologies and Applications, Woodhead Publishing Series in Energy, 2016.

Eastman: www.eastman.com, 06/2018

EES, S. A. Klein and G. Nellis, Mastering EES. (2012), www.fchart.com/ees/, 2018.

Enel video, Stillwater Solar Geothermal Hybrid Project in Fallon, USA (ENG), 07/2018.

Eric W. Lemmon, Roland Span, *Short Fundamental Equations of State for 20 Industrial Fluids, Journal of Chemical and Engineering Data*, 51(3),785-850, 2006.

Evangelos Bellos, Christos Tzivanidis, Vassilis Belessiotis. *Daily performance of parabolic trough solar collectors*, 2017.

Gabriel Morin, Jürgen Dersch, Werner Platzer, Markus Eck, Andreas Häberle. *Comparison of Linear Fresnel and Parabolic Trough Collector power plants*, 2011.

Giorgio Bonvicini, *Applicazione di cicli ORC per il recupero di potenza in impianti turbogas di piccola taglia*, 2014.

Giuseppe DiMarzio, Lorenzo Angelini, William Price, Chun Chin and Steve Harris. *The Stillwater Triple Hybrid Power Plant: Integrating Geothermal, Solar Photovoltaic and Solar Thermal Power Generation*, Proceedings World Geothermal Congress 2015.

Gobierno de España, Ministerio de Fomento, *Documento Básico HE Ahorro de energía, Código técnico de la edificación*, 2017.

Greenprogress: www.greenprogress.com, 07/2018.

Gro Harlem Bruntland*, Our Common Future*, Oxford: Oxford University Press, Oxford, 1987.

Liang Hongbo, Zheng Chenxiao, Zheng Wandong, You Shijun, Zhang Huan. *Analysis of Annual Performance of a Parabolic Trough Solar Collector*. Energy Procedia, 2017.

Linde Group: www.linde-gas.com, 07/2018.

M. Orosz, R. Dickes. *Chapter 16. Solar thermal powered Organic Rankine Cycles,* in Organic Rankine Cycle (ORC) Power Systems: Technologies and Applications, Woodhead Publishing Series in Energy, 2016

M.Astolfi, *Chapter 3. Technical options for Organic Rankine Cycle systems*, in Organic Rankine Cycle (ORC) Power Systems: Technologies and Applications, Woodhead Publishing Series in Energy, 2016.

Martin-Hou, A.I.Ch.E. Journal, 1:142,1995.

Meteonorm, www.meteonorm.com, 2018

Michael J. Wagner and Paul Gilman, Technical Manual for the SAM Physical Trough Model, 2011

Michael J. Wagner, Nate Blair, and Aron Dobos, National Renewable Energy Laboratory. *A Detailed Physical Trough Model for NREL's Solar Advisor Model*, SolarPACES, (conferences Paper NREL/CP-5500-49368, October 2010) Perpignan, France, September 21-24, 2010

Mohammed Khennich and Nicolas Galanis. *Optimal Design of ORC Systems with a Low-Temperature Heat Source*. Entropy 2012, 14, 370-389; doi:10.3390/e14020370.

Mónica Borunda, O.A. Jaramillo, R. Dorantes, Alberto Reyes. *Organic Rankine Cycle coupling with a Parabolic Trough Solar Power Plant for cogeneration and industrial processes*, 2015.

Montreal Protocol, UNEP/Earthprint, *Handbook for the Montreal Protocol on Substances that Deplete the Ozone Layer*, 2006.

National Renewable Energy Laboratory: www.nrel.gov, 07/2018.

Pedro Horta, FhG ISE, IEA SHC Task 49, SolarPACES Annex IV, *Solar Process Heat for Production and Advanced Applications, Process Heat Collectors: State of the Art and available medium temperature collectors*, 2012.

Protenders, Construction Intelligence & Tendering platform Protenders: www.protenders.com, 07/2018

Regulation (EU) No. 517/2014 on fluorinated greenhouse gases and repealing Regulation (EC) No 842/2006, European Parliament and Council, 16 April 2014.

Reiner Tillner-Roth, *Fundamental Equations of State*, Shaker, Verlag, Aachan, 1998.

S. Quoilin, M. Orosz, H. Hemond, V. Lemort. *Performance and design optimization of a low-cost solar organic Rankine cycle for remote power generation*, 2011.

SAM: System Advisor Model 2017.9.5 Available from: https://sam.nrel.gov/ National Renewable Energy Laboratory, (NREL).

SankeyMATIC (BETA): www.sankeymatic.com, 07/2018.

Siemens: www.siemens.com, 06/2018.

Soteris A. Kalogirou, 2004, *Solar thermal collectors and applications*, 2004.

Swegon: www.swegon.com, 07/2018.

Sylvain Quoilin, Martijn Van Den Broek, Sébastien Declaye, Pierre Dewallef, Vincent Lemort. *Techno-economic survey of Organic Rankine Cycle (ORC) systems*, Renewable and Sustainable Energy Reviews 22 (2013) 168–186, 2013.

Tchanche BF, Lambrinos G, Frangoudakis A, Papadakis G. *Low-grade heat conversion into power using organic Rankine cycles – A review of various applications*. Renewable Sustainable Energy Reviews, 2011;15:3963–79.

The greenage: www.thegreenage.co.uk, 08/2018.

Therminol: Heat transfer fluid calculators, https://calculators.therminol.com, www.therminol.com, 06/2018.

TRNSYS, a Transient Simulation Program. University of Wisconsin--Madison. Solar Energy Laboratory, Wis.:The Laboratory, 1975.

Turboden: www.turboden.eu, 07/2018.

U. Caldiño-Herrera, L. Castro, O.A. Jaramillo, J.C. Garcia, G. Urquiza, F. Flores. *Small Organic Rankine Cycle Coupled to Parabolic Trough Solar Concentrator*, 2017.

Ulli Drescher, Dieter Brüggemann. *Fluid selection for the Organic Rankine Cycle (ORC) in biomass power and heat plants*, 2006.

United States Environmental Protection Agency: www.epa.gov

Villarini M, Bocci E, Moneti M, Di Carlo A, Micangeli A. *State of art of small scale solar powered ORC systems: a review of the different typologies and technology perspectives*, 2014.

X.D. Wang, L. Zhao, J.L. Wang, W.Z. Zhang, X.Z. Zhao, W. Wu. *Performance evaluation of a low-temperature solar Rankine cycle system utilizing R245fa*, 2010.

Xiaojun Zhang, Lijun Wu, Xiaoliu Wang, Guidong Ju. *Comparative study of waste heat steam SRC, ORC and S-ORC power generation systems in medium-low temperature*, 2016.

12. Acknowledgment

En primer lugar, quiero dar las gracias a los profesores de Zaragoza, Luis y Miguel Ángel, que me han ayudado a realizar esta Tesis, además todos mis compañeros de carrera que me hicieron sentir como en familia.

Inoltre, ringrazio ancora la mia famiglia per l'appoggio ricevuto durante tutti questi anni di università, che come sono stati duri per me, molto di più per loro, è stata un'impresa sopportare le mie pazzie.

Ringrazio tutti i miei amici che hanno condiviso con me il freddo e le difficoltà di Torino, e gli amici di *botellón* dell'Erasmus che hanno vissuto con me questa esperienza indescrivibile.